

Development and Application of Subtype-Selective Fluorescent Antagonists for the Study of the Human Adenosine A₁ Receptor in Living Cells

Eleonora Comeo, Phuc Trinh, Anh T. Nguyen, Cameron J. Nowell, Nicholas D. Kindon, Mark Soave, Leigh A. Stoddart, Jonathan M. White, Stephen J. Hill, Barrie Kellam, Michelle L. Halls,* Lauren T. May,* and Peter J. Scammells*



Cite This: *J. Med. Chem.* 2021, 64, 6670–6695



Read Online

ACCESS |



Metrics & More

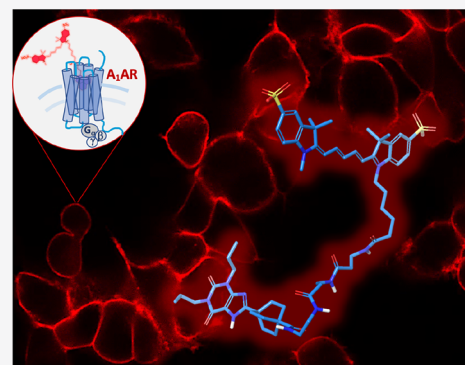


Article Recommendations



Supporting Information

ABSTRACT: The adenosine A₁ receptor (A₁AR) is a G-protein-coupled receptor (GPCR) that provides important therapeutic opportunities for a number of conditions including congestive heart failure, tachycardia, and neuropathic pain. The development of A₁AR-selective fluorescent ligands will enhance our understanding of the subcellular mechanisms underlying A₁AR pharmacology facilitating the development of more efficacious and selective therapies. Herein, we report the design, synthesis, and application of a novel series of A₁AR-selective fluorescent probes based on 8-functionalized bicyclo[2.2.2]octylxanthine and 3-functionalized 8-(adamant-1-yl) xanthine scaffolds. These fluorescent conjugates allowed quantification of kinetic and equilibrium ligand binding parameters using NanoBRET and visualization of specific receptor distribution patterns in living cells by confocal imaging and total internal reflection fluorescence (TIRF) microscopy. As such, the novel A₁AR-selective fluorescent antagonists described herein can be applied in conjunction with a series of fluorescence-based techniques to foster understanding of A₁AR molecular pharmacology and signaling in living cells.



INTRODUCTION

Adenosine is an important endogenous nucleoside, which exerts its modulatory role upon binding to four adenosine receptor (AR) subtypes, namely, A₁, A_{2A}, A_{2B}, and A₃.^{1,2} Adenosine receptors are class A G-protein-coupled receptors (GPCRs)³ and, due to their widespread distribution throughout the human body, are implicated in modulating many biological processes.⁴ The adenosine A₁ receptor (A₁AR) exerts its regulatory role mainly upon coupling with the G_{i/o} family of heterotrimeric G-proteins, resulting in adenylyl cyclase inhibition and a subsequent reduction of cAMP accumulation.¹ A₁ARs are highly expressed in the brain and, to a lesser extent, in peripheral tissues such as the heart, kidney, and lungs,^{1,5} and represent an attractive drug target for the development of therapeutic agents for CNS, cardiovascular, renal, and respiratory disorders.^{4,6,7} For instance, adenosine itself is administered to patients with paroxysmal supraventricular tachycardia (PSVT) to slow heart rate and contractility upon activation of the A₁AR.^{4,8} A₁AR activation can also decrease ischemia–reperfusion injury and neuropathic pain.^{4,9,10} On the other hand, inhibition of A₁AR function may offer therapeutic opportunities for the development of potassium sparing diuretics,^{4,10,11} anti-asthmatic agents,¹² and cognitive enhancers.^{7,13} However, a principal drawback in

developing efficacious and safe A₁AR-selective therapeutics is that this same biological target also mediates the onset of undesirable side effects including bradycardia, dyspnoea, and seizures.^{14–16} As such, the clinical application of A₁AR ligands has been hindered by the difficulty in separating on-target beneficial effects from adverse effects, coupled to the widespread expression of A₁AR in multiple tissues.^{14–16} Alternative therapeutic approaches could be exploited to address the aforementioned issues, which include more selective targeting through A₁AR-biased agonism and allosterism.^{17–19} The development of more selective and efficacious therapies, however, heavily depends on our understanding of how A₁AR pharmacology differs across tissues, cell types, and subcellular compartments.^{20–23} Fluorescent ligands represent valuable tools to enable real-time monitoring of receptor pharmacology, including ligand–receptor interactions, receptor signaling, and trafficking in different cell types, in both

Received: November 27, 2020

Published: March 16, 2021



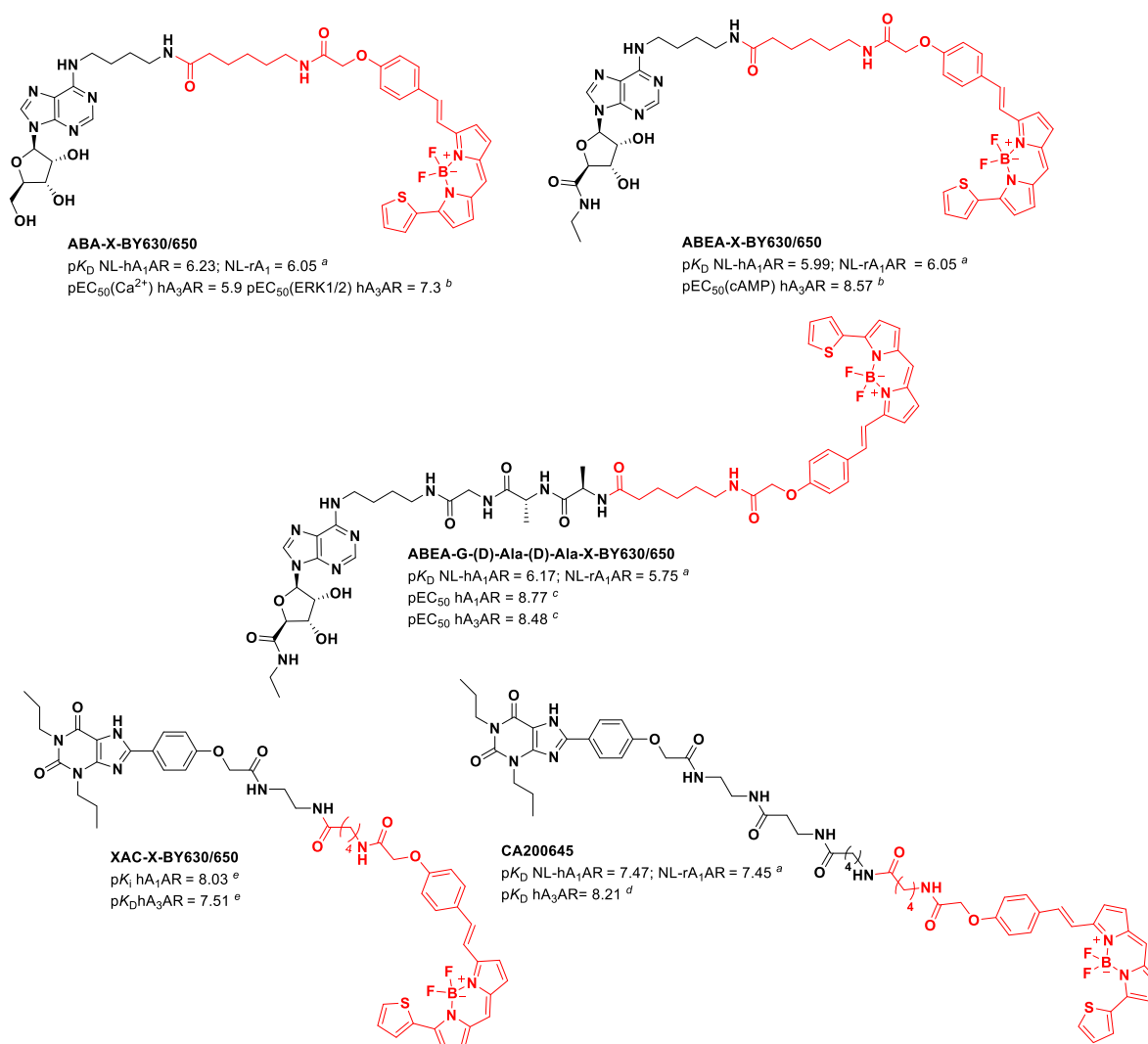


Figure 1. Structures of representative fluorescent ligands available to probe the A₁AR. Fluorescent ligand binding affinity^{a,d,e} (pK_D and pK_i)^{28,42,44} and potency^{b,c} (pEC_{50})^{25,45,46} quantified in cell lines stably expressing the human A₁AR (hA₁AR), rat A₁AR (rA₁AR), or human A₃AR (hA₃AR). NL denotes the presence of an N-terminal NLuc tag.

health and disease.^{24–29} Importantly, fluorescent ligands are amenable to quantifying receptor pharmacology at the single-cell level, in real-time, and in unmodified, endogenously expressing systems.^{30–32} The fluorescent ligand toolbox for the adenosine receptors has rapidly expanded over the past 15 years.^{33–36} Notably, the Jacobson group functionalized the hA_{2A}AR selective antagonist SCH442416 with AlexaFluor 488, resulting in a series of selective fluorescent ligands that have been successfully applied for fluorescence polarization (MRS5346)³⁷ and flow cytometry (MRS7416)³⁸ studies. Additionally, we have recently synthesized a novel series of hA_{2A}AR selective fluorescent probes based on preladenant, which allowed the successful monitoring of ligand binding and visualization of the hA_{2A}AR in living cells.³⁹ Conjugation of a green-emitting 4,4-difluoro-4-bora-3a,4a-diaza-s-indacene (BODIPY) fluorophore with a 8-phenyl-1-propylxanthine scaffold yielded the selective hA_{2B}AR probe (PSB-12105), which could monitor ligand binding at the hA_{2B}AR by flow cytometry.⁴⁰ There are also examples of selective fluorescent ligands that have been successfully developed and applied to probe the hA₃AR.^{41–43}

The fluorescent ligand toolkit available to study the hA₁AR (Figure 1) includes probes prepared from the endogenous A₁AR agonist, adenosine, labeled with fluorescein isothiocyanate (FITC) and nitrobenzoxadiazole (NBD) (FITC-ADAC and NBD-ADAC)⁴⁷ or BODIPY-X-630/650 (ABA-X-BY630).⁴⁸ Additionally, probes prepared from the full agonist NECA (dansyl-NECA,⁴⁹ ABEA-BY630,⁴⁸ and ABEA-G-(D)-Ala-(D)-Ala-X-BY630²⁵) and antagonists based on a xanthine amine congener (XAC)⁵⁰ (XAC-X-BY630)²⁴ and its analogue with a polyamide linker (CA200645) are also available.^{28,51} These probes have enabled researchers to gain important insights into A₁AR spatio-temporal organization^{24,48,52} and signaling in living cells,⁴⁴ yet the ability of these probes to bind other adenosine receptors limits their use to recombinant expression systems. Interrogating A₁AR pharmacology in more physiologically relevant models requires that the fluorescent probe engages with the targeted A₁AR with high selectivity as other closely related adenosine receptors are often coexpressed.^{5,32,53} Efforts to develop A₁AR-selective probes have been undertaken. For example, Singh et al. designed fluorescent ligands based on a (benzimidazolyl)isoquinolinol scaffold. However, these probes did not show measurable

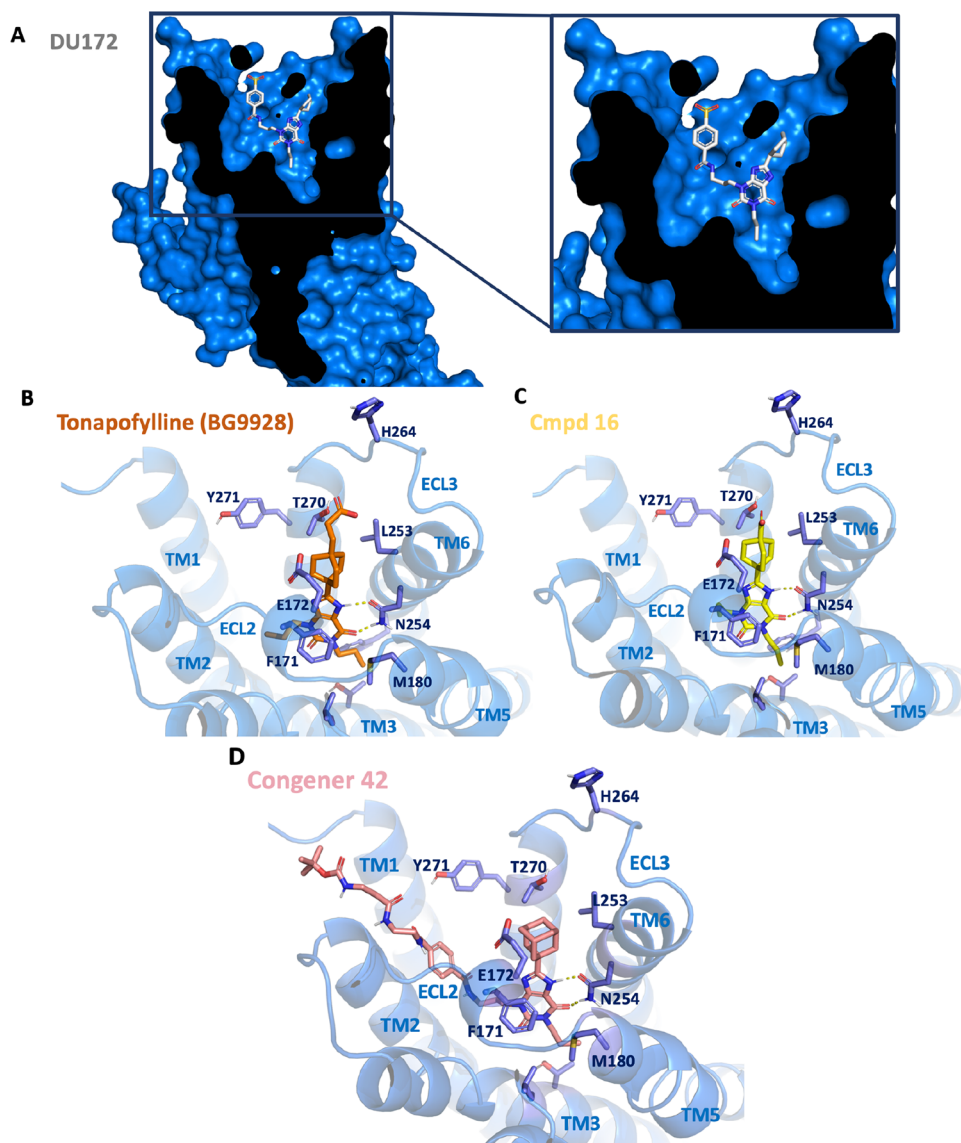


Figure 2. (A) Sectional view of the hA₁AR Connolly surface to show the binding pose adopted by the co-crystallized irreversible ligand DU172 (compound 23a in Beaglehole et al.)⁶⁰ (shown in grey sticks) with the 3-(4-fluorosulfonylbenzamido)propyl group directed toward the extracellular medium. Molecular docking of (B) tonapofylline (BG9928), (C) compound 16, and (D) congener 42 to the crystal structure of the hA₁AR (PDB: 5UEN) performed with Schrödinger's glide (Schrodinger release 2019-2). Tonapofylline is rendered in brick-red sticks, while compound 16 is shown in sticks (colored yellow) and congener 42 is rendered in pink sticks. The hA₁AR is shown in ribbon (colored marine blue). The key residues are shown in sticks (violet) and are labeled. Hydrogen bonds are shown as yellow-dashed lines and the transmembrane (TM) helices 1–3, 5, and 6 are labeled for clarity alongside extracellular loop (ECL) 2 and ECL3.

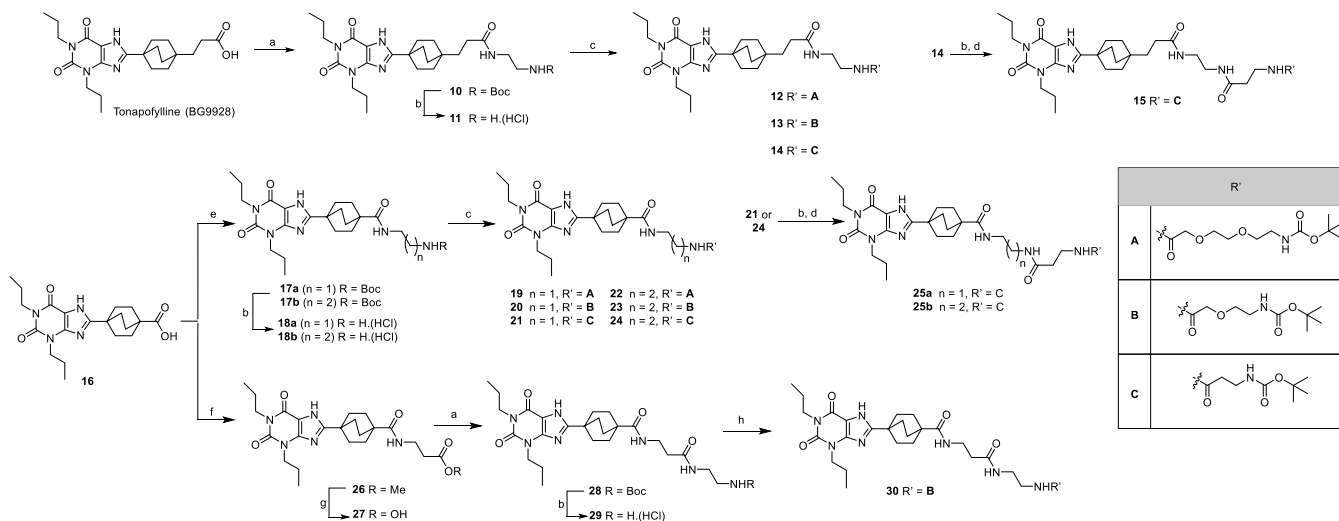
binding affinity to the A₁AR.⁵⁴ Therefore, there still remains a need for fluorescent probes with marked subtype selectivity for the A₁AR.

In the present study, we report the design, synthesis, and pharmacological evaluation of a novel series of subtype-selective fluorescent antagonists targeting the adenosine A₁AR receptor, which are amenable for use in a variety of fluorescence-based techniques. Two different positions of the prototypical xanthine scaffold were assessed for fluorophore/linker functionalization. To this end, the desired fluorescent antagonists were prepared by conjugating 8-bicyclo[2.2.2]-octylxanthine and 3-functionalized 8-(adamant-1-yl)xanthine scaffolds with a series of commercially available far-red fluorophores. We envisage that these novel probes will be valuable pharmacological tools for the wider scientific

community to further the understanding of the role of the A₁AR in health and disease.

RESULTS AND DISCUSSION

Fluorescent Ligand Design. The availability of crystal structures for the hA₁AR^{55,56} allowed us to rationalize the reported structure–activity relationships (SARs) relative to xanthine-based A₁AR antagonists,^{7,11,57,58} thereby helping guide our design strategy. We sought to explore two different positions of the prototypical xanthine scaffold, namely, the 3- and 8-positions, for linker/fluorophore attachment as structural data suggested that functionalization of either of these positions could be harnessed for the development of chemical probes (Figure 2). Tonapofylline (BG9928)^{15,59} and its synthetic precursor, compound 16 (from Kiesman et al.)⁵⁹ with a carboxylate handle directly attached to the

Scheme 1. Synthesis of the 8-Bicyclo[2.2.2]octylxanthine-Based Congeners^{4a}

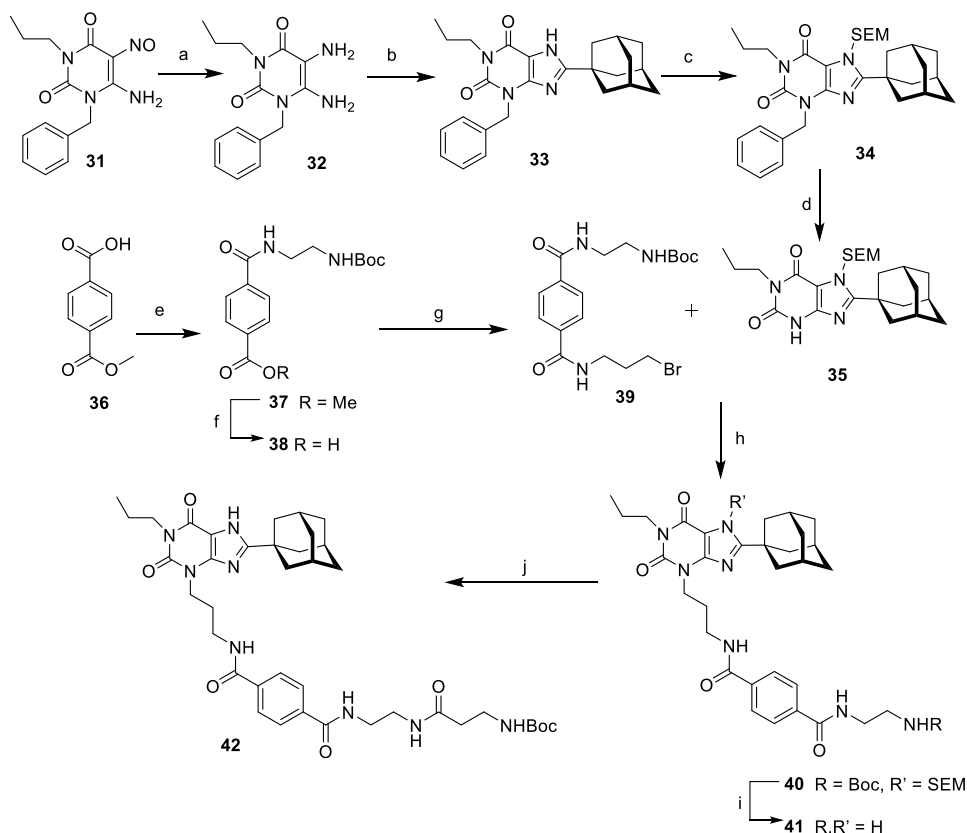
^{4a}Reagents and conditions: (a) *N*-Boc-ethylenediamine, COMU, DIPEA, DMF, rt, 1 h, 58%; (b) 4 N HCl in dioxane, rt, 30 min, quantitative; (c) *N*-Boc-8-amino-3,6-dioxoheptanoic acid or *N*-Boc-5-amino-3-oxapentanoic acid or *N*-Boc- β -alanine, COMU, DIPEA, rt, 1 h, 28–67%; (d) *N*-Boc- β -alanine, COMU, DIPEA, rt, 1 h; (e) *N*¹-Boc-ethylenediamine or *N*-Boc-1,3-propanediamine, BOP, DIPEA, DMF, rt, 1 h, 78–86%; (f) β -alanine methyl ester, BOP, DIPEA, DMF, rt, 56%; (g) LiOH·H₂O, MeOH/H₂O 1:1, rt, 40 min, 84%; (h) *N*-Boc-5-amino-3-oxopentanoic acid, COMU, DIPEA, rt, 1 h.

bicyclo[2.2.2]octane group (Figure 2B,C), were selected as parent molecules for the development of 8-position-functionalized xanthine-based fluorescent ligands. These two molecules exhibit high binding affinities for the hA₁AR ($K_i = 7.4$ nM and $K_i = 33$ nM for tonapofylline and compound **16**, respectively) and good selectivity profiles with respect to binding other adenosine receptor subtypes (hA_{2A}AR $K_i = 6410$ nM, hA_{2B}AR $K_i = 90$ nM, hA₃AR $K_i > 10,000$ nM for tonapofylline, and hA_{2A}AR $K_i = 1070$ nM, hA_{2B}AR (48%)^b, hA₃AR (100%)^b (b: % of specific radioligand binding) for compound **16**).⁵⁹ Additionally, the presence of a carboxylate group in both molecules represented an attractive functional handle for subsequent attachment of a linker and fluorophore.

Molecular docking studies of tonapofylline and compound **16** to the 3.2 Å resolution crystal structure (PDB: SUEN)⁵⁵ of the hA₁AR revealed that both ligands exhibited comparable binding modes, with subtle differences in orientation of the 1- and 3-propyl groups for each ligand (Figure 2B–D). The pattern of key interactions established with the orthosteric site of the receptor was in keeping with those observed for the A₁AR crystal structure co-bound with xanthine-based analogues, including hydrogen-bonding interactions with N254^{6,55} and π -stacking interaction with F171^{ECL2} (ECL2 in superscripts refer to the Ballesteros–Weinstein numbering system).^{61,55,56} For both molecules, the carboxylate group was oriented toward the extracellular face of the A₁AR without making direct interactions with neighboring residues. Structure–activity relationships (SAR) reported by Kiesman et al.,⁵⁹ suggested that receptor affinity was maintained when the carboxylate group was functionalized with amide linkers, thereby further supporting our docking results. Consequently, we set out to probe the area beyond the carboxylate group using linkers of different lengths and chemical compositions with the aim to find the optimal congener template upon which to append a series of commercially available fluorophores.

In addition, we generated a second library of probes featuring 3-functionalized xanthine-based fluorescent ligands. This second library displayed linkers with reduced length compared to the first library as structural data, complemented with docking studies, suggested that shorter linkers would provide sufficient spatial separation between the pharmacophore and fluorophore (Figure 2D). It was also of interest to explore probes lacking the linker in which the fluorophores were directly conjugated to the orthosteric binding moiety as previous studies from our laboratories suggested that such modification was advantageous for the development of A₁AR fluorescent probes.⁶²

The novel series of fluorescent ligands reported here included far-red emitting probes tethered with the 6-(((4,4-difluoro-5-(2-thien-yl)-4-bora-3a,4a-diaza-s-indacene-3-yl)-styryloxy)acetyl)aminohexanoic acid (BODIPY630/650-X) dye and the water-soluble sulfonated cyanine5 (Sulfo-Cy5) dye. Far-red emitting fluorophores were preferred as these fluorophores emit at wavelengths of 650–670 nm, where the degree of overlap with background autofluorescence from living cells is minimized.⁶³ Previous studies have demonstrated that conjugation of the xanthine amine congener (XAC) with green-emitting fluorophores, such as 4,4-difluoro-5,7-dimethyl-4-bora-3a,4a-diaza-s-indacene-3-propionic acid (BODIPY-FL) dye, generated probes with markedly reduced affinity for the hA₁AR and disadvantageous imaging properties due to significant membrane penetration.⁶⁴ For these reasons, BODIPY-FL fluorophores were not included in the present study. BODIPY 630/650 fluorophores are amongst the preferred candidates for fluorescence derivatization due to their advantageous spectral properties, including high fluorescence quantum yield (ϕ) and photochemical stability.^{65,66} Moreover, BODIPY 630/650 fluorophores are brighter when located in lipid environments, such as the plasma membrane, which is particularly advantageous when visualizing specific cell surface fluorescence in imaging studies.^{45,64,67} The application of BODIPY dyes, however, may be limited by their

Scheme 2. Synthesis of the 1-Propyl-3-(3-benzamidopropyl)-8-(3-adamantyl) Xanthine-Based Congeners^a

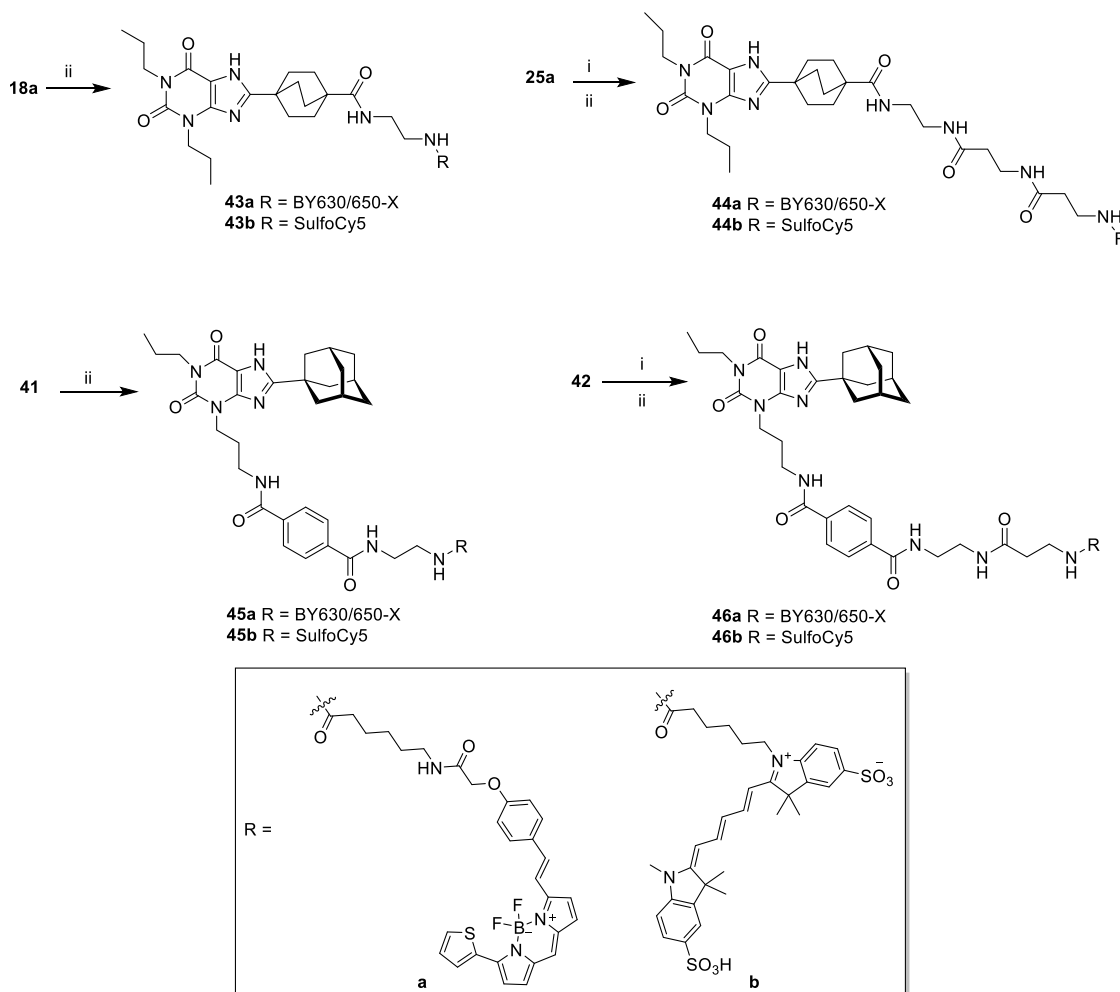
^aReagents and conditions: (a) $\text{Na}_2\text{S}_2\text{O}_4$, 30% NH_4OH in H_2O , 85 °C, 92%; (b) (i) 1-adamantane carboxylic acid, COMU, DIPEA, DMF, rt., 15 min, 87% (ii) 1 M KOH/n -propanol 1:1, reflux, 1 h, 95%; (c) SEM-Cl, K_2CO_3 , DMF, 4 h, 66%; (d) $\text{NH}_4^+\text{HCO}_3^-$, Pd/C, MeOH, 140 °C, 9 h, 67%; (e) *N*¹-Boc ethylenediamine, COMU, DIPEA, DMF, rt., 20 min, 75%; (f) 1 M NaOH, THF, rt., 3 h, 90%; (g) 3-bromopropylamine hydrobromide, COMU, DIPEA, DMF, rt., 15 min, 61%; (h) **35** and **39**, K_2CO_3 , DMF, 25–40 °C, 24 h, 49%; (i) 4 M HCl in dioxane, rt., 30 min, quantitative, then DIPEA; (j) Boc- β -Ala-OH, COMU, DIPEA, DMF, rt., 15 min, 47%.

intrinsic lipophilicity, which could lead to increased levels of nonspecific binding⁶⁸ and reduced stability in plasma. This would thereby limit their utility in more physiologically relevant models such as in vivo models.³⁰ Fluorescent dyes with improved water solubility, such as sulfonated cyanine5 dyes, may overcome these limitations as demonstrated by the Cy5-labeled quinazoline-based probe developed by Ma et al., for the α_1 -adrenoreceptor.⁶⁹ In addition, to the best of our knowledge, there are no reported examples of fluorescent hA_1AR antagonists integrating a Sulfo-Cy5 fluorophore that have been successfully utilized in studies of the hA_1AR in living cells.

Chemistry: Synthesis of the 8-Bicyclo[2.2.2]-octylxanthine-Based Congeners. The chemical synthesis of the 8-bicyclo[2.2.2]octylxanthine-based amino-functionalized congeners is outlined in Scheme 1. Tonapofylline (BG9928) and **16** provided the framework for the development of the series of fluorescent ligands featuring linkers and fluorophores extending from the 8-position of the xanthine scaffold. Tonapofylline (BG9928) and **16** were synthesized as described in Keisman et al.⁵⁹ (detailed procedures are reported in the Supporting Information) and further functionalized with a series of linker variants of different lengths and chemical compositions to afford 10 final *N*-Boc-protected amino-functionalized congeners. Briefly, Tonapofylline (BG9928) was activated with (1-cyano-2-ethoxy-2-oxoethylideneaminoxy)dimethylamino-morpholino-carbenium

hexafluorophosphate (COMU) in the presence of DIPEA and subsequently coupled with *N*-Boc-ethylenediamine in DMF to afford the corresponding monoprotected amine intermediate (**10**). The acidolytic removal of the Boc-protecting group afforded the corresponding amine (**11**) as its HCl salt, which was subsequently functionalized in the presence of DIPEA and COMU with three linker variants of different lengths and chemical compositions: Boc-8-amino-3,6-dioxaoctanoic acid, Boc-5-amino-3-oxapentanoic acid, and Boc- β -alanine to afford **12**, **13**, and **14**, respectively (Scheme 2).

Compound **16** was coupled with either *N*-Boc-ethylenediamine or *N*-Boc-1,3-propanediamine to afford the corresponding monoprotected intermediates **17a** and **17b**, respectively. Following acidolysis, *N*-Boc deprotection gave the corresponding primary amines (**18a** and **18b**) as their HCl salts. COMU-mediated amide coupling of **18a** and **18b** with the *N*-protected linkers Boc-8-amino-3,6-dioxaoctanoic acid, Boc-5-amino-3-oxapentanoic acid, or Boc- β -alanine afforded the Boc-protected congeners **19–24**. An additional chain-extended congener was also synthesized to investigate the effect of this longer linker variant in modulating A_1AR binding affinity. To this end, **16** was activated with (benzotriazol-1-yloxy)tris(dimethylamino)phosphonium hexafluorophosphate (BOP) and coupled with β -alanine methyl ester to afford **26**. Saponification of the latter and subsequent amide coupling with *N*-Boc-ethylenediamine yielded the corresponding Boc-protected intermediate (**28**). Treatment of **28** with 4 M HCl in

Scheme 3. Synthesis of the Fluorescent A₁AR Antagonists^a

^aReagents and conditions: (i) 4 M HCl in dioxane, rt., 30 min, quantitative; (ii) BY630/650-X-NHS or Sulfo-Cy5-NHS, DIPEA, DMF, rt., exclusion of light, 39–100%.

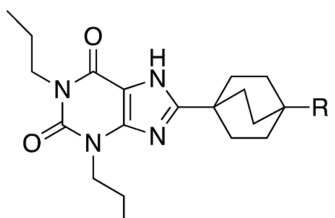
dioxane afforded the corresponding amine (**29**) as its HCl salt, which was coupled with Boc-5-amino-3-oxapentanoic acid to afford the desired protected congener **30**.

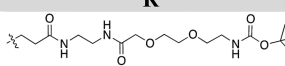
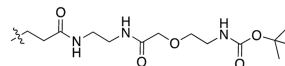
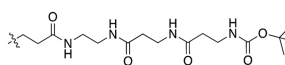
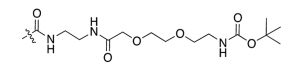
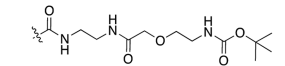
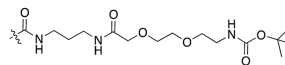
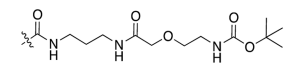
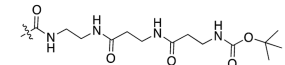
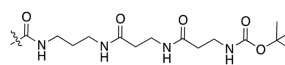
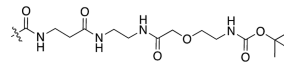
Syntheses of the 1-Propyl-3-(3-benzamidopropyl)-8-(3-adamantyl) Xanthine-Based Congeners. The synthetic approach for the preparation of 3-functionalized analogues is outlined in Scheme 2 and was adapted from procedures reported by Beaglehole et al.⁶⁰ 6-Amino-1-benzyl-5-nitroso-3-propylpyrimidine-2,4(1*H*,3*H*)-dione (**31**) was previously prepared in our laboratory following reported literature procedures.^{70–72} Reduction of the nitroso group of **31** with sodium dithionite afforded the corresponding 5,6-diamino uracil product (**32**), which was subsequently acylated with 1-adamantane carboxylic acid in the presence of COMU⁷³ to afford the corresponding 6-amino-5-carboxamido uracil precursor. The latter then underwent cyclization in the presence of 1 M KOH to the corresponding 8-adamantyl-substituted xanthine (**33**) in excellent yield (95%). To ultimately allow a selective alkylation of the unsubstituted 3-position of the xanthine ring following its debenzoylation, a 2-(trimethylsilyl)ethoxymethyl (SEM) protecting group was introduced at the 7-position to afford the corresponding 7-*N*-SEM-protected intermediate (**34**) in good yield (66%). Subsequent debenzoylation was achieved under transfer hydro-

genation conditions using ammonium formate in the presence of 10% palladium on carbon (Pd/C) in methanol at high temperature,⁷⁴ affording the corresponding deprotected xanthine **35** in good yield (67%). The aryl amide linker variant was prepared starting from commercially available monomethyl terephthalate (**31**), which was coupled with *N*-Boc ethylenediamine by means of COMU, in the presence of DIPEA in DMF, affording intermediate **37**. The latter was then treated with 1 M NaOH to generate the corresponding carboxylic acid (**38**), which was subsequently coupled with 3-bromopropylamine hydrobromide in the presence of DIPEA, affording intermediate **39** with good yield (61%). Alkylation of the xanthine derivative **35** with **39** under basic conditions yielded the corresponding 3-*N*-propyl-3-benzamide intermediate (**40**) in reasonable yield (49%). Concomitant SEM and Boc removal was effected by reacting **40** with 4 M HCl in dioxane for 1 h, followed by treatment of the resulting HCl salt with DIPEA to liberate the corresponding amine (**41**), which was coupled with Boc- β -Ala-OH using COMU in DMF to yield the final Boc-protected congener (**42**).

Synthesis of Fluorescent A₁AR Antagonists. The 8-bicyclo[2.2.2]octylxanthine-based congeners **18a** and **25a** and the 8-adamantyl-3-propyl-3-benzamide-substituted congeners **41** and **42** were subsequently conjugated with a series of

Table 1. Binding Affinities of the Novel 8-Bicyclo[2.2.2]octylxanthine-Based Amino-Functionalized Congeners



Cmpd	R	p <i>K</i> _i (Log M) ± SEM ^a
12		7.88 ± 0.06
13		7.83 ± 0.10
15		8.11 ± 0.09**
19		7.76 ± 0.06
20		7.86 ± 0.05
22		7.65 ± 0.05
23		7.79 ± 0.09
25a		8.36 ± 0.08**
25b		7.89 ± 0.05**
30		7.95 ± 0.04

^ap*K*_i ± SEM values were calculated from the negative logarithm of the equilibrium inhibitory constant (*K*_i in nM) determined at 4 °C using [³H] DPCPX competition binding experiments in FlpIn-CHO cells stably expressing the hA₁AR. Values represent the mean ± SEM from *n* = 3 experiments performed in duplicate. ** *P* < 0.01, compared to congeners lacking the dipeptide linker one-way ANOVA with Tukey's multiple comparison test.

commercially available far-red emitting fluorophores (Scheme 3), namely, BODIPY630/650-X (BY630/650-X) and sulfonated cyanine5 (Sulfo-Cy5) dyes, thereby yielding a focused library of eight fluorescent analogues (43a and 43b to 46a and 46b). The novel synthesized fluorescent probes were purified by reverse-phase high-performance liquid chromatography (RP-HPLC), and the high purity of the final probes was confirmed by analytical RP-HPLC with dual-wavelength detection and measured as ≥96% homogeneity. Furthermore, chemical identity of the final probes was confirmed by high-resolution mass spectroscopy (HRMS) (TOF ES+ and ES-).

Pharmacology. To assess which linker functionality could be harnessed for the development of the first library of fluorescent probes, the 10 newly synthesized Boc-protected 8-bicyclo[2.2.2]octylxanthine congeners 12, 13, 15, 19, 20, 22, 23, 25a, 25b, and 30 (Scheme 1) were characterized using [³H] DPCPX binding in FlpIn-CHO cells stably expressing the hA₁AR (A₁AR-FlpInCHO cells). All congeners were able to

bind the hA₁AR with good affinity (7.65–8.36 p*K*_i range, Table 1), demonstrating that all linker combinations were well tolerated. Comparison of the reported binding affinities⁵⁹ of tonapofylline (BG9928) and 16 with our newly synthesized congeners corroborated the original observation that functionalization of the carboxylate handle of either tonapofylline or 16 could be exploited for linker conjugation. Despite the similar affinity of these ligands, subtle differences in SARs were observed. There was a general trend for congeners integrating the β-Ala-β-Ala linker moiety to display higher hA₁AR affinities relative to congeners lacking the dipeptide linker (15, 25a, and 25b; Table 1. ** *P* < 0.01 one-way ANOVA with the Tukey's multiple comparison test). Likewise, congeners with an ethylenediamine spacer seemed to be better tolerated than those with a propane-1,3-diamine. Based on these initial results, compound 25a (Table 1 and Scheme 1) was therefore selected as our model-functionalized congener for the development of the 8-bicyclo[2.2.2]octylxanthine-based fluo-

rescent ligands. Given the greater A₁AR affinity observed with congeners conjugated with β -alanine, we also used the β -alanine linker for the development of the 1-propyl-3-(3-benzamidopropyl)-8-(3-noradamantyl)xanthine-based fluorescent ligands. Furthermore, structural data suggested that a single β -alanine linker, coupled with an ethylenediamine spacer, should provide the optimal linker length for conjugating the 1-propyl-3-(3-benzamidopropyl)-8-(3-noradamantyl) xanthine-based scaffold with the desired fluorophore.

The novel-synthesized 8-bicyclo[2.2.2]octylxanthine- and 1-propyl-3-(3-benzamidopropyl)-8-(3-noradamantyl) xanthine-based fluorescent ligands (Scheme 3) were characterized in a variety of pharmacological assays. First, the fluorescent ligand binding was quantified using [³H] DPCPX competition binding in A₁AR-FlpInCHO cells (Figure 3 and Table 2).

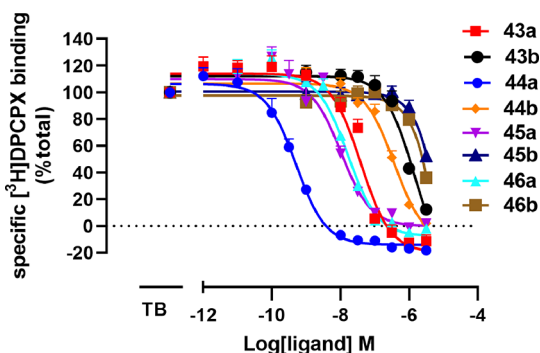


Figure 3. Inhibition of [³H] DPCPX specific binding (1 nM) in the presence of increasing concentrations of fluorescent antagonist (43a and 43b to 46a and 46b) at 37 °C in hA₁AR-FlpInCHO cells. TB stands for total radioligand binding. Each data point represents the combined mean \pm SEM from $n = 5$ experiments performed in triplicate.

There was a broad variability of the binding affinities measured across the novel fluorescent ligands synthesized (Table 2). These results are consistent with previous studies, which demonstrated a significant contribution of the fluorophore in modulating the pharmacology of the final conjugates.^{39,41,64} Indeed, there was a statistical difference for the BY630/650-X-labeled compounds (43a–46a) to display the highest affinities of the series compared to the corresponding Sulfo-Cy5-labeled analogues (43b–46b) (Table 2). Overall, conjugation with the Sulfo-Cy5 probe was detrimental with regard to binding to the hA₁AR. Fluorescent analogue 44a displayed the highest affinity of the series at the hA₁AR ($pK_i = 9.54 \pm 0.05$). The addition of the BY630/650-X fluorophore resulted in a circa 16-fold increase of hA₁AR affinity compared to the Boc-protected congener 25a. Replacement of the BY630/650-X fluorophore with Sulfo-Cy5 yielded fluorescent antagonist 44b ($pK_i = 6.70 \pm 0.06$), which resulted in a significant reduction in hA₁AR binding affinity (690-fold) compared to the BY630/650-X-labeled analogue. The fluorophore moiety alone, however, was not the only driver of hA₁AR affinity as demonstrated by compounds 43a and 43b, which had lower affinity compared to 44a and 44b. These two fluorescent analogues lacked the dipeptide β -Ala- β -Ala linker and were synthesized to explore the effect of moving the fluorophore closer to the 8-bicyclo[2.2.2]-octylxanthine scaffold. Despite the reasonable hA₁AR affinity displayed by compounds 43a and 43b, the removal of the dipeptide β -Ala- β -Ala linker proved to be disadvantageous.

Table 2. Binding Affinities of the Novel 8-Bicyclo[2.2.2]octylxanthine-Based (43a, 43b, 44a, and 44b) and 1-Propyl-3-(3-benzamidopropyl)-8-(3-noradamantyl) Xanthine-Based (45a, 45b, 46a, and 46b) Fluorescent Antagonists

cmpd	linker	fluorophore	pK_i (Log M) \pm SEM ^a
SLV320			8.77 ± 0.05
43a		BY630/650-X	7.69 ± 0.06 ####
43b		Sulfo-Cy5	6.07 ± 0.09
44a	β -Ala- β -Ala	BY630/650-X	9.54 ± 0.05 ****
44b	β -Ala- β -Ala	Sulfo-Cy5	6.70 ± 0.06
45a		BY630/650-X	8.23 ± 0.07
45b		Sulfo-Cy5	<5
46a	β -Ala	BY630/650-X	8.01 ± 0.03
46b	β -Ala	Sulfo-Cy5	<5

^a pK_i values were calculated from the negative logarithm of the equilibrium inhibitory constant (K_i in nM) measured at 37 °C by radioligand competition binding employing [³H] DPCPX as the radiotracer in FlpIn-CHO cells stably expressing the hA₁AR. Values represent the mean \pm SEM from $n = 5$ experiments performed in triplicate (statistical significance was defined as **** $p < 0.0001$ one-way ANOVA with the Tukey's multiple comparison test comparing the pK_i of 44a vs 44b. ##### $p < 0.0001$ one-way ANOVA with the Tukey's multiple comparison test comparing the pK_i of 44a vs 43a).

This suggests that there may be a synergistic effect of both linker and fluorophore in influencing the binding affinity of the final fluorescent conjugates. The introduction of the Sulfo-Cy5 fluorophore to the 1-propyl-3-(3-benzamidopropyl)-8-(3-noradamantyl) xanthine scaffold (probes 45b and 46b) effectively abolished hA₁AR affinity ($pK_i < 5$). In contrast, conjugation with BY630/650-X fluorophore yielded fluorescent analogues 45a and 46a with good hA₁AR affinity ($pK_i = 8.23 \pm 0.07$ and $pK_i = 8.01 \pm 0.03$, respectively). These results supported our original hypothesis, whereby fluorophore derivatization could be achieved at both the 8- and 3-positions of the prototypical xanthine scaffold.

The SAR of these novel fluorescent ligands could be rationalized in the context of A₁AR structural information. For example, crystal structures for the hA₁AR^{55,56,75} revealed the presence of a secondary hydrophobic pocket defined by residues F171^{ECL2}, E170^{ECL2}, V83^{3.28}, I69^{2.64}, and L65^{2.60}. Molecular dynamics simulation (MD) studies suggest that this pocket provides an important recognition mechanism for ligand binding, with A₁AR ligand affinity and selectivity being influenced by their ability to engage with this accessory hydrophobic site.^{76,77} The importance of hydrophobic pockets in influencing ligand binding has been suggested for various GPCRs, including the A_{2A}AR and the C–C chemokine receptor type 5 (CCRS).^{78,79} Accordingly, the lipophilic nature of the BODIPY probes may enable the boron dipyrromethene scaffold to establish favorable interactions with this accessory hydrophobic site with concomitant displacement of weakly associated water molecules from this pocket, thereby further

Table 3. Binding Affinities of Fluorescent 8-Bicyclo[2.2.2]octylxanthine-Based Conjugates **44a** and **44b** and Fluorescent 1-Propyl-3-(3-benzamidopropyl)-8-(3-noradamantyl) Xanthine-Based Conjugate **46a** at NanoLuc-hA₁AR, NanoLuc-hA_{2A}AR, NanoLuc-hA_{2B}AR, and NanoLuc-hA₃AR

cmpd	binding	NLuc-hA ₁ AR	NLuc-hA _{2A} AR	NLuc-hA _{2B} AR	NLuc-hA ₃ AR
44a	pK_D (Log M) ^a	8.93 ± 0.02	7.55 ± 0.09	8.11 ± 0.08	6.87 ± 0.04
	B_{max}	0.018 ± 0.002	0.035 ± 0.001	0.016 ± 0.003	0.012 ± 0.001
46a	pK_D (Log M)	8.50 ± 0.07	7.30 ± 0.15	7.26 ± 0.08	7.23 ± 0.09
	B_{max}	0.019 ± 0.0005	0.003 ± 0.0003****	0.004 ± 0.0004****	0.001 ± 0.00007****
44b	pK_D (Log M)	7.35 ± 0.09	<6	<6	<6
	B_{max}	0.030 ± 0.006	N.D. ^b	N.D. ^b	N.D. ^b

^a pK_D values were calculated from the negative logarithm of the equilibrium dissociation constant (K_D) measured at 37 °C by NanoBRET saturation binding using increasing concentration of the fluorescent ligand in the absence or presence (to define nonspecific binding) of selective unlabeled AR antagonist (1 μ M SLV320 for NanoLuc-A₁AR, 1 μ M ZM241385 for NanoLuc-A_{2A}AR, 1 μ M PSB603 for NanoLuc-A_{2B}AR, and 1 μ M MRS1220 for NanoLuc-A₃AR). Data are represented as mean ± SEM of $n = 3$ experiments, where each experiment was performed in duplicate. ^bN.D. = not determined. **** $P < 0.0001$, compared to NanoLucA₁ B_{max} one-way ANOVA with the Tukey's multiple comparison test.

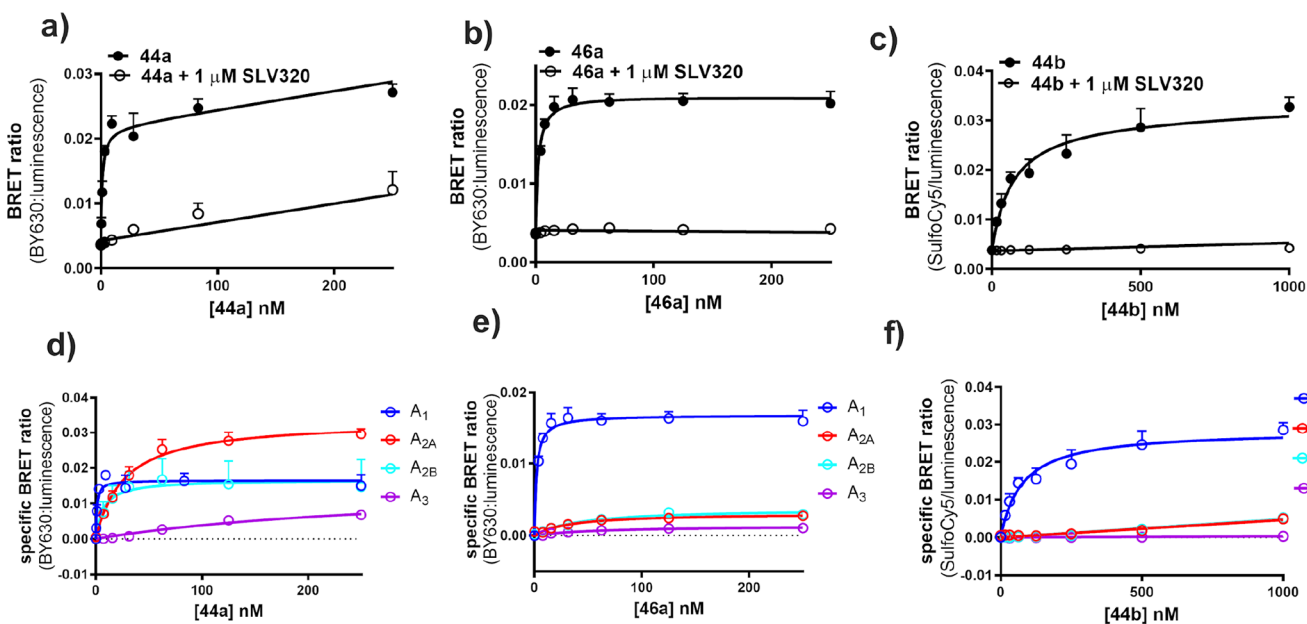


Figure 4. NanoBRET saturation ligand binding curves (a)–(c) measured in HEK293A cells transiently expressing the NanoLuc-hA₁AR for (a) **44a**, (b) **46a**, and (c) **44b** in the presence (open circles) and absence (closed circles) of 1 μ M SLV320. Graphs (d)–(f) depict the selectivity profiles of the probes tested against each subtype of adenosine receptors. Specific binding (d)–(f) of (d) **44a**, (e) **46a**, and (f) **44b** at each subtype of adenosine receptor was measured from saturation binding curves (a)–(c) after subtraction of the nonspecific binding component from the total binding. Nonspecific binding was determined in the presence of 1 μ M of ZM241385 for NanoLuc-hA_{2A}AR, 1 μ M PSB603 for NanoLuc-hA_{2B}AR, and 1 μ M MRS1220 for NanoLuc-hA₃AR. Data points represent the combined mean ± SEM from $n = 3$ experiments performed in duplicate.

enhancing the overall free energy of binding for the probe bound to the A₁AR. In contrast, molecular interactions of this type could not be established with the corresponding water-soluble Sulfo-Cy5 analogues as, due to their hydrophilic nature, the interaction with the solvent could be more favorable.

One of the principal objectives of this study was to develop subtype-selective probes that can selectively bind A₁ARs in cells where other adenosine receptors are co-expressed. To this end, the selectivity profile of the newly synthesized probes was quantified using a bioluminescent resonance energy transfer (BRET)^{29,80,81} ligand binding assay, a proximity assay (<10 nm), which relies upon the energy transfer between a donor bioluminescent protein (NanoLuc)⁸² tagged on the N-terminus of the receptor of interest (NanoLuc-hA₁AR), and an acceptor fluorophore. The binding affinity of the most promising fluorescent ligands of both BODIPY- and Sulfo-Cy5-bearing probes (**44a**, **44b**, and **46a**; Scheme 3), selected based on [³H]DPCPX binding results (Table 2), was

quantified at each adenosine receptor subtype using NanoBRET saturation ligand binding assay in HEK293A cells transiently expressing either the NanoLuc-A₁AR, NanoLuc-A_{2A}AR, NanoLuc-A_{2B}AR, or the NanoLuc-A₃AR. A robust, specific, and saturable BRET signal was detected at the NanoLuc-A₁AR for each fluorescent analogue investigated (**44a**, **44b**, and **46a**), with low levels of nonspecific binding for all concentrations tested. Fluorescent analogue **44b** showed reasonable NanoLuc-hA₁AR affinity ($pK_D = 7.35 \pm 0.09$, $n = 3$) and the most promising selectivity profile among the fluorescent probes tested in the NanoBRET assay (Table 3 and Figure 4f). Indeed, minimal BRET signal was detected at either NanoLuc-hA_{2A}AR, NanoLuc-hA_{2B}AR, or NanoLuc-hA₃AR at 500 nM–1 μ M **44b** (Figure 4f). A concentration-dependent BRET signal was observed for fluorescent analogues **44a** and **46a** at the NanoLuc-hA_{2A}AR, NanoLuc-hA_{2B}AR, and NanoLuc-hA₃AR (Figure 4e), allowing estimation of their equilibrium dissociation constant (K_D) (Table 3). **44a**

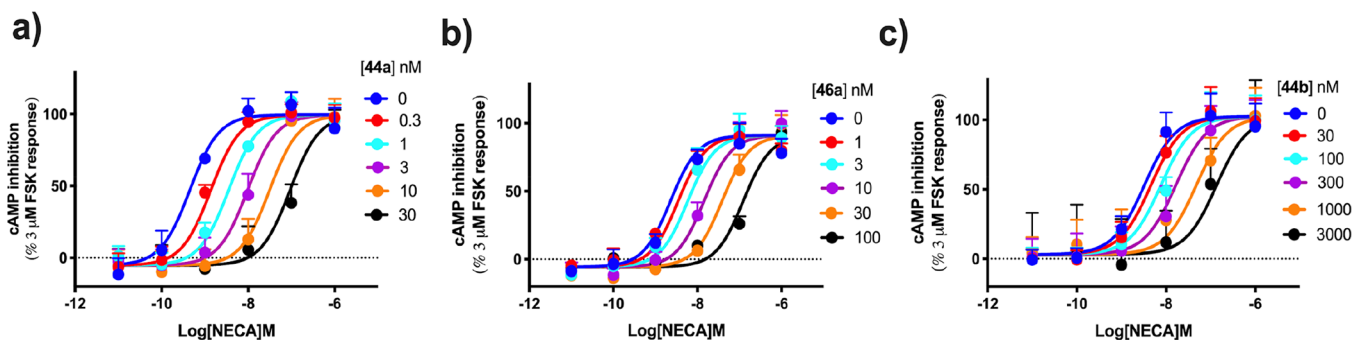


Figure 5. Effects of antagonists **44a** (a), **46a** (b), and **44b** (c) on the NECA-mediated inhibition of forskolin-stimulated cAMP accumulation. hA₁AR-FlpInCHO cells were stimulated with increasing concentrations of NECA in the absence and presence of increasing concentrations of the fluorescent antagonist. Data have been presented as percentage of cAMP accumulation in response to 3 μ M forskolin (0%) or buffer (100%) alone. Each data point represents the combined mean \pm SEM from n separate experiments ($n = 3$ for **44a**, $n = 3$ for **46a**, and $n = 4$ for **44b**) performed in duplicate.

exhibited high affinity for the NanoLuc-hA₁AR ($pK_D = 8.93 \pm 0.02$, $n = 3$), which was 25-fold, 7-fold, and 117-fold greater than its affinity for the NanoLuc-hA_{2A}AR, NanoLuc-hA_{2B}AR, and NanoLuc-hA₃AR, respectively. Fluorescent analogue **46a** also displayed high affinity at the NanoLuc-hA₁AR ($pK_D = 8.50 \pm 0.07$, $n = 3$), while the affinities measured at the other adenosine receptor subtypes were appreciably lower, displaying approximately 20-fold greater affinity for the NanoLuc-hA₁AR compared to the NanoLuc-hA_{2A}AR, NanoLuc-hA_{2B}AR, and NanoLuc-hA₃AR.

The maximal binding capacity (B_{max}) value of probe **46a** was significantly higher at the NanoLuc-hA₁AR compared to binding to either of the NanoLuc-hA_{2A}AR, NanoLuc-hA_{2B}AR, and NanoLuc-hA₃AR receptor subtypes (maximum BRET ratios of 0.003, 0.004, and 0.001, respectively) (Table 3). They were also substantially different to the B_{max} values obtained at the NanoLuc-hA_{2A}AR, NanoLuc-hA_{2B}AR, and NanoLuc-hA₃AR receptor subtypes with **44a** (0.035, 0.016, and 0.012, respectively). These findings are unlikely to reflect a lack of receptor expression for A_{2A}AR, A_{2B}AR, and A₃AR when assessing **46a**, as these assays were performed in parallel with **44a**, which exhibited robust expression for all adenosine receptor subtypes. We therefore hypothesized that the BRET signal resulting from probe **46a** binding to the NanoLuc-hA_{2A}AR, NanoLuc-hA_{2B}AR, and NanoLuc-hA₃AR could be a result of the so-called “bystander” BRET,^{83–85} that is, non-specific enrichment of probe **46a** at the plasma membrane of cells expressing hA_{2A}AR, hA_{2B}AR, or hA₃AR receptors could produce a measurable BRET signal owing to the close proximity between the probe and bioluminescent protein NanoLuc. Alternatively, HEK293 cells are known to express hA₁AR at very low levels^{86,87} and it is therefore possible that the low BRET signal detected with **46a** at the NanoLuc-hA_{2A}AR and NanoLuc-hA_{2B}AR is a result of close proximity between the endogenous hA₁AR and NanoLuc-hA_{2A}AR or NanoLuc-hA_{2B}AR receptors (such as might occur in oligomeric complexes).

To further assess its subtype selectivity, probe **46a** was therefore evaluated for its ability to antagonize NECA-mediated cAMP accumulation in FlpIn-CHO cells expressing either of hA_{2A}AR, hA_{2B}AR, or hA₃AR. If the affinity of **46a** for the other AR subtypes measured in the NanoBRET saturation assay was “true affinity”, one would expect to measure comparable affinity values in this functional assay. At the hA_{2A}AR and hA_{2B}AR, **46a** caused a small but significant

rightward shift of the NECA concentration response curve only at the highest concentration tested (1 μ M) (Figure S9), with no detectable effect at the hA₃AR. Therefore, the estimated affinity of **46a** for each of the adenosine receptor subtypes, quantified using the Gaddum equation as previously described, was relatively low (pK_D hA_{2A}AR = 6.11 ± 0.08 , pK_D hA_{2B}AR = 6.16 ± 0.07 , pK_D hA₃AR < 6, $n = 3$)^{41,88} compared to that observed from the NanoBRET assay (Figure 4 and Table 3). Therefore, the small BRET signal detected with **46a** in HEK293 cells expressing NanoLuc-hA_{2A}AR and NanoLuc-hA_{2B}AR may reflect BRET between **46a** bound to endogenous hA₁ARs and the transfected NanoLuc-tagged A₂AR receptors as a result of oligomerization. The lower binding affinity obtained for **46a** in cells expressing NanoLuc-hA_{2A}AR and NanoLuc-hA_{2B}AR, compared to NanoLuc-hA₁AR, would be consistent with negative allosterism across oligomeric receptor interfaces.⁸⁹

The ability of probes **44a**, **46a**, and **44b** (Scheme 3) to retain functional antagonism at the hA₁AR was also investigated. This was performed in FlpIn-CHO cells stably expressing the hA₁AR. All three fluorescent probes proved to be competitive antagonists at the A₁AR, causing a parallel rightward shift of the NECA response curve in a concentration-dependent manner (Figure 5). From this data, we performed Schild regression analysis and the pK_B value for each of the compounds tested was calculated (Table 4). All three fluorescent ligands **44a**, **46a**, and **44b** retained a functional antagonism activities at the hA₁AR comparable to the parent Tonapofylline⁵⁹ and DU172.⁵⁵ Moreover, the functional affinity values (pK_B) measured for each of the fluorescent ligands were in agreement with the binding

Table 4. pK_B Values of Fluorescent Analogues **44a**, **46a**, and **44b**

cmpd	hA ₁ AR pK_B ^a	n
44a (BY630/650)	9.75 ± 0.11	3
46a (BY630/650)	8.72 ± 0.02	3
44b (Sulfo-Cy5)	7.12 ± 0.12	4

^aAffinities of the fluorescently-labeled antagonists **44a**, **46a**, and **44b** measured from the antagonism of NECA-mediated inhibition of forskolin-stimulated cAMP accumulation in hA₁AR-FlpInCHO cells. Schild slopes were 1.14, 1.22, and 0.89 for **44a**, **46a**, and **44b**, respectively. Data represent mean value \pm SEM of n separate experiments, where each experiment was performed in duplicate.

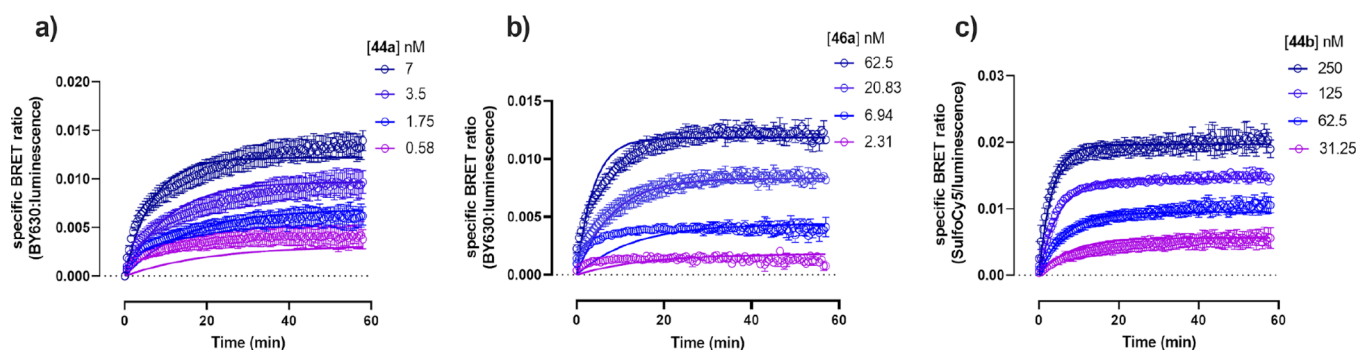


Figure 6. NanoBRET association binding kinetic curves of specific **44a** (a), **46a** (b), and **44b** (c) binding to NanoLuc-hA₁AR at 37 °C. HEK293A cells transiently expressing the NanoLuc-hA₁AR were treated with the indicated concentration of the fluorescent ligand, and the NanoBRET signal was monitored every 30 s for 1 h. Nonspecific binding was determined in the presence of 1 μM SLV320. Each data point represents the combined mean value ± SEM of *n* = 3 separate experiments performed in triplicate.

Table 5. Kinetic Parameters of Fluorescent Analogues 44a, 44b, and 46a Binding to the NanoLuc-hA₁AR^a

compd	k_{on} ($\times 10^6 \text{ M}^{-1} \text{ min}^{-1}$)	k_{off} (min^{-1})	RT ($1/k_{\text{off}}$) (min)	kinetic $\text{p}K_{\text{D}}$ (Log <i>M</i>)	saturation $\text{p}K_{\text{D}}$ (Log <i>M</i>)
44a	17.90 ± 3.69	0.054 ± 0.009	19.7 ± 3.7	8.51 ± 0.18	8.93 ± 0.02
44b	0.86 ± 0.13	0.117 ± 0.016	9.0 ± 1.0	$6.86 \pm 0.03^*$	7.35 ± 0.09
46a	3.60 ± 0.90	0.046 ± 0.008	23.8 ± 3.9	$7.88 \pm 0.04^*$	8.50 ± 0.07

^aThe kinetic parameters k_{on} , k_{off} , and $\text{p}K_{\text{D}}$ were calculated by monitoring the specific BRET signal of four concentrations of the fluorescent ligand every 30 s for 1 h at 37 °C. The residence time (RT) was calculated from the reciprocal of the k_{off} value, and the $\text{p}K_{\text{D}}$ was derived from the negative logarithm of the kinetic K_{D} . The values listed represent the mean ± SEM of *n* = 3 performed in triplicate. **p* < 0.05, kinetically derived $\text{p}K_{\text{D}}$ versus equilibrium saturation derived $\text{p}K_{\text{D}}$ value, Student's unpaired *t*-test.

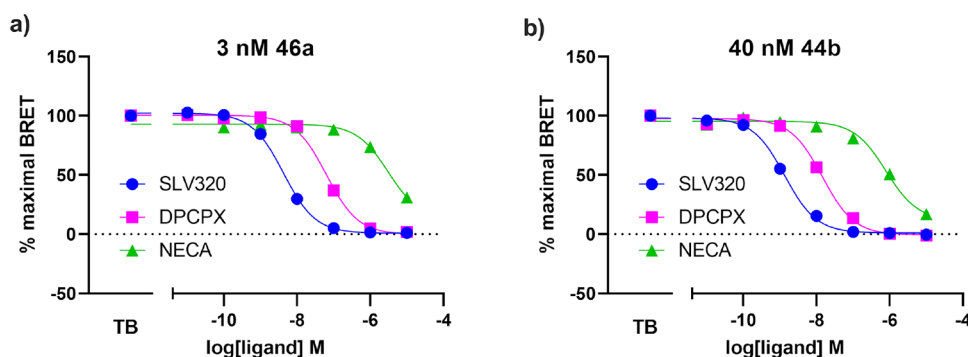


Figure 7. Displacement of 3 nM **46a** (a) and 40 nM **44b** (b) by unlabeled A₁AR antagonists SLV320 and DPCPX and agonist NECA in HEK293A cells transiently expressing the NanoLuc-hA₁AR. The reduction of BRET signal was monitored as a function of increasing concentration of the competing ligand. Data were normalized to maximal BRET signal in the absence of the unlabeled competing ligand (total binding, TB). Each data point represents the combined mean ± SEM from *n* = 3 experiments performed in duplicate.

affinities measured in the same cell line (hA₁AR-FipInCHO) by radioligand binding experiments.

The kinetics of ligand–receptor binding is emerging as a powerful pharmacological paradigm for predicting the efficacy of drug candidates *in vivo*.^{90,91} The availability of probes and techniques, which allow real-time monitoring of the rate at which a drug binds to its biological target (k_{on}) and dissociates from it (k_{off}), are therefore of great utility.^{32,92,93} It has been recently observed with the A₃AR that the kinetics of the labeled probe can influence the kinetic parameters of the unlabeled ligands under investigation, suggesting that a labeled probe should be chosen with regard to its adequate kinetic profile for the given study.⁴³ In this regard, the ligand binding kinetics of fluorescent analogues **44a**, **44b**, and **46a** were monitored by the NanoBRET ligand binding kinetic assay in HEK293A cells transiently expressing the NanoLuc-hA₁AR. The kinetic parameters of each fluorescent ligand were derived by measuring the observed association constant (k_{obs}) at four

concentrations of the fluorescent probe over a time frame of 1 h. The specific BRET signal for each fluorescent probe was calculated after subtraction of the nonspecific binding, defined using 1 μM of unlabeled antagonist SLV320, from the total binding component at each time point (Figure 6). The kinetic parameters k_{on} , k_{off} , and $\text{p}K_{\text{D}}$, along with the calculated residence time ($1/k_{\text{off}}$), were measured by globally fitting the resulting BRET data (Table 5).

The results obtained showed that all three fluorescent ligands displayed relatively fast kinetics. Additionally, for probe **44a**, the $\text{p}K_{\text{D}}$ values measured from the kinetic analyses were in agreement with that obtained from saturation ligand binding assays, while for **44b** and **46a**, the kinetic $\text{p}K_{\text{D}}$ values were significantly lower compared to the saturation $\text{p}K_{\text{D}}$. There were, however, large differences in the measured association rates (k_{on}) between the compounds. In particular, the BY630/650-X-labeled probe **44a** displayed k_{on} two orders of magnitude faster ($1.79 \pm 3.69 \times 10^7 \text{ M}^{-1} \text{ min}^{-1}$) than its

Sulfo-Cy5-labeled analogue **44b** ($8.6 \pm 0.13 \times 10^5 \text{ M}^{-1} \text{ min}^{-1}$). These two fluorescent analogues differ only by the attached fluorophore motif, demonstrating the potential of the fluorescent pharmacophore to establish different interactions with the receptor and nearby environment in a way that affects the observed binding kinetics. This would be consistent with observations described recently for the $A_3\text{AR}$.⁴³ Moreover, in an elegant study with the β_2 -adrenoreceptor, Sykes et al., showed that the lipophilic nature of some structural motifs in a molecule can influence the observed binding kinetics, dependent on direct interactions between these motifs and the plasma membrane.⁹⁴ This could therefore be the case for the BODIPY moiety in our fluorescent analogues.⁹⁵

After having thoroughly characterized the pharmacology of the synthesized fluorescent $A_1\text{AR}$ antagonists, we then investigated their utilities in a broad range of fluorescence-based techniques. For example, fluorescent analogues **44b** and **46a** were subsequently applied to monitor the ligand binding of unlabeled ligands to the $hA_1\text{AR}$. This was achieved through the NanoBRET competition ligand binding assay in HEK293A cells transiently expressing the NanoLuc- $hA_1\text{AR}$. Cells were incubated with the indicated concentration of fluorescent ligand and increasing concentrations of $hA_1\text{AR}$ antagonists SLV320, DPCPX, and the nonselective agonist NECA. A clear concentration dependent inhibition of the BRET signal was observed for all the compounds tested (Figure 7), allowing for the relative half-maximal inhibitory concentrations (IC_{50}) to be measured. These values were converted to the corresponding inhibitory constant (K_i) by means of the Cheng–Prusoff equation and are listed in Table 6.

Table 6. Binding Affinities of $A_1\text{AR}$ Ligands Measured by the NanoBRET Competition Ligand Binding Assay and Affinities Reported in Literature

compd	pK_i (Log M) \pm SEM ^d		pK_i (literature)
	44b (Sulfo-Cy5)	46a (BY630/650)	
SLV320	9.15 ± 0.07	8.85 ± 0.07	9 ^a
DPCPX	8.13 ± 0.05	7.68 ± 0.01	7.4–9.2 ^b
NECA	6.40 ± 0.10	5.96 ± 0.06	5.3–8.2 ^c

^aReported binding affinities.² Value determined in radioligand binding experiments in $hA_1\text{AR}$ -CHO-K1 cells using [³H] DPCPX.⁹⁶

^bValues determined in radioligand binding experiments in $A_1\text{AR}$ -COS-7⁹⁷ or $hA_1\text{AR}$ -CHO-K1 cell membranes^{57,98} or whole cells⁹⁹ using [³H] DPCPX. ^cValues determined in radioligand binding experiments in cells expressing the wild-type $hA_1\text{AR}$ using [³H] DPCPX^{57,100,101} or [³H]R-PIA.¹⁰² ^dMeasured pK_i in NanoBRET competition binding experiments in whole NanoLuc- $hA_1\text{AR}$ HEK293A cells using the fluorescent ligand indicated. Values are mean \pm SEM of $n = 3$ experiments performed in duplicate.

NanoBRET competition binding assays with fluorescent ligands **46a** and **44b** and the unlabeled competing $A_1\text{AR}$ ligands yielded pK_i values that were comparable to the reported literature values measured by radioligand binding assays ($R^2 = 0.95$ using **46a**, $R^2 = 0.94$ using **44b**; Figure S10a,b) and comparable to those measured in NanoBRET binding assays by Stoddart et al.²⁹ and Cooper et al.⁴⁴ Overall, the pK_i values measured using both fluorescent probes were also comparable ($R^2 = 0.99$ **44b** vs **46a**; Figure S10c).

To further expand the utility of the novel synthesized probes, we assessed whether fluorescent analogues **44a**, **46a**, and **44b** would allow visualization of the $hA_1\text{AR}$ expressed at

the plasma membrane of living cells. To be suitable for imaging studies, a fluorescent ligand must possess adequate properties, showing specific binding of the target protein at the cell surface coupled with both low levels of nonspecific membrane incorporation and diffusion into the cell cytosol. To this end, confocal microscopy studies of fluorescent probes **44a**, **46a**, and **44b** were carried out in HEK293A cells transiently transfected with the engineered SNAP-tagged human $A_1\text{AR}$.

The equatorial images acquired with the confocal microscope (Figure 8) revealed high levels of fluorescent labeling of the SNAP-tagged- $hA_1\text{AR}$ localized at the cell membrane for all the three red-shifted fluorescent probes tested. Moreover, pre-incubation of the cells with $10 \mu\text{M}$ unlabeled $A_1\text{AR}$ antagonist SLV320 prevented the binding of the fluorescent probes to the SNAP-tagged $hA_1\text{AR}$ causing a reduction of fluorescence. This demonstrated that the binding of the probes was specific at the SNAP-tagged- $hA_1\text{AR}$ localized at the cell membrane. Furthermore, when nontransfected (NT) HEK293 cells were treated with probes **44a**, **46a**, and **44b**, under the same experimental conditions as the SNAP-tagged- $hA_1\text{AR}$ HEK293 cells, no fluorescence signal was detected, further confirming the specificity of these fluorescent ligands for binding to the $hA_1\text{AR}$ and their low levels of nonspecific binding (Figure S11).

Finally, we investigated the suitability of the most $hA_1\text{AR}$ selective probes reported here for high resolution fluorescence microscopy. To this end, the Sulfo-Cy5-labeled ligand **44b** and BODIPY-630/650-X-labeled ligand **46a** were used in total internal reflection fluorescence microscopy (TIRF-M) to probe receptor distribution at the plasma membrane of living HEK293 cells transiently expressing the SNAP-tagged $hA_1\text{AR}$. TIRF-M is a wide-field imaging method that allows for the visualization of molecule localization and organization on the surface of living cells with high spatial and temporal resolution.^{103–105} Imaging living cells with probe **44b** allowed for the detection of the SNAP- $hA_1\text{AR}$ as single red fluorescent spots localized at the plasma membrane (Figure 9a). The location of the red fluorescent spots correlated with the green fluorescent spots of AF488-labeled SNAP- $hA_1\text{AR}$ and is shown in Figure 9a. Additionally, pre-incubation of the cells with $10 \mu\text{M}$ SLV320 prevented the visualization of SNAP- $hA_1\text{AR}$ s by probe **44b**, further validating the specificity of probe **44b** (bottom frames, Figure 9a). While we found that the fluorescent ligand **44b** had a high signal-to-noise ratio for high resolution microscopy applications, fluorescent ligand **46a** also did not perform in this way. Indeed, when **46a** was used in TIRF-M experiments, it was not possible to distinguish the same localization patterns as the AF488-labeled SNAP- $hA_1\text{AR}$ (Figure S12). The BY630/650 moiety increases the lipophilicity of the fluorescent conjugate and might allow probe **46a** to stick either to the plasma membrane of the cell or to the glass coverslip surface, resulting in higher background signal in this particular microscopy approach.

CONCLUSIONS

In the study presented herein, we have reported the successful design, synthesis, and pharmacological evaluation of a series of novel, high affinity, and subtype-selective fluorescent probes for the study of human $A_1\text{AR}$ in living cells. We have demonstrated that both positions of the prototypical xanthine scaffold, namely, the 3- and 8-positions, could be harnessed for linker/fluorophore functionalization. Additionally, modifications at both positions yielded fluorescent probes that retained

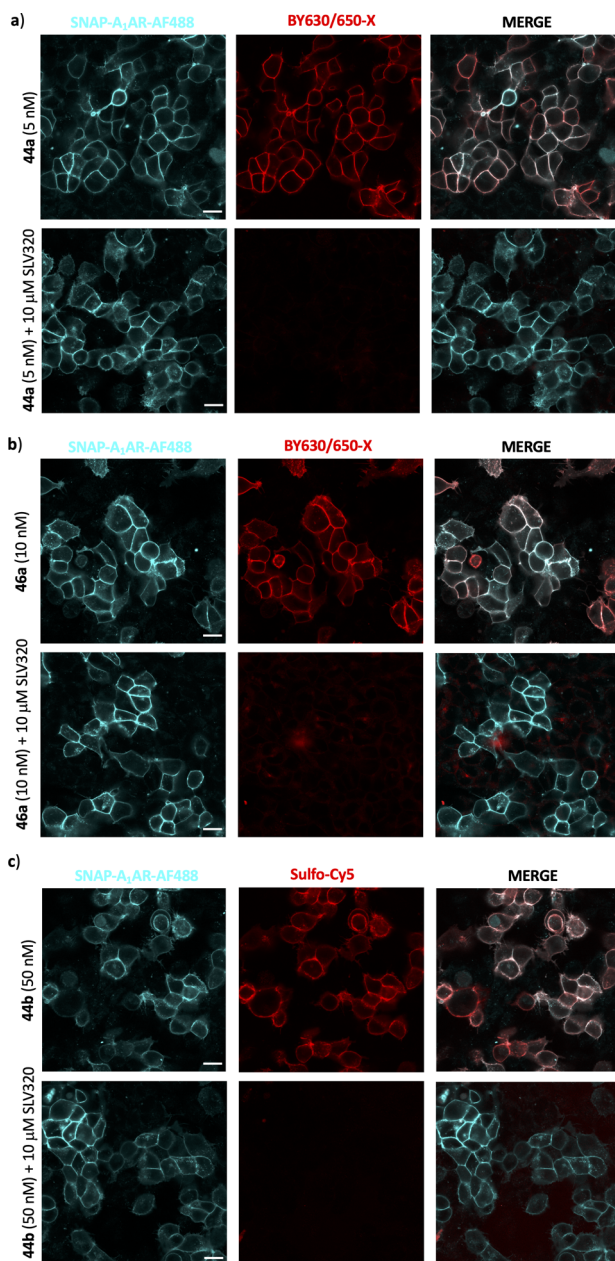


Figure 8. Live-cell confocal imaging studies of fluorescent analogues **44a** (5 nM) (a), **46a** (10 nM) (b), and **44b** (50 nM) (c) binding to SNAP-tagged human A_1AR expressed in HEK293 cells in the absence (top frames) or presence (bottom frames) of 10 μM unlabeled A_1AR antagonist SLV320. Cells were treated with BG-Alexa Fluor 488 for 30 min at 37 $^{\circ}C$ to label the SNAP-tag on the N-terminus of the A_1AR (left hand frames). Middle frames show fluorescent labeling of SNAP-tagged- hA_1AR by the red-shifted fluorescent analogues tested at the given concentration. The images presented here are representative of images captured in three independent experiments. Scale bar = 15 μm

binding affinity and functional activity at the hA_1AR . Overall, a good selectivity profile for the probes synthesized was observed, with the Sulfo-Cy5-bearing probe **44b** and BY630/650-X-bearing probe **46a** displaying the best selectivity profile for the hA_1AR compared to the other adenosine receptors. To the best of our knowledge, probes **44b** and **46a** represent the first examples of subtype-selective fluorescent hA_1AR antagonists reported to date.

Furthermore, fluorescent conjugates **44b** and **46a** were successfully applied to monitor ligand binding of known A_1AR ligands by the recently described NanoBRET ligand binding assay, demonstrating that these probes can be used as alternatives to radioligands. Confocal microscopy studies showed that fluorescent analogues **44a**, **46a**, and **44b** could be applied to visualize the hA_1AR expressed at the membrane of living cells as demonstrated by the high degree of fluorescence intensity observed at the plasma membrane. The binding of the probes could be prevented by incubating the cells with a high concentration of nonfluorescent A_1AR antagonist, demonstrating the specificity of the binding of the probes to the SNAP-tagged- hA_1AR with very little nonspecific cellular uptake detected across all the compounds tested.

Finally, the Sulfo-Cy5-labeled probe **44b** was successfully combined with TIRF microscopy to map hA_1AR distribution at the plasma membrane of HEK293 cells, suggesting that probe **44b** could be coupled with advanced microscopy techniques for the study of the spatial organization of A_1AR s at the plasma membrane of living cells. Remarkably, despite the introduction of the Sulfo-Cy5 fluorescent tag causing a reduced affinity for the hA_1AR compared to the corresponding BY630/650-labeled analogues, we found that the Sulfo-Cy5-labeled probe (**44b**) proved as specific and effective as the BY630/650-labeled analogues (**44a** and **46a**) and possessed even superior physicochemical properties for single-molecule microscopy applications. These results highlight the importance of developing small-molecule probes labeled with dyes of different physicochemical properties and that the characterization and selection of these probes should not be merely based on their apparent binding affinity for the target protein under investigation, but, principally, for the specific biological application.

In summary, we have expanded the available fluorescent A_1AR ligand toolbox. The novel probes reported herein were thoroughly characterized, displayed improved A_1AR pharmacology, and were amenable to a broad range of fluorescence-based techniques. We envisage that these novel A_1AR fluorescent probes will be valuable pharmacological tools to the wider scientific community to aid in understanding the molecular mechanisms underlying A_1AR pharmacology in health and disease.

EXPERIMENTAL SECTION

Chemistry: Materials and Methods. Chemicals and solvents were purchased from commercial suppliers and used without further purification. Davis silica gel (40–63 mm) was supplied by Grace Davison Discovery Science (Victoria, Australia), and a deuterated solvent was purchased from Cambridge Isotope Laboratories (USA, distributed by Novachem Pty. Ltd., Victoria, Australia). Reactions were monitored by thin-layer chromatography on commercially available precoated silica aluminium-backed plates (Merck Kieselgel 60F₂₅₄). Visualization was by examination under UV light (254 and 366 nm), followed by staining with ninhydrin or $KMnO_4$ dips. All organic extracts collected after aqueous workup procedures were dried over anhydrous $MgSO_4$, before gravity filtering and evaporation to dryness. Organic solvents were evaporated in vacuo at 40 $^{\circ}C$ (water bath temperature). NMR spectra were recorded on a Bruker Avance Nanobay III 400 MHz Ultrashield Plus spectrometer. 1H NMR spectra were recorded at 400.13, and ^{13}C NMR were recorded at 101.62 MHz. Chemical shifts (δ) are recorded in parts per million (ppm) with reference to the chemical shift of the deuterated solvent used, and coupling constants are recorded in Hz. The following abbreviation are used to describe the signal shape and multiplicities: singlet (s), doublet (d), triplet (t), quadruplet (q), broad (br),

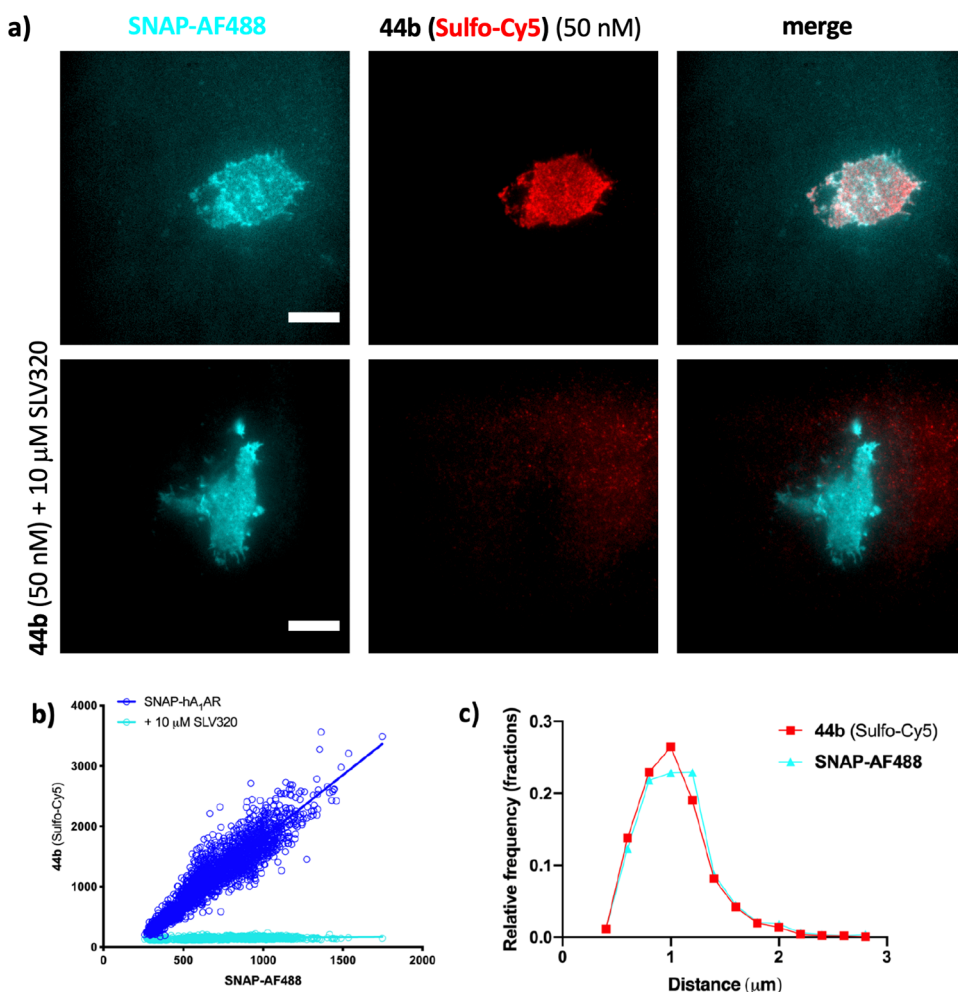


Figure 9. Fluorescent ligand **44b** (50 nM) allowed the visualization of the organization of SNAP-tagged-hA₁AR localized at the plasma membrane of living HEK293 cells by total internal reflection fluorescence microscopy (TIRF-M) in the absence (top frames) or presence (bottom frames) of 10 μ M unlabeled A₁AR selective antagonist SLV320. (a) Cells were labeled with 0.2 μ M BG-Alexa Fluor 488 dye for 30 min at 37 $^{\circ}$ C (left hand frames). Top middle frame shows the labeling of SNAP-hA₁AR by probe **44b** (Sulfo-Cy5) at the given concentration. Bottom middle frame shows that pretreatment of the cells with high concentration (10 μ M) of A₁AR selective antagonist SLV320 prevents the binding of fluorescent ligand **44b** to the hA₁AR. Right hand frames represent merged green (AF488) and red (Sulfo-Cy5) channels. (b) Plot of fluorescence intensities of Sulfo-Cy5-labeled (**44b**) spots vs AF488-labeled spots, in the absence (blue) or presence (cyan) of 10 μ M SLV320. (c) Distribution of the nearest neighbor distances between single SNAP-hA₁ARs labeled with probe **44b** (red) and the BG-Alexa Fluor 488 (cyan). The images reported here are representative TIRF-M images from three independent experiments, each of which included the analysis of 14–18 cells. The data reported in graphs (b) and (c) is the average of data analyzed from 14 to 18 cells in a single representative experiment of three independent experiments. Scale bar = 12 μ m

doublet of doublets (dd), doublet of triplets (dt), triplet of doublets (td), and multiplet (m). Processing of the NMR data was carried out using NMR software Mnova 12.0.4. LC–MS spectra were recorded on an Agilent 6100 series single quad coupled to an Agilent 1200 series HPLC instrument using the following buffers: buffer A, 0.1% formic acid in H₂O; buffer B, 0.1% formic acid in CH₃CN. The following gradient was used with a Poroshell 120 EC-C18 3.0 \times 50mm, 2.7 μ m column a flow rate of 0.5 mL/min and a total run time of 5 min: 0–1 min 95% buffer A and 5% buffer B, 1–2.5 min 0% buffer A and 100% buffer B, 2.5–3.8 min 0% buffer A and 100% buffer B, 3.8–4 min 95% buffer A and 5% buffer B, 4–5 min 95% buffer A and 5% buffer B (method A). Mass spectra were acquired in positive and negative ion modes with a scan range of 100–1000 m/z , and UV detection was monitored at 254 and 214 nm. All high-resolution mass spectra (HRMS) were recorded on an Agilent 6624 TOF LC–MS spectrometer coupled to an Agilent 1290 Infinity system (Agilent, Palo Alto, CA). All data were acquired, and reference mass corrected via a dual-spray electrospray ionization (ESI) source. Acquisition was performed using Agilent Mass Hunter Data

Acquisition software version B.05.00 Build 5.0.5042.2, and analysis was performed using Mass Hunter Qualitative Analysis version B.05.00 Build 5.0.519.13. Preparative HPLC was performed on an Agilent 1260 infinity system coupled with a binary preparative pump and Agilent 1260 FC-PS fraction collector using an Altima C8, 250 \times 22 mm, 5 μ m column. The following conditions were used for this system: buffer A, H₂O and buffer B, CH₃CN with a gradient of 30–100% buffer B over 11 min, with a flow rate of 20 mL/min (method B). Spectra were analyzed using Agilent OpenLAB CDS software. Purity was verified on an analytical reverse-phase Agilent HPLC system coupled directly to a photodiode array detector and using a Zorbax Eclipse Plus C18 Rapid resolution 4.6 \times 100 mm, 3.5 μ m column using the following solvent system: buffer A, 0.1% TFA in H₂O; buffer B, 0.1% TFA in CH₃CN. The elution was performed on a gradient of 95% buffer A and 5% buffer A to 0% buffer A and 100% buffer B over 12 min at a flow rate of 1 mL/min (method C). Final products were one single peak and >95% purity.

General Procedure A: Amide Coupling. To a solution of the respective carboxylic acid (1.0 equiv) in DMF (1–2 mL) were added

DIPEA (1.10 equiv) and COMU or BOP (1.10 equiv). After stirring for 5 min at rt, the respective amine (1.10 equiv) was added to the reaction mixture and the resulting solution was stirred at rt. for 15–60 min. Upon completion of the reaction, checked by LC/MS and TLC, the reaction mixture was evaporated to dryness. The residue was taken up in EtOAc and washed with 1 M aq. HCl, sat. NaHCO₃, and brine. The organic layer was collected, dried over anhydrous MgSO₄, filtered, and evaporated to dryness. The resulting residue was purified by flash column chromatography as indicated.

General Procedure B: Deprotection of *tert*-Butyl Carbamate (Boc-Group). To the respective Boc-protected amine (1 equiv) was added an excess of 4 M HCl in dioxane (1 mL). The resulting mixture was stirred at rt. for 30 min. Upon completion of the reaction, monitored by TLC and LC/MS, the solvent was evaporated to dryness to give the corresponding amine as its HCl salt, which was used for the subsequent step without further purification.

General Procedure C: Syntheses of the Fluorescent Ligands. The respective amine congener (as HCl salt) (1.1 equiv) was dissolved in DMF (0.5 mL), treated with DIPEA (3 equiv), and reacted with BODIPY 630/650-X-NHS (0.5 mg, 1 equiv) or Sulfo-Cy5-NHS (0.5 mg, 1 equiv). The resulting mixture was stirred at rt. under the exclusion of light for 15–60 min. Upon completion of the reaction, monitored by TLC and LC/MS, the solvent was removed in vacuo and the residue was dissolved in a mixture of 1:1 CH₃CN/H₂O. Purification by reverse-phase preparative HPLC (followed by preparative TLC with DCM/MeOH 80:20 for the Sulfo-Cy5 probes) and subsequent lyophilization yielded the pure fluorescent ligand as a bright blue solid.

***tert*-Butyl(2-(3-(4-(2,6-dioxo-1,3-dipropyl-2,3,6,9-tetrahydro-1H-purin-8-yl)bicyclo[2.2.2]octan-1-yl)propanamido)ethyl)carbamate (10).** Following general procedure A, to a solution of 3-(4-(2,6-dioxo-1,3-dipropyl-2,3,6,9-tetrahydro-1H-purin-8-yl)bicyclo[2.2.2]octan-1-yl)propanoic acid, tonapofylline (120 mg, 288 μmol, 1.0 equiv) in DMF (1 mL), were added DIPEA (55 μL, 317 μmol, 1.10 equiv) and COMU (136 mg, 317 μmol, 1.10 equiv) followed by a solution of *tert*-butyl (2-aminoethyl)carbamate (51 mg, 317 μmol, 1.10 equiv) in DMF (0.5 mL). Purification by flash column chromatography using a gradient of 97:3 to 94:6 DCM/MeOH gave the title compound as colorless oil (93 mg, 58%). LC/MS *m/z* calcd for C₂₉H₄₇N₆O₅ [MH]⁺: 559.20, found 559.20 *t_R* = 3.78 min (method A). ¹H NMR (CDCl₃) δ 12.13 (s, 1H), 6.33 (s, 1H), 5.03 (s, 1H), 4.08 (t, *J* = 7.0 Hz, 2H), 4.00 (t, *J* = 7.3 Hz, 2H), 3.35 (q, *J* = 5.4 Hz, 2H), 3.26 (q, *J* = 5.7 Hz, 2H), 2.16–2.08 (m, 2H), 2.03–1.93 (m, 6H), 1.79 (h, *J* = 7.4 Hz, 2H), 1.70 (h, *J* = 6.7, 6.0 Hz, 2H), 1.54–1.38 (m, 17H), 0.95 (t, *J* = 6.5 Hz, 6H). ¹³C NMR (CDCl₃) δ 174.2, 161.9, 157.2, 155.5, 151.2, 148.9, 106.9, 79.8, 45.3, 43.2, 41.1, 40.3, 36.8, 34.0, 31.5, 30.6, 30.6, 28.5, 21.5, 11.7, 11.3.

***tert*-Butyl(15-(4-(2,6-dioxo-1,3-dipropyl-2,3,6,9-tetrahydro-1H-purin-8-yl)bicyclo[2.2.2]octan-1-yl)-8,13-dioxo-3,6-dioxo-9,12-diazapentadecyl)carbamate (12).** Following general procedure B, compound 11 (as HCl salt) was synthesized (75 mg, quantitative) and was used for the next steps without further purification. LC/MS *m/z* calcd for C₂₄H₃₉N₆O₃ [MH]⁺: 459.20, found 459.20 *t_R* = 3.07 min (method A). Following general procedure A, to a solution of 2,2-dimethyl-4-oxo-3,8,11-trioxo-5-azatridecan-13-oic acid (linker A) (15 mg, 57 μmol, 1.0 equiv) in DMF (0.5 mL) was added DIPEA (40 μL, 228 μmol, 4.0 equiv), followed by COMU (26.84 mg, 63 μmol, 1.10 equiv) and a solution of compound 11 (29 mg, 63 μmol, 1.10 equiv) in DMF (0.5 mL). Purification by flash column chromatography using a gradient of 97:3 to 95:5 DCM/MeOH gave the title compound as colorless oil (15 mg, 38%). LC/MS *m/z* calcd for C₃₅H₅₆N₇O₈ [MH]⁺: 702.20, found 702.20 *t_R* = 3.63 min (method A). HRMS (TOF ES⁺) calcd for C₃₅H₅₈N₇O₈ 704.4341, found 704.4356; calcd for C₃₅H₅₈N₇O₈Na 726.4161, found 726.4178. ¹H NMR (CDCl₃) δ 11.86 (br s, 1H), 7.33 (t, *J* = 5.7 Hz, 1H), 6.42 (s, 1H), 5.19 (s, 1H), 4.09 (t, *J* = 6.7 Hz, 2H), 4.00 (m, 4H), 3.68–3.61 (m, 4H), 3.57 (t, *J* = 5.3 Hz, 2H), 3.47–3.38 (m, 4H), 3.36–3.29 (m, 2H), 2.15–2.07 (m, 2H), 2.02–1.95 (m, 6H), 1.79 (h, *J* = 7.4 Hz, 2H), 1.69 (h, *J* = 7.1 Hz, 2H), 1.54–1.46 (m, 8H), 1.43 (s, 9H), 0.95 (t, *J* = 7.4 Hz, 6H). ¹³C NMR (CDCl₃) δ 174.2, 161.7, 156.3, 155.1, 151.3, 148.8, 106.9,

71.2, 70.5, 70.1, 45.3, 43.2, 40.6, 38.9, 36.8, 34.0, 31.5, 30.6, 30.6, 28.5, 21.5, 21.5, 11.7, 11.3. Analytical RP-HPLC *t_R* = 5.77 min, purity >99% (method C).

***tert*-Butyl(2-(2-((2-(3-(4-(2,6-dioxo-1,3-dipropyl-2,3,6,9-tetrahydro-1H-purin-8-yl)bicyclo[2.2.2]octan-1-yl)propanamido)ethyl)amino)-2-oxoethoxy)ethyl)carbamate (13).** Following general procedure A, to a solution of 2-(2-((*tert*-butoxycarbonyl)amino)ethoxy)acetic acid (linker B) (12 mg, 55 μmol, 1.0 equiv) in DMF (0.5 mL) were added DIPEA (38 μL, 219 μmol, 4.0 equiv) and COMU (25.80 mg, 60 μmol, 1.10 equiv), followed by a solution of 11 (28 mg, 60 μmol, 1.10 equiv) in DMF (0.5 mL). Purification by flash column chromatography using a gradient of 96:4 to 94:6 DCM/MeOH gave the title compound as colorless oil (10 mg, 28%). LC/MS *m/z* calcd for C₃₃H₅₂N₇O₇ [MH]⁺: 658.20, found 658.40 *t_R* = 3.70 min (method A). HRMS (TOF ES⁺) calcd for C₃₃H₅₄N₇O₇ 660.4079, found 660.4096; calcd for C₃₃H₅₄N₇O₇Na 682.3899, found 682.3917. ¹H NMR (CDCl₃) δ 7.43 (s, 1H), 6.44 (s, 1H), 5.57 (s, 1H), 4.09 (t, *J* = 6.9 Hz, 2H), 4.00 (t, *J* = 6.9 Hz, 2H), 3.95 (s, 2H), 3.56 (t, *J* = 5.0 Hz, 2H), 3.45–3.40 (m, 4H), 3.40–3.33 (m, 2H), 2.17–2.11 (m, 2H), 2.02–1.95 (m, 6H), 1.78 (h, *J* = 7.4 Hz, 2H), 1.69 (h, *J* = 7.0 Hz, 2H), 1.55–1.47 (m, 8H), 1.44 (s, 9H), 0.95 (t, *J* = 7.4 Hz, 6H). ¹³C NMR (CDCl₃) δ 174.9, 170.8, 161.7, 156.5, 155.4, 151.2, 148.8, 106.8, 79.4, 71.3, 70.4, 70.4, 45.4, 43.2, 40.0, 36.8, 34.0, 31.5, 30.6, 30.6, 28.6, 21.5, 21.5, 11.6, 11.3. Analytical RP-HPLC *t_R* = 5.77 min, purity >99% (method C).

***tert*-Butyl(3-((2-(3-(4-(2,6-dioxo-1,3-dipropyl-2,3,6,9-tetrahydro-1H-purin-8-yl)bicyclo[2.2.2]octan-1-yl)propanamido)ethyl)amino)-3-oxopropyl)carbamate (14).** Following general procedure A, to a solution of 3-((*tert*-butoxycarbonyl)amino)propanoic acid (Boc-β-Ala-OH) (10 mg, 53 μmol, 1.0 equiv) in DMF (0.5 mL) were added DIPEA (37 μL, 211 μmol, 4.0 equiv) and COMU (25 mg, 58 μmol, 1.10 equiv), followed by a solution of 11 (27 mg, 58 μmol, 1.10 equiv) in DMF (0.5 mL). Purification by flash column chromatography using a gradient of 96:4 to 94:6 DCM/MeOH gave the title compound as an off-white solid (29 mg, 78%). LC/MS *m/z* calcd for C₃₂H₅₂N₇O₆ [MH]⁺: 630.20, found 630.40 *t_R* = 3.69 min (method A). ¹H NMR (CD₃OD) δ 4.07 (t, *J* = 6.3 Hz, 2H), 3.95 (t, *J* = 6.8, 2H), 3.29 (br s, 4H), 2.37 (t, *J* = 6.8 Hz, 2H), 2.20–2.14 (m, 2H), 2.00–1.93 (m, 6H), 1.78 (h, *J* = 6.8 Hz, 2H), 1.66 (h, *J* = 6.8 Hz, 2H), 1.59–1.48 (m, 8H), 1.45 (s, 9H), 0.95 (t, *J* = 7.5 Hz, 6H). ¹³C NMR (CD₃OD) δ 176.9, 174.1, 162.7, 155.8, 152.6, 149.3, 107.8, 79.9, 45.8, 43.6, 39.8, 37.9, 37.3, 34.9, 31.8, 31.4, 31.4, 31.2, 28.5, 22.2, 22.1, 11.3, 11.1. Analytical RP-HPLC *t_R* = 5.65 min, purity >99% (method C).

***tert*-Butyl(3-((3-((2-(3-(4-(2,6-dioxo-1,3-dipropyl-2,3,6,9-tetrahydro-1H-purin-8-yl)bicyclo[2.2.2]octan-1-yl)propanamido)ethyl)amino)-3-oxopropyl)amino)-3-oxopropyl)carbamate (15).** Following general procedure B, compound 14 (27 mg, 1.0 equiv) was reacted with 4 M HCl in dioxane (1 mL), and after the removal of the solvent in vacuo, the resulting HCl salt was used for the subsequent step without further purification. The synthesis of 15 was carried out as described for xanthine 14, following general procedure A, reacting a solution of the 3-((2-(3-(4-(2,6-dioxo-1,3-dipropyl-2,3,6,7-tetrahydro-1H-purin-8-yl)bicyclo[2.2.2]octan-1-yl)propanamido)ethyl)amino)-3-oxopropan-1-aminium chloride intermediate (22 mg, 41 μmol, 1.10 equiv) in DMF (0.5 mL) with a solution of 3-((*tert*-Butoxycarbonyl)amino)propanoic acid (Boc-β-Ala-OH) (7 mg, 37 μmol, 1.0 equiv), DIPEA (32 μL, 185 μmol, 5 equiv), COMU (17.43 mg, 41 μmol, 1.10 equiv) in DMF (0.5 mL). Purification by flash column chromatography using a gradient of 96:4 to 93:7 DCM/MeOH gave the title compound as an off-white solid (12 mg, 46%). LC/MS *m/z* calcd for C₃₅H₅₇N₈O₇ [MH]⁺: 701.20, found 701.40 *t_R* = 3.57 min (method A). HRMS (TOF ES⁺) calcd for C₃₅H₅₇N₈O₇ 701.4350, found 701.4360; calcd for C₃₅H₅₇N₈O₇Na 723.4164, found 723.4184. ¹H NMR (CD₃OD) δ 4.07 (t, *J* = 6.3 Hz, 2H), 3.95 (t, *J* = 6.3 Hz, 2H), 3.45 (t, *J* = 6.8 Hz, 2H), 3.33–3.31 (m, 2H), 3.30 (br s, 4H), 2.38 (dt, *J* = 9.0, 6.8 Hz, 4H), 2.20–2.14 (m, 2H), 2.00–1.92 (m, 6H), 1.78 (h, *J* = 7.5 Hz, 2H), 1.66 (h, *J* = 7.0 Hz, 2H), 1.59–1.49 (m, 8H), 1.44 (s, 9H), 0.95 (t, *J* = 7.4, 6H). ¹³C NMR (CD₃OD) δ 177.1, 174.1, 162.7, 158.3, 156.0, 152.9, 149.5, 80.1, 45.9, 43.8, 40.2, 40.0, 38.1, 37.4, 37.1,

35.1, 32.1, 31.6, 31.4, 28.8, 22.4, 22.3, 11.5, 11.3. Analytical RP-HPLC $t_R = 5.52$ min, purity >99% (method C).

tert-Butyl(2-(4-(2,6-dioxo-1,3-dipropyl-2,3,6,9-tetrahydro-1H-purin-8-yl) bicyclo[2.2.2]octane-1-carboxamido)ethyl)carbamate (17a). Following general procedure A, to a solution of (2,6-dioxo-1,3-dipropyl-2,3,6,9-tetrahydro-1H-purin-8-yl) bicyclo [2.2.2] octane-1-carboxylic acid (compound **16** from Kiesman et al.)⁵⁹ (80 mg, 206 μ mol, 1.0 equiv), *tert*-butyl (2-aminoethyl) carbamate (33 mg, 206 μ mol, 1.0 equiv), and BOP (137 mg, 309 μ mol, 1.50 equiv) in dry DMF (2 mL) was added DIPEA (143 μ L, 824 μ mol, 4.0 equiv). Purification by flash column chromatography using a gradient of 97:3 to 96:4 DCM/MeOH gave the title compound as off-white solid (85 mg, 78%). LC/MS m/z calcd for $C_{27}H_{43}N_6O_5$ [MH]⁺: 531.30, found 531.30 $t_R = 3.61$ min (method A). ¹H NMR (CDCl₃) δ 11.67 (br s, 1H), 6.53 (br s, 1H), 4.90 (br s, 1H), 4.09 (t, $J = 6.3$ Hz, 2H), 4.02 (t, $J = 6.6$ Hz, 2H), 3.37–3.26 (m, 4H), 2.08–2.01 (m, 6H), 1.93–1.87 (m, 6H), 1.80 (h, $J = 6.5$ Hz, 2H), 1.70 (h, $J = 6.5$ Hz, 2H), 1.45 (s, 9H), 0.96 (t, $J = 7.5$ Hz, 6H). ¹³C NMR (CDCl₃) δ 176.1, 155.5, 152.2, 151.3, 148.9, 106.9, 30.2, 28.5, 21.5, 11.6, 11.3.

tert-Butyl(3-(4-(2,6-dioxo-1,3-dipropyl-2,3,6,9-tetrahydro-1H-purin-8-yl) bicyclo[2.2.2]octane-1-carboxamido)propyl)carbamate (17b). The synthesis of the title compound **17b** was carried out as described for xanthine (**17a**), following general procedure A. To a stirred solution of (2,6-dioxo-1,3-dipropyl-2,3,6,9-tetrahydro-1H-purin-8-yl) bicyclo [2.2.2] octane-1-carboxylic acid (compound **16** from Kiesman et al.) (110 mg, 283 μ mol, 1 equiv), *tert*-butyl (3-aminopropyl) carbamate (49 mg, 283 μ mol, 1.0 equiv), and BOP (188 mg, 425 μ mol, 1.50 equiv) in dry DMF (2 mL) was added DIPEA (197 μ L, 1.13 μ mol, 4.0 equiv). Purification by flash column chromatography using a gradient of 97:3 to 96:4 DCM/MeOH gave the title pure compound as an off-white solid (132 mg, 86%). LC/MS m/z calcd for $C_{28}H_{45}N_6O_5$ [MH]⁺: 545.30, found 545.40 $t_R = 3.66$ min (method A). ¹H NMR (CDCl₃) δ 12.20 (br s, 1H), 6.55 (br s, 1H), 4.91 (br s, 1H), 4.08 (t, $J = 6.9$ Hz, 2H), 4.02 (t, $J = 6.2$ Hz, 2H), 3.30 (q, $J = 4.6$ Hz, 2H), 3.16 (q, $J = 4.6$ Hz, 2H), 2.10–2.04 (m, 6H), 1.94–1.88 (m, 6H), 1.78 (h, $J = 6.5$ Hz, 2H), 1.70 (h, $J = 6.5$ Hz, 2H), 1.62–1.54 (m, 2H), 1.43 (s, 9H), 0.95 (t, $J = 7.0$ Hz, 6H). ¹³C NMR (CDCl₃) δ 177.6, 161.4, 156.9, 155.6, 151.2, 149.0, 107.0, 79.6, 45.3, 43.2, 39.1, 36.9, 35.6, 33.9, 30.2, 28.5, 21.5, 11.6, 11.3.

tert-Butyl(1-(4-(2,6-dioxo-1,3-dipropyl-2,3,6,9-tetrahydro-1H-purin-8-yl) bicyclo[2.2.2]octan-1-yl)-1,6-dioxo-8,11-dioxo-2,5-diazatridecan-13-yl)carbamate (19). Following general procedure B, compound **17a** (85 mg, 206 μ mol, 1.0 equiv) was treated with 4 M HCl in dioxane (1 mL) to afford compound **18a** (68 mg, quantitative) as HCl salt, which was used in the next step without further purification. LC/MS m/z calcd for $C_{22}H_{35}N_6O_3$ [MH]⁺: 431.34, found 431.30 $t_R = 3.10$ min. Compound **19** was synthesized according to general procedure A, reacting a solution of compound **18a** (25 mg, 57 μ mol, 1.1 equiv) in DMF (0.5 mL) with 2,2-dimethyl-4-oxo-3,8,11-trioxa-5-azatridecan-13-oic acid (15 mg, 57 μ mol, 1.0 equiv), DIPEA (40 mL, 228 μ mol, 4.0 equiv), and BOP (38 mg, 85 μ mol, 1.50 equiv). Purification by flash column chromatography using a gradient of 98:2 to 96:4 DCM/MeOH gave the title compound as colorless oil (15 mg, 38%). LC/MS m/z calcd for $C_{33}H_{54}N_7O_8$ [MH]⁺: 676.20, found 676.40 $t_R = 3.50$ min (method A). HRMS (TOF ES⁺) calcd for $C_{33}H_{54}N_7O_8$ 676.4028, found 676.4045; calcd for $C_{33}H_{54}N_7O_8Na$ 698.3848, found 698.3869. ¹H NMR (CD₃OD) δ 4.07 (t, $J = 6.9$ Hz, 2H), 4.01 (s, 2H), 3.95 (t, $J = 7.1$ Hz, 2H), 3.72–3.66 (m, 4H), 3.56 (t, $J = 5.7$ Hz, 2H), 3.41–3.37 (m, 2H), 3.37–3.34 (m, 2H), 3.27 (td, $J = 5.7, 4.4$ Hz, 2H), 2.05–1.98 (m, 6H), 1.93–1.86 (m, 6H), 1.79 (h, $J = 7.3$ Hz, 2H), 1.65 (h, $J = 7.3$ Hz, 2H), 1.44 (s, 9H), 0.96 (t, $J = 7.4, 6.3$ Hz, 6H). ¹³C NMR (CD₃OD) δ 180.5, 173.3, 160.9, 156.0, 152.9, 151.6, 149.5, 108.2, 80.1, 72.0, 71.3, 71.2, 71.1, 49.6, 45.9, 43.8, 41.3, 40.5, 40.5, 40.1, 39.7, 34.9, 31.0, 29.2, 28.8, 22.4, 22.3, 11.5, 11.4. Analytical RP-HPLC $t_R = 5.85$ min, purity >99% (method C).

tert-Butyl(2-(2-(4-(2,6-dioxo-1,3-dipropyl-2,3,6,9-tetrahydro-1H-purin-8-yl) bicyclo[2.2.2]octane-1-carboxamido)ethyl)amino)-2-oxoethoxy)ethyl)carbamate (20). The synthesis of **20** was carried out as described for 8-bicyclo[2.2.2]octylxanthine **19**, following

general procedure A. Compound **18a** (20 mg, 46 μ mol, 1.1 equiv) was added to a solution of 2-(2-((*tert*-butoxycarbonyl)amino)-ethoxy)acetic acid (10 mg, 46 μ mol, 1.0 equiv), BOP (30 mg, 68 μ mol, 1.50 equiv), and DIPEA (32 mL, 182 μ mol, 4.0 equiv) in DMF (1 mL). Purification by flash column chromatography using a gradient of 97:3 to 96:4 DCM/MeOH gave the title compound as colorless oil, which slightly solidified upon cooling (10 mg, 36%). LC/MS m/z calcd for $C_{31}H_{50}N_7O_7$ [MH]⁺: 632.20, found 632.40 $t_R = 3.53$ min (method A). HRMS (TOF ES⁺) calcd for $C_{31}H_{50}N_7O_7$ 632.3766, found 632.3781; calcd for $C_{31}H_{50}N_7O_7Na$ 654.3586, found 654.3601. ¹H NMR (CDCl₃) δ 11.86 (s, 1H), 7.38 (s, 1H), 6.57 (s, 1H), 5.46 (s, 1H), 4.09 (t, $J = 6.4$ Hz, 2H), 4.01 (t, $J = 6.4$ Hz, 2H), 3.96 (s, 2H), 3.57 (t, $J = 5.0$ Hz, 2H), 3.47–3.41 (m, 4H), 3.40–3.33 (m, 2H), 2.09–2.01 (m, 6H), 1.92–1.85 (m, 6H), 1.79 (h, $J = 6.9$ Hz, 2H), 1.69 (h, $J = 6.9$ Hz, 2H), 1.45 (s, 9H), 0.95 (t, $J = 7.5$ Hz, 6H). ¹³C NMR (CDCl₃) δ 178.5, 171.1, 156.4, 155.5, 151.2, 106.9, 79.7, 70.4, 69.5, 43.3, 40.7, 39.9, 39.0, 33.9, 30.1, 29.8, 28.6, 28.5, 21.5, 21.5, 11.6, 11.3. Analytical RP-HPLC $t_R = 5.87$ min, purity >97% (method C).

tert-Butyl(3-((2-(4-(2,6-dioxo-1,3-dipropyl-2,3,6,9-tetrahydro-1H-purin-8-yl) bicyclo[2.2.2]octane-1-carboxamido)ethyl)amino)-3-oxopropyl)carbamate (21). Compound **18a** (22 mg, 53 μ mol, 1.0 equiv) was reacted with Boc- β -Ala-OH (10 mg, 53 μ mol, 1.0 equiv) in the presence of BOP (35 mg, 79 μ mol, 1.50 equiv) and DIPEA (37 μ L, 211 μ mol, 4.0 equiv) in DMF (2 mL) according to general procedure A. Purification by flash column chromatography using a gradient of 97:3 to 96:4 DCM/MeOH gave the title compound as colorless oil, which slightly solidified upon cooling (12 mg, 38%). LC/MS m/z calcd for $C_{30}H_{48}N_7O_6$ [MH]⁺: 602.20, found 602.40 $t_R = 3.48$ min (method A). ¹H NMR (CD₃OD) δ 4.07 (t, $J = 6.9$ Hz, 2H), 3.95 (t, $J = 6.9$ Hz, 2H), 3.32 (s, 2H), 3.30 (s, 4H), 2.37 (t, $J = 6.8$ Hz, 2H), 2.05–1.98 (m, 6H), 1.95–1.87 (m, 6H), 1.77 (h, $J = 7.5$ Hz, 2H), 1.66 (h, $J = 7.5$ Hz, 2H), 1.45 (s, 9H), 0.96 (t, $J = 7.4$ Hz, 6H).

tert-Butyl(3-((3-((2-(4-(2,6-dioxo-1,3-dipropyl-2,3,6,9-tetrahydro-1H-purin-8-yl) bicyclo[2.2.2]octane-1-carboxamido)ethyl)amino)-3-oxopropyl)amino)-3-oxopropyl)carbamate (25a). Compound **21** (12 mg, 1.0 equiv) was treated with 4 M HCl in dioxane following general procedure B to yield the corresponding 3-((2-(4-(2,6-dioxo-1,3-dipropyl-2,3,6,7-tetrahydro-1H-purin-8-yl) bicyclo[2.2.2]octane-1-carboxamido)ethyl)amino)-3-oxopropan-1-aminium chloride intermediate (9 mg, quantitative), which was used for the next step without any further purification. The synthesis of the title compound **25a** was carried out as described for 8-bicyclo[2.2.2]octylxanthine **21**, treating the 3-((2-(4-(2,6-dioxo-1,3-dipropyl-2,3,6,7-tetrahydro-1H-purin-8-yl) bicyclo[2.2.2]octane-1-carboxamido)ethyl)amino)-3-oxopropan-1-aminium chloride intermediate (5 mg, 1.10 equiv) with DIPEA (31 μ L, 186 μ mol, 10.0 equiv), Boc- β -Ala-OH (4 mg, 19 μ mol, 1.0 equiv), and BOP (12 mg, 28 μ mol, 1.50 equiv) in DMF (1 mL). Purification by flash column chromatography using a gradient of 96:4 to 94:6 DCM/MeOH gave the title compound as colorless oil, which solidified upon cooling (8 mg, 67%). LC/MS m/z calcd for $C_{33}H_{53}N_8O_7$ [MH]⁺: 673.20, found 673.40 $t_R = 3.42$ min (method A). HRMS (TOF ES⁺) calcd for $C_{33}H_{53}N_8O_7$ 673.4032, found 673.4043; calcd for $C_{33}H_{53}N_8O_7Na$ 695.3851, found 695.3866. ¹H NMR (CD₃OD) δ 4.07 (t, $J = 6.3$ Hz, 2H), 3.95 (t, $J = 5.7$ Hz, 2H), 3.45 (t, $J = 6.8$ Hz, 2H), 3.30 (s, 4H), 2.38 (t, $J = 6.8$ Hz, 4H), 2.04–1.98 (m, 6H), 1.93–1.87 (m, 6H), 1.77 (h, $J = 7.4$ Hz, 2H), 1.66 (h, $J = 6.4$ Hz, 2H), 1.43 (s, 9H), 0.96 (t, $J = 7.2$ Hz, 6H). ¹³C NMR (CD₃OD) δ 179.1, 172.9, 161.5, 160.8, 151.5, 95.1, 78.7, 46.8, 42.5, 39.1, 38.7, 35.7, 35.5, 33.6, 33.3, 29.6, 27.8, 27.4, 20.9, 20.9, 10.1, 9.9. Analytical RP-HPLC $t_R = 5.58$ min, purity >97% (method C).

Methyl 3-(4-(2,6-Dioxo-1,3-dipropyl-2,3,6,9-tetrahydro-1H-purin-8-yl) bicyclo[2.2.2]octane-1-carboxamido)propanoate (26). To a solution of 4-(2,6-dioxo-1,3-dipropyl-2,3,6,9-tetrahydro-1H-purin-8-yl) bicyclo[2.2.2]octane-1-carboxylic acid (compound **16** from Kiesman et al.) (80 mg, 206 μ mol, 1.0 equiv) in DMF (1 mL) were added DIPEA (0.143 mL, 824 μ mol, 4.0 equiv), β -Ala-methyl ester (29 mg, 206 μ mol, 1.0 equiv), and BOP (136 mg, 309 μ mol, 1.50 equiv). The resulting mixture was stirred at rt. for 1 h.

Upon completion of the reaction, checked by TLC and LC/MS, DMF was evaporated to dryness and the resulting residue was taken up in water (20 mL) and extracted with EtOAc. The organic layer was collected and washed with 1 M HCl, sat. NaHCO₃, and brine. The organic layer was then dried over anhydrous Na₂SO₄, filtered, and evaporated to dryness to give the crude as pale yellow oil. Purification by flash column chromatography using a gradient of 96:4 to 94:6 DCM/MeOH gave the title compound as an off-white solid (76 mg, 56%). LC/MS *m/z* calcd for C₂₄H₃₆N₅O₅ [MH]⁺: 474.20, found 474.30 *t_R* = 3.57 min (method A). ¹H NMR (CDCl₃) δ 12.25 (s, 1H), 6.33 (t, *J* = 6.0 Hz, 1H), 4.08 (t, *J* = 7.6, 6.1 Hz, 2H), 4.01 (t, *J* = 6.7 Hz, 2H), 3.69 (s, 3H), 3.51 (q, *J* = 6.0 Hz, 2H), 2.52 (t, *J* = 6.2 Hz, 2H), 2.10–2.02 (m, 6H), 1.87 (m, 6H), 1.79 (h, *J* = 7.4 Hz, 2H), 1.74–1.64 (h, *J* = 7.4 Hz, 2H), 0.95 (t, *J* = 7.4 Hz, 6H). ¹³C NMR (CDCl₃) δ 177.1, 173.5, 161.2, 155.5, 151.2, 149.0, 107.1, 51.9, 45.3, 43.3, 38.9, 34.9, 33.9, 33.7, 30.1, 28.5, 21.5, 11.6, 11.3.

3-(4-(2,6-Dioxo-1,3-dipropyl-2,3,6,9-tetrahydro-1H-purin-8-yl)-bicyclo[2.2.2]octane-1-carboxamido)propanoic acid (**27**). Methyl 3-(4-(2,6-dioxo-1,3-dipropyl-2,3,6,9-tetrahydro-1H-purin-8-yl)-bicyclo[2.2.2]octane-1-carboxamido)propanoate (**26**) (76 mg, 160 μmol, 1.0 equiv) was dissolved in MeOH (5 mL). To the mixture was added a solution of LiOH·H₂O (33.67 mg, 802 μmol, 5.0 equiv) in water (5 mL). The resulting mixture was stirred at rt. for 40 min. By that time, TLC and LC/MS showed that the reaction was completed. MeOH was then removed under reduced pressure, and the water layer was acidified with 2 M HCl to pH = 1. The water layer was extracted with EtOAc (2 × 20 mL). The organic layer was separated, dried over anhydrous MgSO₄, filtered, and evaporated to dryness to give the title compound as an off-white solid (61 mg, 84%). ¹H NMR (CDCl₃) δ 12.10 (s, 1H), 6.45 (t, *J* = 6.0 Hz, 1H), 4.08 (t, *J* = 6.6 Hz, 2H), 3.98 (t, *J* = 7.0 Hz, 2H), 3.58 (q, *J* = 6.0 Hz, 2H), 2.66 (t, *J* = 4.9 Hz, 2H), 2.07–2.00 (m, 6H), 1.96–1.91 (m, 6H), 1.78 (h, *J* = 7.0 Hz, 2H), 1.65 (h, *J* = 7.0 Hz, 2H), 0.94 (t, *J* = 7.4, 6H). ¹³C NMR (CDCl₃) δ 178.2, 176.6, 161.4, 156.4, 150.8, 149.7, 106.5, 45.5, 43.6, 38.9, 34.6, 33.8, 30.2, 28.5, 21.4, 11.4, 11.3.

tert-Butyl(2-(3-(4-(2,6-dioxo-1,3-dipropyl-2,3,6,9-tetrahydro-1H-purin-8-yl)bicyclo[2.2.2]octane-1-carboxamido)propanamido)ethyl)carbamate (**28**). Following general procedure A, to a solution of compound **27** (61.00 mg, 133 μmol, 1 equiv) in DMF (1 mL) were added DIPEA (92 μL, 531 μmol, 4.0 equiv), *tert*-butyl (2-aminoethyl)carbamate (21.27 mg, 133 μmol, 1.0 equiv), and BOP (88 mg, 199 μmol, 1.50 equiv). Purification by flash column chromatography using a gradient of 96:4 to 94:6 DCM/MeOH gave the title compound as an off-white solid (62 mg, 70%). LC/MS *m/z* calcd for C₃₀H₄₈N₇O₆ [MH]⁺: 602.20, found 602.40 *t_R* = 3.62 min (Method A). ¹H NMR (CDCl₃) δ 6.86 (br s, 1H), 6.65 (br s, 1H), 5.02 (br s, 1H), 4.10 (t, *J* = 6.4 Hz, 2H), 4.00 (t, *J* = 6.4 Hz, 2H), 3.57–3.48 (m, 2H), 3.39–3.32 (m, 2H), 3.31–3.22 (m, 2H), 2.46–2.37 (m, 2H), 2.10–2.00 (m, 6H), 1.95–1.85 (m, 6H), 1.79 (h, *J* = 7.3 Hz, 2H), 1.68 (h, *J* = 7.4 Hz, 2H), 1.44 (s, 9H), 0.95 (t, *J* = 7.5 Hz, 6H).

tert-Butyl(1-(4-(2,6-dioxo-1,3-dipropyl-2,3,6,9-tetrahydro-1H-purin-8-yl)bicyclo[2.2.2]octan-1-yl)-1,5,10-trioxo-12-oxa-2,6,9-triazatetradecan-14-yl)carbamate (**30**). Following general procedure B, compound 2-(3-(4-(2,6-dioxo-1,3-dipropyl-2,3,6,9-tetrahydro-1H-purin-8-yl)bicyclo[2.2.2]octane-1-carboxamido)propanamido)ethan-1-aminium chloride (**29**) was synthesized reacting **28** (64 mg, 1.0 equiv) with 4 M HCl in dioxane (1 mL). The resulting intermediate **29** was used for the subsequent step without further purification. The synthesis of the title compound **30** was carried out following general procedure A, reacting a solution of 2-(3-(4-(2,6-dioxo-1,3-dipropyl-2,3,6,9-tetrahydro-1H-purin-8-yl)bicyclo[2.2.2]octane-1-carboxamido)propanamido)ethan-1-aminium chloride (**29**) (54 mg, 100 μmol, 1.10 equiv) in DMF (0.5 mL) with a solution of 2-(2-((*tert*-butoxycarbonyl)amino)ethoxy)acetic acid (20 mg, 91 μmol, 1.0 equiv), DIPEA (64 μL, 365 μmol, 4.0 equiv), and COMU (43 mg, 100 μmol, 1.10 equiv) in DMF (0.5 mL). Purification by flash column chromatography using a gradient of 97:3 to 94:6 DCM/MeOH gave the title compound as an off-white solid (37 mg, 58%). LC/MS *m/z* calcd for C₃₄H₅₅N₈O₈ [MH]⁺: 703.20, found 703.40 *t_R* = 3.37 min

(method A). HRMS (TOF ES⁺) calcd for C₃₄H₅₅N₈O₈ 703.4137, found 703.4155; calcd for C₃₄H₅₅N₈O₈Na 725.3957, found 725.3974. ¹H NMR (CDCl₃) δ 12.05 (s, 1H), 7.57 (s, 1H), 7.10 (s, 1H), 6.71 (s, 1H), 5.62 (s, 1H), 4.07 (t, *J* = 6.1 Hz, 2H), 4.01–3.93 (m, 4H), 3.59–3.50 (m, 4H), 3.43–3.38 (m, 4H), 3.38–3.32 (m, 2H), 2.56–2.42 (m, 2H), 2.07–1.98 (m, 6H), 1.90–1.82 (m, 6H), 1.78 (h, *J* = 7.4 Hz, 2H), 1.67 (h, *J* = 7.4 Hz, 2H), 1.43 (s, 9H), 0.94 (t, *J* = 7.5 Hz, 6H). ¹³C NMR (CDCl₃) δ 161.5, 160.9, 156.5, 155.4, 151.2, 148.8, 107.0, 101.7, 79.9, 70.5, 45.3, 43.2, 39.9, 39.0, 35.9, 35.8, 33.9, 30.1, 28.6, 28.4, 21.5, 11.6, 11.3. Analytical RP-HPLC *t_R* = 5.62 min, purity >98% (method C).

tert-Butyl(1-(4-(2,6-dioxo-1,3-dipropyl-2,3,6,9-tetrahydro-1H-purin-8-yl)bicyclo[2.2.2]octan-1-yl)-1,7-dioxo-9,12-dioxo-2,6-diazatetradecan-14-yl)carbamate (**22**). The title compound was synthesized as described for 8-bicyclo[2.2.2]octylxanthine **19**, following general procedure A: to a solution of 2,2-dimethyl-4-oxo-3,8,11-trioxa-5-azatridecan-13-oic acid (11 mg, 42 μmol, 1.0 equiv) in DMF (0.7 mL) was added DIPEA (15 μL, 85 μmol, 4.0 equiv) followed by COMU (20 mg, 46 μmol, 1.10 equiv) and intermediate **18b** (21 mg, 46 μmol, 1.10 equiv) previously dissolved in DMF (0.5 mL). Purification by flash column chromatography using a gradient of 97:3 to 95:5 DCM/MeOH gave the title compound as colorless oil (15 mg, 39%). LC/MS *m/z* calcd for C₃₄H₅₆N₇O₈ [MH]⁺: 690.20, found 690.40 *t_R* = 3.57 min (method A). HRMS (TOF ES⁺) calcd for C₃₄H₅₆N₇O₈ 690.4185, found 690.4199; calcd for C₃₄H₅₆N₇O₈ Na 712.4004, found 712.4020. ¹H NMR (CDCl₃) δ 11.86 (s, 1H), 7.17 (t, *J* = 6.6 Hz, 1H), 6.86 (t, *J* = 6.8 Hz, 1H), 4.92 (br s, 1H), 4.10 (t, *J* = 6.5 Hz, 2H), 4.04–3.99 (m, 4H), 3.71–3.66 (m, 2H), 3.66–3.63 (m, 2H), 3.57 (t, *J* = 5.3 Hz, 2H), 3.35 (dt, *J* = 10.5, 5.7 Hz, 4H), 3.26 (q, *J* = 6.1 Hz, 2H), 2.10–2.03 (m, 6H), 1.97–1.90 (m, 6H), 1.79 (m, 2H), 1.74–1.67 (m, 2H), 1.67–1.60 (m, 2H), 1.44 (s, 9H), 0.96 (t, *J* = 7.5 Hz, 6H). ¹³C NMR (CDCl₃) δ 177.5, 171.2, 166.7, 156.1, 155.5, 151.2, 148.7, 106.9, 75.4, 71.2, 70.5, 70.5, 70.5, 70.1, 43.3, 39.1, 35.4, 35.3, 33.9, 30.2, 29.7, 28.6, 28.5, 21.5, 21.5, 11.6, 11.3. Analytical RP-HPLC *t_R* = 5.92 min, purity >99% (method C).

tert-Butyl(2-(2-(3-(4-(2,6-dioxo-1,3-dipropyl-2,3,6,9-tetrahydro-1H-purin-8-yl)bicyclo[2.2.2]octane-1-carboxamido)propyl)amino)-2-oxoethoxy)ethyl)carbamate (**23**). The synthesis of **23** was carried out as described for 8-bicyclo[2.2.2]octylxanthine **20**, following general procedure A: to a solution of 2-(2-((*tert*-butoxycarbonyl)amino)ethoxy)acetic acid (13 mg, 59.30 μmol, 1.0 equiv) in DMF (0.7 mL) was added DIPEA (21 mL, 118.6 μmol, 4.0 equiv), followed by COMU (27.93 mg, 65 μmol, 1.10 equiv) and intermediate **18b** (29 mg, 65.23 μmol, 1.10 equiv) previously dissolved in DMF (0.5 mL). Purification by flash column chromatography using a gradient of 96:4 to 95:5 DCM/MeOH gave the title compound as colorless oil (14 mg, 37%). LC/MS *m/z* calcd for C₃₂H₅₂N₇O₇ [MH]⁺: 646.20, found 646.40 *t_R* = 2.82 min (method A). HRMS (TOF ES⁺) calcd for C₃₂H₅₂N₇O₇ 646.3923, found 646.3937; calcd for C₃₂H₅₂N₇O₇ Na 668.3742, found 668.3758. ¹H NMR (CDCl₃) δ 12.08 (s, 1H), 7.43 (br s, 1H), 6.52 (br s, 1H), 5.54 (br s, 1H), 4.09 (t, *J* = 6.0 Hz, 2H), 4.01 (t, *J* = 6.3 Hz, 2H), 3.98 (s, 2H), 3.58 (t, *J* = 5.0 Hz, 2H), 3.40–3.35 (m, 2H), 3.34–3.27 (m, 4H), 2.11–2.04 (m, 6H), 1.96–1.90 (m, 6H), 1.79 (h, *J* = 6.5 Hz, 2H), 1.71 (h, *J* = 6.5 Hz, 2H), 1.66–1.57 (m, 2H), 1.43 (s, 9H), 0.95 (t, *J* = 7.5 Hz, 6H). ¹³C NMR (CDCl₃) δ 178.1, 170.5, 161.1, 156.4, 155.5, 151.2, 148.8, 106.9, 79.4, 71.4, 70.5, 45.4, 43.3, 40.7, 39.2, 35.4, 34.9, 33.9, 30.2, 29.7, 28.6, 21.5, 21.5, 11.6, 11.3. Analytical RP-HPLC *t_R* = 5.95 min, purity >99% (method C).

tert-Butyl(3-(3-(4-(2,6-dioxo-1,3-dipropyl-2,3,6,9-tetrahydro-1H-purin-8-yl)bicyclo[2.2.2]octane-1-carboxamido)propyl)amino)-3-oxopropyl)carbamate (**24**). The synthesis of compound **24** was carried out as described for 8-bicyclo[2.2.2]octylxanthine **21**, following general procedure A: to a solution of Boc-β-Ala-OH (12 mg, 61 μmol, 1.0 equiv) in DMF (0.5 mL) was added DIPEA (21 μL, 122 μmol, 2.0 equiv) followed by COMU (29 mg, 67 μmol, 1.10 equiv) and intermediate **18b** (30 mg, μmol, 1.10 equiv) previously dissolved in DMF (0.5 mL). Purification by flash column chromatography using a gradient of 96:4 to 94:6 DCM/MeOH gave the title compound as an off-white solid (36 mg, 92%). LC/MS

m/z calcd for $C_{31}H_{50}N_7O_6$ $[MH]^+$: 616.37, found 616.40 t_R = 3.43 min (method A). 1H NMR ($CDCl_3$) δ 6.58–6.49 (m, 2H), 5.20 (s, 1H), 4.09 (t, J = 6.5 Hz, 2H), 4.02 (t, J = 6.7 Hz, 2H), 3.41 (t, J = 5.3 Hz, 2H), 3.31–3.23 (m, 4H), 2.45 (t, J = 6.1 Hz, 2H), 2.11–2.04 (m, 6H), 1.96–1.89 (m, 6H), 1.79 (h, J = 6.5 Hz, 2H), 1.70 (h, J = 6.4 Hz, 2H), 1.65–1.56 (m, 2H), 1.42 (s, 9H), 0.96 (t, J = 7.4 Hz, 6H). ^{13}C NMR ($CDCl_3$) δ 177.9, 161.1, 157.9, 156.4, 155.5, 151.2, 148.8, 106.9, 47.7, 45.4, 43.3, 39.2, 36.8, 35.8, 35.5, 33.9, 30.2, 29.8, 28.6, 28.5, 21.5, 21.5, 11.6, 11.3.

tert-Butyl(3-((3-(4-(2,6-dioxo-1,3-dipropyl-2,3,6,9-tetrahydro-1H-purin-8-yl)bicyclo[2.2.2]octane-1-carboxamido)propyl)amino)-3-oxopropyl)carbamate (**25b**). Following general procedure B, the intermediate 3-((3-(4-(2,6-dioxo-1,3-dipropyl-2,3,6,7-tetrahydro-1H-purin-8-yl)bicyclo[2.2.2]octane-1-carboxamido)propyl)amino)-3-oxopropan-1-aminium chloride was synthesized and used for the subsequent step without further purification. The synthesis of the title compound **25b** was carried out as described for xanthine **24**, following general procedure A: to a solution of Boc- β -Ala-OH (11 mg, 58 μ mol, 1.0 equiv), DIPEA (41 μ L, 233 μ mol, 4.0 equiv), and COMU (22 mg, 64 μ mol, 1.10 equiv) in DMF (0.5 mL) was added a solution of 3-((3-(4-(2,6-dioxo-1,3-dipropyl-2,3,6,7-tetrahydro-1H-purin-8-yl)bicyclo[2.2.2]octane-1-carboxamido)propyl)amino)-3-oxopropan-1-aminium chloride (33 mg, 64 μ mol, 1.10 equiv) in DMF (0.5 mL). Purification by flash column chromatography using a gradient of 96:4 to 93:7 DCM/MeOH gave the title compound as an off-white solid (12 mg, 31%). LC/MS m/z calcd for $C_{34}H_{55}N_8O_7$ $[MH]^+$: 687.20, found 687.40 t_R = 3.38 min (method A). HRMS (TOF ES⁺) calcd for $C_{34}H_{55}N_8O_7$ 687.4188, found 687.4202; calcd for $C_{34}H_{55}N_8O_7$ Na 709.4008, found 709.4026. 1H NMR (CD_3OD) δ 4.07 (t, J = 6.9 Hz, 2H), 3.95 (t, J = 6.9 Hz, 2H), 3.46 (t, J = 6.7 Hz, 2H), 3.31 (s, 2H), 3.22 (dt, J = 6.7, 4.2 Hz, 4H), 2.39 (dt, J = 15.7, 6.8 Hz, 4H), 2.06–1.99 (m, 6H), 1.95–1.89 (m, 6H), 1.78 (h, J = 6.9 Hz, 2H), 1.72–1.61 (m, 4H), 1.44 (s, 9H), 0.96 (t, J = 7.3 Hz, 6H). ^{13}C NMR (CD_3OD) δ 190.9, 181.9, 159.9, 156.0, 153.9, 143.9, 109.1, 108.3, 83.8, 82.3, 73.34, 57.9, 40.2, 36.9, 34.9, 31.0, 29.3, 28.8, 22.4, 22.3, 19.4, 11.5, 11.3. Analytical RP-HPLC t_R = 5.30 min, purity >99% (method C).

5,6-Diamino-1-benzyl-3-propylpyrimidine-2,4(1H,3H)-dione (**32**).⁷² A solution of 6-amino-1-benzyl-5-nitroso-3-propylpyrimidine-2,4(1H,3H)-dione (**31**) (0.250 g, 0.87 mmol, 1 equiv) in water (25 mL) and 30% NH_3OH (10 mL) was heated to 85 °C, and sodium dithionite (3.0 equiv) was added in small portions until the color disappeared. The reaction was cooled to rt., and the mixture was extracted with EtOAc. The organic phase was dried over anhydrous $MgSO_4$, filtered, and evaporated to dryness to give the title compound as yellow solid (0.218 g, 92%). LC/MS m/z calcd for $C_{14}H_{19}N_4O_2$ $[MH]^+$: 275.14, found 275.10 t_R = 2.90 min (method A). 1H NMR ($DMSO-d_6$) δ 7.36–7.30 (m, 2H), 7.27–7.22 (m, 1H), 7.21–7.15 (m, 2H), 6.13 (s, 2H), 5.13 (s, 2H), 3.76 (t, J = 6.2 Hz, 2H), 2.95 (br s, 2H), 1.51 (h, J = 7.3 Hz, 2H), 0.82 (t, J = 7.5 Hz, 3H). ^{13}C NMR ($DMSO-d_6$) δ 158.9, 149.8, 144.1, 136.9, 128.4, 127.1, 126.4, 96.3, 44.9, 42.0, 20.9, 11.2.

8-((1R,3R,5S)-Adamantan-1-yl)-3-benzyl-1-propyl-3,7-dihydro-1H-purine-2,6-dione (**33**). To a solution of xanthine **32** (0.201 g, 0.73 mmol, 1.0 equiv) in DMF (1 mL) was added DIPEA (0.13 mL, 0.73 mmol, 1.10 equiv). The resulting mixture was added to a solution of 1-adamantane carboxylic acid (0.120 g, 0.67 mmol, 1 equiv) and COMU (0.314 g, 0.73 mmol, 1.10 equiv) in DMF (1 mL). The resulting solution was stirred at rt. for 15 min. Upon completion of the reaction (LC–MS), cold water was added to the reaction mixture and subsequent precipitation of a white solid occurred. The solid was filtrated, washed with cold water, and dried. The title intermediate (1R,3R,5S)-*N*-(6-amino-1-benzyl-2,4-dioxo-3-propyl-1,2,3,4-tetrahydropyrimidin-5-yl)adamantane-1-carboxamide was obtained as an off-white solid (0.254 g, 87%).⁷³ LC/MS m/z calcd for $C_{25}H_{33}N_4O_4$ $[MH]^+$: 437.14, found 437.20 t_R = 2.99 min (method A). 1H NMR ($DMSO-d_6$) δ 7.83 (s, 1H), 7.37–7.31 (m, 2H), 7.27–7.22 (m, 1H), 7.23–7.17 (m, 2H), 6.28 (s, 2H), 5.16 (s, 2H), 3.71 (t, J = 7.2, 2H), 2.00–1.92 (m, 3H), 1.89–1.86 (m, 5H), 1.71–1.60 (m, 6H), 1.49 (h, J = 7.3 Hz, 2H), 0.82 (t, J = 7.5 Hz, 3H). ^{13}C NMR ($DMSO-d_6$)

δ 177.9, 159.0, 151.5, 150.7, 136.6, 128.6, 127.3, 126.4, 88.3, 45.2, 42.1, 36.3, 27.8, 20.9, 11.3. (1R,3R,5S)-*N*-(6-Amino-1-benzyl-2,4-dioxo-3-propyl-1,2,3,4-tetrahydropyrimidin-5-yl)adamantane-1-carboxamide (0.254 g, 0.58 mmol, 1.0 equiv) was dissolved in propan-2-ol (7 mL). To the resulting mixture was added 1 M KOH (7 mL), and the resulting solution was heated to reflux for 1 h. Upon completion of the reaction, the solvent was removed under reduced pressure and the residue was taken up in water and extracted with DCM (2 \times 20 mL). The organic layers were combined, dried over anhydrous $MgSO_4$, filtered, and evaporated to dryness to give the title compound as a pale yellow solid. Subsequent recrystallization from hot ethanol and water gave the title compound as a fluffy off-white solid (0.232 g, 95%). LC/MS m/z calcd for $C_{25}H_{31}N_4O_4$ $[MH]^+$: 419.20, found 419.20 t_R = 4.73 min (method A). 1H NMR ($CDCl_3$) δ 12.10 (s, 1H), 7.60–7.56 (m, 2H), 7.34–7.24 (m, 3H), 5.32 (s, 2H), 4.04 (t, J = 6.3 Hz, 2H), 2.19–2.09 (m, 9H), 1.90–1.77 (m, 6H), 1.69 (h, J = 6.5 Hz, 2H), 0.94 (t, J = 7.4 Hz, 3H). ^{13}C NMR ($CDCl_3$) δ 162.8, 155.5, 151.3, 148.9, 136.9, 129.3, 128.5, 127.8, 106.7, 46.9, 43.3, 41.0, 36.6, 35.9, 28.3, 21.4, 11.4.

Methyl 4-((2-((*tert*-Butoxycarbonyl)amino)ethyl)carbamoyl)benzoate (**37**). 4-(Methoxycarbonyl)benzoic acid **36** (0.200 g, 1.11 mmol, 1.0 equiv) was dissolved in DMF (2 mL). To the resulting solution were added DIPEA (0.21 mL, 1.22 mmol, 1.10 equiv), COMU (0.523 g, 1.22 mmol, 1.10 equiv), and *tert*-butyl (2-aminoethyl) carbamate (0.19 mL, 1.22 mmol, 1.10 equiv). The reaction was stirred at rt. for 20 min. Upon completion of reaction, checked by LC–MS and TLC, cold water (7 mL) was added and a pale pink precipitate was developed, which was collected by suction filtration and washed with cold water. The title compound was obtained after air drying (0.270 g, 75%). LC/MS m/z calcd for $C_{16}H_{22}N_2O_5$ $[MH]^+$: 223.15, found 223.10 (–Boc); t_R = 2.69 min (method A). 1H NMR ($CDCl_3$) δ 8.08 (d, J = 8.0 Hz, 2H), 7.89 (d, J = 7.3 Hz, 2H), 7.43 (br s, 1H), 5.00 (br s, 1H), 3.94 (s, 3H), 3.56 (dt, J = 6.5, 4.8 Hz, 2H), 3.45–3.39 (m, 2H), 1.43 (s, 9H). ^{13}C NMR ($CDCl_3$) δ 166.9, 166.5, 155.6, 138.2, 132.8, 129.9, 127.2, 80.4, 52.5, 28.5.

4-((2-((*tert*-Butoxycarbonyl)amino)ethyl)carbamoyl)benzoic Acid (**38**). Methyl 4-((2-((*tert*-butoxycarbonyl)amino)ethyl)carbamoyl)benzoate (**37**) (0.260 g, 0.81 mmol, 1.0 equiv) was dissolved in THF (10 mL). To the resulting mixture was added 1 M NaOH (8 mL), and the solution was stirred at rt. for 3 h. Upon completion of the reaction checked by TLC and LCMS, the organic layer was removed under reduced pressure. The dropwise addition of conc. HCl gave the title compound as white solid, which was obtained after suction filtration and vacuum drying (0.223, 90%). LC/MS m/z calcd for $C_{15}H_{21}N_2O_5$ $[MH]^+$: 209.14, found 209.10 (–Boc); calcd for $C_{15}H_{21}N_2O_5Na$ $[MH]^+$ 331.14, found 331.10; t_R = 3.18 min. (method A). 1H NMR (CD_3OD) δ 8.08 (d, 2H), 7.89 (d, J = 8.3 Hz, 2H), 3.46 (t, J = 5.6 Hz, 2H), 3.28 (t, J = 6.1 Hz, 2H), 1.41 (s, 9H). ^{13}C NMR (CD_3OD) δ 169.0, 158.8, 139.6, 134.8, 130.8, 128.4, 80.2, 41.5, 40.8, 28.7.

tert-Butyl(2-(4-((3-bromopropyl)carbamoyl)benzamido)ethyl)carbamate (**39**). To a solution of 4-((2-((*tert*-Butoxycarbonyl)amino)ethyl)carbamoyl)benzoic acid **38** (0.100 g, 0.32 mmol, 1.0 equiv) in DMF (2 mL) were added COMU (0.153 g, 0.36 mmol, 1.10 equiv) and 3-bromopropyl amine hydrobromide (0.092 g, 0.42 mmol, 1.30 equiv). DIPEA (0.112 mL, 0.65 mmol, 2.0 equiv) was subsequently added to the reaction mixture dropwise. The resulting mixture was stirred at rt. for 15 min. Completion of the reaction was checked by TLC (R_f 0.35 in DCM/MeOH 95:5) and LCMS. The resulting mixture was diluted with water and extracted with EtOAc. The organic layer was subsequently washed with 1 M HCl (10 mL), dried over $MgSO_4$, filtered, and concentrated to dryness to afford the crude product as orange oil. Purification by flash column chromatography on a gradient of 97:3 to 94:6% DCM/MeOH afforded the title product as an off-white solid (0.085 g, 61%). 1H NMR ($DMSO-d_6$) δ 8.70 (t, J = 5.6 Hz, 1H), 8.55 (t, J = 5.3 Hz, 1H), 7.83 (s, 4H), 3.51 (t, J = 6.6 Hz, 2H), 3.40–3.33 (m, 2H), 3.31–3.26 (m, 2H), 3.10 (t, J = 6.1 Hz, 2H), 2.05 (p, J = 6.7 Hz, 2H), 1.31 (s,

9H). ^{13}C NMR (DMSO- d_6) δ 167.6, 155.1, 129.9, 128.2, 36.8, 36.0, 34.3, 33.1, 28.8 (two quaternary carbon not observed).

8-((1R,3R,5S)-Adamantan-1-yl)-3-benzyl-1-propyl-7-((2-trimethylsilyloxy)methyl)-3,7-dihydro-1H-purine-2,6-dione (34). Potassium carbonate was added to a solution of xanthine **33** (0.232 g, 0.55 mmol, 1.0 equiv) in DMF (3 mL), and the resulting mixture was stirred at rt. for 2 h. (2-(Chloromethoxy)ethyl)-trimethylsilane (0.110 g, 0.67 mmol, 1.20 equiv) was added dropwise, and the solution was stirred at rt. for additional 2 h. TLC showed complete consumption of the starting material. The reaction was then evaporated to dryness, and the residue was adsorbed on isolute. Purification by flash column chromatography using a gradient of 100:0 to 80:20 PE/EtOAc gave the title compound as colorless oil, which solidified upon cooling (0.200 g, 66%). ^1H NMR (CDCl_3) δ 7.61–7.56 (m, 2H), 7.34–7.24 (m, 3H), 5.91 (s, 2H), 5.26 (s, 2H), 3.94 (t, J = 6.9 Hz, 2H), 3.70 (t, J = 6.9 Hz, 2H), 2.23–2.17 (m, 6H), 2.15–2.09 (m, 3H), 1.85–1.78 (m, 6H), 1.64 (h, J = 7.2 Hz, 2H), 0.96–0.90 (m, 5H), –0.02 (s, 9H). ^{13}C NMR (CDCl_3) δ 161.6, 155.3, 151.3, 147.0, 137.0, 129.5, 128.5, 127.9, 107.6, 73.6, 66.5, 46.5, 43.1, 40.9, 37.9, 36.6, 28.5, 21.5, 18.2, 11.5, –1.3.

8-((1R,3R,5S)-Adamantan-1-yl)-1-propyl-7-((2-trimethylsilyloxy)methyl)-3,7-dihydro-1H-purine-2,6-dione (35).¹⁰⁶ Xanthine **34** (0.188 g, 0.34 mmol, 1.0 equiv) was dissolved in methanol, and to the solution was added 10% Pd/C (100 mg), followed by ammonium formate (3.53 mmol, 15 equiv). The flask was equipped with a condenser with a balloon with N_2 at the top and heated to 140 °C for 9 h. The completion of the reaction was monitored by TLC. The reaction mixture was then cooled to rt. and filtered through Celite. The pad was washed with MeOH and DCM. The colorless solution was concentrated to dryness to give the title compound as an off-white solid (0.105 g, 67%). ^1H NMR (CDCl_3) δ 5.93 (s, 2H), 3.95 (t, J = 7.2, 5.4 Hz, 2H), 3.71 (t, J = 7.2 Hz, 2H), 2.19 (s, 6H), 2.09 (s, 3H), 1.78 (s, 6H), 1.66 (h, J = 7.6 Hz, 2H), 0.98–0.89 (m, 5H), –0.02 (s, 9H). ^{13}C NMR (CDCl_3) δ 162.1, 155.9, 107.7, 73.6, 66.5, 42.5, 40.8, 37.9, 36.5, 28.4, 21.5, 18.2, 11.5, –1.3.

tert-Butyl(2-(4-((3-(8-((3R,5R,7R)-adamantan-1-yl)-2,6-dioxo-1-propyl-7-((2-trimethylsilyloxy)methyl)-1,2,6,7-tetrahydro-3H-purin-3-yl)propyl)carbamoyl)benzamido)ethyl)carbamate (40). To a solution of xanthine **35** (105 mg, 1.0 equiv) in DMF (2 mL) was added K_2CO_3 (42 mg, 1.3 equiv). The resulting mixture was stirred at rt. for 1 h. After that time, a solution of *tert*-butyl (2-(4-((3-bromopropyl)carbamoyl)benzamido)ethyl)carbamate (**39**) (113 mg, 1.15 equiv) in DMF (1 mL) was added to the reaction mixture, which was stirred at 40 °C for 23 h. The reaction was subsequently filtered and concentrated to dryness. The crude material was adsorbed on isolute and purified by flash column chromatography using a gradient of 50:50 to 20:80 PE/EtOAc to give the title compound as off-white foam (90 mg, 49%). ^1H NMR (CDCl_3) δ 7.90 (s, 4H), 7.78 (t, J = 6.1 Hz, 1H), 7.47 (s, 1H), 5.92 (s, 2H), 5.14 (br s, 1H), 4.26 (t, J = 5.6 Hz, 2H), 3.98 (t, J = 7.3 Hz, 2H), 3.71 (t, J = 8.0 Hz, 2H), 3.56 (q, J = 4.8 Hz, 2H), 3.45–3.37 (m, 4H), 2.13–2.08 (m, 6H), 2.08–1.97 (m, 5H), 1.76–1.60 (m, 8H), 1.42 (s, 9H), 0.93 (m, 5H), –0.03 (s, 9H). ^{13}C NMR (CDCl_3) δ 166.9, 161.9, 155.1, 151.8, 147.0, 137.7, 136.7, 107.7, 80.2, 73.7, 66.6, 43.1, 40.9, 40.4, 37.9, 36.4, 35.9, 28.5, 28.3, 21.5, 18.2, 11.5, –1.3.

N^1 -(3-(8-((3R,5R,7R)-Adamantan-1-yl)-2,6-dioxo-1-propyl-1,2,6,7-tetrahydro-3H-purin-3-yl)propyl)- N^4 -(2-aminoethyl)terephthalamide (41). The synthesis of the title compound **41** was achieved by following general procedure B. The title compound **31** was used for the subsequent step without any further purification (29 mg, quantitative). LC–MS m/z calcd for $\text{C}_{31}\text{H}_{42}\text{N}_7\text{O}_4$ $[\text{MH}]^+$: 576.20, found 576.40; t_{R} = 3.16 min (method A).

tert-Butyl(3-((2-(4-((3-(8-((3R,5R,7R)-adamantan-1-yl)-2,6-dioxo-1-propyl-1,2,6,7-tetrahydro-3H-purin-3-yl)propyl)carbamoyl)benzamido)ethyl)amino)-3-oxopropyl)carbamate (42). The title compound **42** was synthesized by following general procedure A, reacting a solution of Boc- β -Ala-OH (10 mg, 1.0 equiv), DIPEA (18 μL , 2.0 equiv) and COMU (24.90 mg, 1.10 equiv) in DMF (0.5 mL) with a solution of N^1 -(3-(8-((1R,3R,5S)-adamantan-1-yl)-2,6-dioxo-1-propyl-1,2,6,7-tetrahydro-3H-purin-3-yl)propyl)- N^4 -(2-aminoethyl)terephthalamide (**41**) (34 mg, 1.10 equiv) in DMF (0.5

mL). Purification by flash column chromatography using a gradient of 96:4 to 93:7 DCM/MeOH gave the title compound as an off-white solid (18 mg, 47%). LC/MS m/z calcd for $\text{C}_{39}\text{H}_{55}\text{N}_8\text{O}_7$ $[\text{MH}]^+$: 747.40, found 747.40; t_{R} = 3.71 min (method A). ^1H NMR (CD_3OD) δ 7.93 (s, 4H), 4.59 (s, 1H), 4.26 (t, J = 6.6 Hz, 2H), 3.95 (t, J = 6.3 Hz, 2H), 3.52 (t, J = 5.8 Hz, 2H), 3.48–3.39 (m, 4H), 3.36 (s, 2H), 2.37 (t, J = 6.7 Hz, 2H), 2.10 (q, J = 6.5 Hz, 2H), 2.02–1.96 (m, 9H), 1.81–1.70 (m, 6H), 1.69–1.62 (m, 2H), 1.42 (s, 9H), 0.94 (t, J = 7.5 Hz, 3H). ^{13}C NMR (CD_3OD) δ 187.4, 181.9, 169.2, 163.6, 156.0, 152.9, 149.5, 138.7, 138.2, 128.6, 128.5, 107.9, 80.2, 43.9, 42.2, 41.9, 40.9, 40.1, 38.0, 37.6, 37.4, 36.9, 29.5, 28.9, 28.7, 22.3, 11.6.

(E)-N-(2-(6-(2-(4-(2-(5,5-Difluoro-7-(thiophen-2-yl)-5H-4 H ,5 I -dipyrrrolo[1,2-c:2',1'-f][1,3,2]diazaborinin-3-yl)vinyl)phenoxy)acetamido)hexanamido)ethyl)-4-(2,6-dioxo-1,3-dipropyl-2,3,6,7-tetrahydro-1H-purin-8-yl)bicyclo[2.2.2]octane-1-carboxamide (43a). Following general procedure C, amine congener **18a** (0.5 mg, 1.10 equiv) was converted to the BODIPY 630/650 conjugate. Purification by RP-HPLC (method B) gave, after lyophilization, the title compound as a blue solid (0.4 mg, 39%). LC/MS m/z calcd for $\text{C}_{51}\text{H}_{61}\text{BF}_2\text{N}_9\text{O}_6\text{S}$ $[\text{MH}]^+$: 976.30, found 976.30 t_{R} = 3.98 min (method A). HRMS (TOF ES $^+$) calcd for $\text{C}_{51}\text{H}_{61}\text{BF}_2\text{N}_9\text{O}_6\text{S}$ $[\text{MH}]^+$: 976.4530, found 976.4530; calcd for $\text{C}_{51}\text{H}_{61}\text{BF}_2\text{N}_9\text{O}_6\text{SNa}$ $[\text{M} + \text{Na}]^+$: 998.4349, found 998.4335. Analytical RP-HPLC t_{R} = 6.86 min, purity >99% (method C).

1-(6-((2-(4-(2,6-Dioxo-1,3-dipropyl-2,3,6,7-tetrahydro-1H-purin-8-yl)bicyclo[2.2.2]octane-1-carboxamido)ethyl)amino)-6-oxohexyl)-3,3-dimethyl-2-((1E,3E)-5-((E)-1,3,3-trimethyl-5-sulfoindolin-2-ylidene)penta-1,3-dien-1-yl)-3H-indol-1-ium-5-sulfonate (43b). Following general procedure C, amine congener **18a** (0.5 mg, 1.10 equiv) was converted to the Sulfo-Cy5 conjugate **43b**. Purification by RP-HPLC (method B) gave after lyophilization the title compound as a bright blue solid (0.5 mg, 56%). LC/MS m/z calcd for $\text{C}_{54}\text{H}_{71}\text{N}_8\text{O}_{10}\text{S}_2$ $[\text{MH}]^+$: 1055.30, found 1055.30; t_{R} = 3.09 min (method A). HRMS (TOF ES $^+$) calcd for $\text{C}_{54}\text{H}_{71}\text{N}_8\text{O}_{10}\text{S}_2$ $[\text{MH}]^+$: 1055.4729, found 1055.4705; calcd for $\text{C}_{54}\text{H}_{71}\text{N}_8\text{O}_{10}\text{S}_2\text{Na}$ $[\text{M} + \text{Na}]^+$: 1077.4549, found 1077.4527. Analytical RP-HPLC t_{R} = 4.93 min, purity >99% (method C).

(E)-N-(20-(4-(2-(5,5-Difluoro-7-(thiophen-2-yl)-5H-4 H ,5 I -dipyrrrolo[1,2-c:2',1'-f][1,3,2]diazaborinin-3-yl)vinyl)phenoxy)-4,8,12,19-tetraoxo-3,7,11,18-tetraazacocoyl)-4-(2,6-dioxo-1,3-dipropyl-2,3,6,9-tetrahydro-1H-purin-8-yl)bicyclo[2.2.2]octane-1-carboxamide (44a). Following general procedure B, compound **25a** (5 mg, 1.0 equiv) was subjected to acidolysis, and after the removal of the solvent, the resulting intermediate (as HCl salt) was used for the next step without further purification (4 mg, quantitative). LC–MS m/z calcd for $\text{C}_{28}\text{H}_{45}\text{N}_8\text{O}_5$ $[\text{MH}]^+$: 573.34, found 573.30 t_{R} = 3.13 min. Following general procedure C, the resulting amine congener was converted to the BODIPY 630/650 conjugate. Purification by RP-HPLC (method B) gave, after lyophilization, the title compound as a blue solid (0.9 mg, 70%). LC/MS m/z calcd for $\text{C}_{57}\text{H}_{71}\text{BF}_2\text{N}_{11}\text{O}_5\text{S}$ $[\text{MH}]^+$: 1118.30, found 1118.40 t_{R} = 3.78 min (method A). HRMS (TOF ES $^+$) calcd for $\text{C}_{57}\text{H}_{71}\text{BF}_2\text{N}_{11}\text{O}_5\text{S}$ $[\text{MH}]^+$: 1118.5273 found 1118.5252; calcd for $\text{C}_{57}\text{H}_{71}\text{BF}_2\text{N}_{11}\text{O}_5\text{SNa}$ $[\text{M} + \text{Na}]^+$: 1140.5092, found 1140.506. Analytical RP-HPLC t_{R} = 6.73 min, purity >99% (method C).

1-(1-(4-(2,6-Dioxo-1,3-dipropyl-2,3,6,7-tetrahydro-1H-purin-8-yl)bicyclo[2.2.2]octane-1-yl)-1,6,10,14-tetraoxo-2,5,9,13-tetraazanonadecan-19-yl)-3,3-dimethyl-2-((1E,3E)-5-((E)-1,3,3-trimethyl-5-sulfoindolin-2-ylidene)penta-1,3-dien-1-yl)-3H-indol-1-ium-5-sulfonate (44b). Following Boc-deprotection of **25a**, the resulting amine congener (0.5 mg, 1.10 equiv) was converted to the Sulfo-Cy5 conjugate **44b** by following general procedure C. Purification by RP-HPLC (method B) gave, after lyophilization, the title compound as a bright blue solid (1.1 mg, quantitative). LC/MS m/z calcd for $\text{C}_{60}\text{H}_{79}\text{N}_{10}\text{O}_{12}\text{S}_2$ $[\text{MH}]^+$: 1195.54, found 1195.60; t_{R} = 3.05 min (method A). HRMS (TOF ES $^+$) calcd for $\text{C}_{60}\text{H}_{81}\text{N}_{10}\text{O}_{12}\text{S}_2$ $[\text{MH}]^+$: 1197.5471, found 1197.5450; calcd for $\text{C}_{60}\text{H}_{81}\text{N}_{10}\text{O}_{12}\text{S}_2\text{Na}$ $[\text{M} + \text{Na}]^+$: 1219.5291, found 1219.5255. Analytical RP-HPLC t_{R} = 4.88 min, purity >99% (method C).

N^1 -(3-(8-((3R,5R,7R)-Adamantan-1-yl)-2,6-dioxo-1-propyl-1,2,6,7-tetrahydro-3H-purin-3-yl)propyl)- N^4 -(2-(6-(2-(4-(E)-2-(5-5-

difluoro-7-(thiophen-2-yl)-5H-4^H,5^H-dipyrrolo[1,2-c:2',1'-f][1,3,2]-diazaborinin-3-yl(vinyl)phenoxyacetamido)hexanamido)ethyl)terephthalamide (**45a**). Following general procedure C, amine congener **41** (0.7 mg, 1.10 equiv) was converted to the BODIPY 630/650 conjugate. Purification by RP-HPLC (method B) gave, after lyophilization, the title compound as a blue solid (0.7 mg, 59%). LC/MS *m/z* calcd for C₆₀H₆₈BF₂N₁₀O₇S [MH]⁺: 1121.30, found 1121.30 *t_R* = 4.05 min (method A). HRMS (TOF ES⁺) calcd for C₆₀H₆₈BF₂N₁₀O₇S [MH]⁺: 1121.5059, found 1121.5060; calcd for C₆₀H₆₈BF₂N₁₀O₇SNa [M + Na]⁺: 1143.4878, found 1143.4855. Analytical RP-HPLC *t_R* = 7.00 min, purity >99% (method C).

1-(6-((2-(4-(3-(8-(3R,5R,7R)-Adamantan-1-yl)-2,6-dioxo-1-propyl-1,2,6,7-tetrahydro-3H-purin-3-yl)propyl)carbamoyl)benzamido)ethyl)amino)-6-oxohexyl)-3,3-dimethyl-2-((1E,3E)-5-((E)-1,3,3-trimethyl-5-sulfoindolin-2-ylidene)pent-1,3-dien-1-yl)-3H-indol-1-ium-5-sulfonate (**45b**). Following general procedure C, amine congener **41** (0.6 mg, 1.10 equiv) was converted to the Sulfo-Cy5 conjugate **45b**. Purification by RP-HPLC (method B), followed by preparative TLC using 80:20 DCM/MeOH as an eluent, after lyophilization, the title compound as a bright blue solid (0.9 mg, 83%). LC/MS *m/z* calcd for C₆₃H₇₈N₉O₁₁S₂ [M-2]⁺: 600.76, found 600.8; *t_R* = 3.19 min (method A). HRMS (TOF ES⁺) calcd for C₆₃H₇₈N₉O₁₁S₂ [MH]⁺: 1200.5257, found 1200.5220; [M-2]⁺: 600.7665, found 600.7680. Analytical RP-HPLC *t_R* = 5.19 min, purity >99% (method C).

N¹-(3-(8-(3R,5R,7R)-Adamantan-1-yl)-2,6-dioxo-1-propyl-1,2,6,7-tetrahydro-3H-purin-3-yl)propyl)-N⁴-(2-(3-(6-(2-(4-((E)-2-(5,5-difluoro-7-(thiophen-2-yl)-5H-4^H,5^H-dipyrrolo[1,2-c:2',1'-f][1,3,2]-diazaborinin-3-yl(vinyl)phenoxyacetamido)hexanamido)propanamido)ethyl)terephthalamide (**46a**). Following general procedure B, compound **42** (5 mg, 1.0 equiv) was converted to the corresponding HCl salt intermediate, which, after the removal of the solvent in vacuo, was used for the subsequent step without further purification. LC/MS *m/z* calcd for C₃₄H₄₇N₈O₈ [MH]⁺: 647.34, found 647.40 *t_R* = 3.18 min. Following general procedure C, the resulting amine congener (0.7 mg, 1.10 equiv) was converted to the BODIPY 630/650 conjugate. Purification by RP-HPLC (method B) gave the title compound as a blue solid (0.7 mg, 56%). LC-MS *m/z* calcd for C₆₃H₇₃BF₂N₁₀O₈S [MH]⁺: 1192.40, found 1192.40 *t_R* = 3.95 min (method A). HRMS (TOF ES⁺) calcd for C₆₃H₇₃BF₂N₁₀O₈S [MH]⁺: 1192.5430, found 1192.5433; calcd for C₆₃H₇₃BF₂N₁₀O₈SNa [M + Na]⁺: 1214.5250, found 1214.5229. Analytical RP-HPLC *t_R* = 6.98 min, purity >97% (method C).

1-(6-((3-(2-(4-(3-(8-(3R,5R,7R)-Adamantan-1-yl)-2,6-dioxo-1-propyl-1,2,6,7-tetrahydro-3H-purin-3-yl)propyl)carbamoyl)benzamido)ethyl)amino)-3-oxopropyl)amino)-6-oxohexyl)-3,3-dimethyl-2-((1E,3E)-5-((E)-1,3,3-trimethyl-5-sulfoindolin-2-ylidene)pent-1,3-dien-1-yl)-3H-indol-1-ium-5-sulfonate (**46b**). Following general procedure C, the amine congener (0.6 mg, 1.10 equiv) was converted to the Sulfo-Cy5 conjugate **46b**. Purification by RP-HPLC (method B), followed by preparative TLC using 80:20 DCM/MeOH, after lyophilization, was isolated the title compound as a bright blue solid (0.9 mg, 79%). LC-MS *m/z* calcd for C₆₆H₈₃N₁₀O₁₂S₂ [M-2]⁺: 636.3, found 636.3; *t_R* = 3.17 min (method A). HRMS (TOF ES⁺) calcd for C₆₆H₈₃N₁₀O₁₂S₂ [MH]⁺: 1271.5628, found 1271.5571; calcd for C₆₆H₈₃N₁₀O₁₂S₂Na [M + Na]⁺: 1293.5447, found 1293.5364; [M-2]⁺: 636.2850, found 636.2861. Analytical RP-HPLC *t_R* = 5.25 min, purity >99% (method C).

Molecular Modeling of Tonapofylline (BG9928) and Compound 16. Molecular docking simulation of tonapofylline (BG9928) and **16** to the 3.2 Å resolution A₁AR crystal structure was performed using Schrödinger software suite (release 2019-2). The 3.2 Å A₁AR crystal structure in complex with the irreversible ligand DU172 was retrieved from the Protein Data Bank (PDB: 5UEN) depository and was firstly prepared in PyMOL (2.2.0) as follows: one copy of the A₁AR-dimer crystal structure was removed and the covalent bond between the Y271 and irreversible antagonist DU172 was broken to facilitate the definition of docking site during the Grid generation step. This structure was subsequently imported on Maestro and was prepared with the Protein Preparation Wizard tool. Hydrogen atoms were added, and the H-bonding network was

optimized using PROPKA at pH = 7.0. The structure of the protein was energy minimized using an OPLS3 force field. The docking site was defined using Glide Grid generation with the barycenter of the co-crystallized DU172 representing the center of the grid. Tonapofylline **16** and congener **42** were prepared for docking using a LigPrep tool. Molecular docking of these two ligands was performed using Glide with XP (extra precision) mode and flexible ligand sampling with no restriction applied. For both ligands, the highest docking scoring pose was selected and depicted with PyMOL to include key binding interactions and distance measurements.

Pharmacology: Materials and Methods. Dulbecco's modified Eagle's medium (DMEM), fetal bovine serum (FBS), and trypsin were purchased from Invitrogen (Carlsbad, CA). Adenosine deaminase (ADA) and hygromycin B were purchased from Roche Diagnostics (Mannheim, Germany). Ultima Gold scintillation cocktail, [³H] DPCPX (8-cyclopentyl-1,3-dipropylxanthine, [dipropyl-2,3-³H(N)], specific activity 137 Ci/mmol), and LANCE→ cAMP kit were purchased from PerkinElmer Life Sciences (Glen Waverley, Australia). All plates were obtained from Corning Costar (Corning Incorporated, Corning, NY, USA). Furimazine was purchased from Promega (Alexandria, Australia). Adenosine receptor ligands, 8-(4-(4-(4-chlorophenyl)piperazine-1-sulfonyl)phenyl)-1-propylxanthine (PSB-603), *N*-[9-chloro-2-(2-furanyl)[1,2,4]-triazolo[1,5-*c*]-quinazolin-5-yl]benzene acetamide (MRS1220), 4-(2-[7-Amino-2-(2-furyl)[1,2,4]triazolo[2,3-*a*][1,3,5]triazin-5-ylamino]ethyl)phenol (ZM241385), and *trans*-4-((2-phenyl-7H-pyrrolo[2,3-*d*]pyrimidin-4-yl)amino)cyclohexanol (SLV320) were purchased from Tocris Bioscience (Bristol, UK). 8-Cyclopentyl-1,3-dipropylxanthine (DPCPX), 5'-(*N*-ethylcarboxamido)adenosine (NECA), and all other reagents were purchased from Sigma-Aldrich (Castel Hill, Australia) and were of analytical quality.

Cell Culture. Chinese Hamster Ovary FlpIn (FlpIn-CHO) cells stably expressing the human A₁AR were generated as described previously.¹⁰⁷ A₁AR-FlpIn-CHO cell lines were cultured in DMEM, supplemented with 10% (v/v) FBS and the selection antibiotic hygromycin B (500 μg/mL) to maintain adenosine receptor expression. Nontransfected HEK293 adherent (HEK293A) cells were cultured in DMEM, supplemented with 10% (v/v) FBS. All cells were cultured at 37 °C in a humidified incubator containing 5% CO₂, grown to confluence, and then seeded into 96-well culture plates at assay-specific densities. All tissue culture procedures were performed in a class II laminar flow hood using sterile conditions. Transfection of NanoLuc-tagged human A₁AR, A_{2A}AR, A_{2B}AR, and A₃AR and SNAP-tagged-hA₁AR in HEK293A cells was performed using polyethylamine (PEI) at the 4:1 ratio of PEI/DNA. Cells were transfected with 3 μg of DNA in 10 mm × 20 mm style dishes at a density of 5 × 10⁶ cells per dish and used 48 h following transfection.

Experiments: [³H] DPCPX Binding Assay. A₁AR-FlpIn-CHO cells were seeded into white 96-well isoplates at 40,000 cells/well and incubated overnight. Before the experiment, DMEM was replaced with binding buffer (10 mM HEPES, 10 mM D-glucose, 145 mM NaCl, 5 mM KCl, 1 mM MgSO₄, 1.5 mM NaHCO₃, 2 mM CaCl₂, 1 U/mL ADA, pH 7.4), and cells were incubated with increasing concentrations of competing ligands, followed by the addition of 1 nM [³H] DPCPX (the precise concentration in each experiment was determined by β-counting). The cells were incubated for 4 h in binding buffer at 37 °C with 5% CO₂. Buffer was removed, and cells were washed three times with ice-cold phosphate buffer saline (PBS, 10 mM Na₂HPO₄, 1.8 mM KH₂PO₄, 137 mM NaCl, 2.7 mM KCl) and then dissolved in Ultima Gold scintillation liquid (100 μL/well). Isoplates were sealed and allowed to incubate at rt. for 1 h before radioactivity was determined by β-counting using a MicroBeta 2 LumijET microplate counter (PerkinElmer). In all radioligand binding experiments, nonspecific binding was determined in the presence of 1 mM SLV320.

NanoBRET Binding Assays. HEK293A cells were transiently transfected to express either the NanoLuc-tagged human A₁AR, A_{2A}AR, A_{2B}AR, and A₃AR. 24 h following transfection, cells were seeded into 96-well poly-D-lysine-coated solid white bottom plates at 40,000 cells/well and incubated overnight in serum-free DMEM.

Before the experiment, DMEM was replaced with binding buffer. For saturation and competition assays, the required concentration of fluorescent ligand, and competing ligands, was added at the same time and the plates were then incubated at 37 °C for 1 h. After 50 min incubation, 1 μM furimazine was added to each well and plates were incubated for additional 10 min (1 h total) at 37 °C. For association kinetic experiments, 1 μM furimazine was added to each well and incubated at 37 °C for 15 min in the dark allowing the luminescence signal to reach equilibrium. The required concentration of the fluorescent ligand in the presence or absence of 1 μM SLV320 (to define nonspecific binding) was added simultaneously. The plates were then read immediately, with each well read once every 30 s for 60 min. Bioluminescence emission at two different wavelengths was measured at room temperature (for saturation and competition binding experiments) or at 37 °C (for kinetic binding assays) using a PheraSTAR Omega plate reader (BMG Labtech) using 460 nm (80 nm bandpass; donor NanoLuc emission) and >610 nm (long pass filter; fluorescent ligand emission). The raw BRET ratio was calculated by dividing the >610 nm emission by the 420 nm emission. In all NanoBRET binding experiments, nonspecific binding was determined in the presence of 1 μM SLV320.

CAMP Assay. A₁AR-FlpIn-CHO cells were seeded into 96-well culture plates at 20,000 cells/well and incubated overnight. The G_{i/o}-protein-mediated inhibition of cAMP accumulation was determined as described previously.¹⁰⁸ Briefly, media were removed and cells were incubated with stimulation buffer (140 mM NaCl, 5.4 mM KCl, 0.8 μM MgSO₄, 0.2 mM Na₂HPO₄, 0.44 mM KH₂PO₄, 1.3 mM CaCl₂, 5.6 mM D-glucose, 5 mM HEPES, 0.1% bovine serum albumin (BSA), 0.1 U/mL ADA, and 10 μM rolipram, pH 7.4) and incubated at 37 °C for 30 min. Inhibition of cAMP was assessed by pre-incubation with increasing concentrations of antagonists for 10 min. NECA concentration response curves were performed by subsequent incubation of increasing concentrations of NECA in the presence of 3 μM forskolin for additional 30 min at 37 °C. The reactions were terminated by the addition of 50 μL ice-cold 100% ethanol. The lysis buffer (0.1% BSA, 0.3% tween-20, 5 mM HEPES, pH 7.4) was added to the cells after ethanol evaporation. The level of cAMP was detected using LANCE cAMP 384 kits (PerkinElmer) following the manufacturer's protocol, and fluorescence was measured with an EnVision plate reader (PerkinElmer). Ligand concentration-response curves were normalized to the response mediated by 3 μM forskolin (0% or buffer (100%) alone. All experiments were performed in duplicate.

Confocal Imaging. Transiently transfected SNAP-tagged human A₁AR HEK293 cells were grown to 80–90% confluence in a μ-Slide 8 well-chambered coverslip (Ibidi GmbH, Gräfelfing, Germany) precoated with poly-D-lysine. On the day of the experiment, culture media were removed and the cells were labeled for 30 min at 37 °C with a 0.2 μM SNAP AlexaFluor488 label as required in binding buffer (10 mM HEPES, 10 mM D-glucose, 145 mM NaCl, 5 mM KCl, 1 mM MgSO₄, 1.5 mM NaHCO₃, 2 mM CaCl₂, 1 U/mL ADA, pH 7.4). After washing twice with binding buffer, the cells were treated with or without 10 μM SLV320 for 30 min at 37 °C. After that time, the cells were treated with the required concentration of fluorescent ligand under investigation. Live cell imaging was performed at 37 °C on a Leica TCS SP8 X confocal running system fitted with an HC PL APO CS2 40x/1.1 NA water immersion objective. A diode 633 laser was used for the excitation of BODIPY-630/650 and Sulfo-Cy5 fluorophores and a beam splitter TD 488/552/638 and the emission was collected using a hybrid detector (HyD) (emission filter range 642–782 nm). A 488 optically pumped semiconductor laser (OPLS) was used for the excitation of the SNAP AF488 label, and the emission was detected using a hybrid detector (HyD) (emission filter range 493–572 nm). The pinhole diameter (1 Airy Unit; 1.1 μm optical slice), laser power, and gain remained constant in all the experiments. The images were captured using 1024 × 1024 pixel resolution, 16-bit depth, and a scan speed of 200 Hz with a line averaging of 6. Images were processed in FIJI (ImageJ)¹⁰⁹ version 2.0.0 software, and linear adjustments to the brightness and contrast have been applied equally across all the images.

Total Internal Reflection Fluorescence Microscopy (TIRF-M). HEK293A cells were seeded into 10 mm × 20 mm style dishes at a density of 5 × 10⁶ cells per dish in complete DMEM. After 12 h, cells were transiently transfected with 2 μg cDNA of SNAP-hA₁AR using the 1:4 ratio of DNA/PEI to achieve lower receptor expression levels. After 12 h, transiently transfected SNAP-hA₁AR HEK293 cells were seeded onto a poly-D-lysine-precoated FluoroDish (35 mm, 23 mm well) to 70–80% confluency. On the day of the experiment (24 h following transfection), DMEM was removed and the cells were incubated with 0.2 μM BG-AF488 in binding buffer (10 mM HEPES, 10 mM D-glucose, 145 mM NaCl, 5 mM KCl, 1 mM MgSO₄, 1.5 mM NaHCO₃, 2 mM CaCl₂, 1 U/mL ADA, pH 7.4) for 30 min at 37 °C. The binding buffer was removed, and the cells were washed twice with warm binding buffer to remove any unbound BG-AF488. Subsequently, the cells were treated with or without 10 μM SLV320 for 30 min at 37 °C. After that time, the cells were treated with the required concentration of fluorescent ligand under investigation.

TIRF Imaging. Images were captured on a Leica DMI6000 3D GSD TIRF microscope running LAS X version 1.9 using a HC Plan Apo 100× NA 1.43 TIRF Objective. Excitation was provided from a 633 nm laser for the BODIPY-630/650 and Sulfo-Cy5 fluorophores. Detection was through either a 540–620 nm emission filter or 640–700 nm emission filter. The TIRF field penetration depth was kept at 80 nm for all wavelengths and samples. Images were captured with an Andor iXon3 897 Ultra EM-CCD camera with exposure times and gain settings being consistent across all images.

TIRF Image Analysis. Analysis of TIRF images were carried out using a custom macro written in the Fiji distribution of ImageJ (Schindelin et al., 2012). In brief, the user was asked to manually outline the cell of interest. Both image channels were then filtered to remove noise (Gaussian filter-Sigma = 1) and discrete spots were extracted from the red channel using the find maxima command (prominence = 3) and displaying the same as single-binary points. The extracted binary points were used to measure the intensity in both the red and far red channel for each discrete spot.

Data Analysis. All data are represented as mean ± SEM of *n* experiments performed either in duplicate or triplicate. *n* refers to the number of separate experiments. A separate experiment required a separate flask of cells and a separate drug dilution used throughout the experiment. The data were presented and analyzed using Prism software (GraphPad Prism 8.0, San Diego, CA) and Excel.

[³H] DPCPX Binding Assay and NanoBRET Competition Binding Assays. The competition binding curves were fit to the following equation:

$$\text{uninhibited specific binding} = 100 - \frac{100 \times [A]}{[A] + (IC_{50})}$$

where [A] is the concentration of competing drug and the IC₅₀ is the molar concentration of ligand required to inhibit 50% of the specific binding of specified concentrations of fluorescent ligands or 1 nM [³H] DPCPX.

The Cheng–Prusoff equation was used to correct fitted IC₅₀ values to K_i values:

$$K_i = \frac{IC_{50}}{1 + \frac{L}{K_D}}$$

where *L* is the concentration of fluorescent ligand or [³H] DPCPX in nM and K_D is the dissociation constant of fluorescent ligand or [³H] DPCPX in nM. The K_D values used were calculated from the saturation binding experiments. The concentration in the assay of [³H] DPCPX was directly determined by measuring DPM counts with a scintillation counter using the following equation:

$$[I] = \frac{\text{DPM}}{\frac{SA \times 2.2 \times 10^6}{\text{volume}}}$$

where SA is the specific activity of the radioligand in Ci/mmol and volume is the final volume of the assay in liter.

NanoBRET Saturation Binding Assay. Total and nonspecific saturation binding curves were fit simultaneously using the following equation:

$$\text{BRET ratio} = \frac{B_{\max}[B]}{B + (K_D)} + M(B) + C$$

where B_{\max} is the maximal response, $[B]$ is the concentration of fluorescent ligand in nM, K_D is the equilibrium dissociation constant in nM, M is the slope of the nonspecific binding component, and C is the intercept with the y axis.

cAMP Assay. Antagonism by fluorescent ligands of the NECA-induced inhibition of cAMP accumulation in FlpIn-CHO cells expressing the human A_1 AR was analyzed. For each concentration of the antagonists, the ratio (DR, dose ratio) of NECA concentrations required to produce the same magnitude of response in the presence and absence of the antagonist was determined. To estimate antagonist affinity values, functional interaction studies between NECA and single concentration of each antagonist in the cAMP assays were fitted to the following form of Schild regression analysis:

$$\text{response} = \text{bottom} + \frac{(E_{\max} - \text{bottom})}{1 + \left(\frac{10^{-\text{pEC}_{50}} \left[1 + \left(\frac{[B]}{10^{-\text{pA}_2}} \right)^S \right]^{\text{HillSlope}}}{[A]} \right)}$$

where pEC_{50} is the negative logarithm of the EC_{50} of NECA (A) in the absence of antagonist (B). HillSlope is the slope of the agonist curve, S is the Schild slope, and pA_2 is the negative logarithm of the molar concentration of antagonist necessary to shift the agonist EC_{50} by a factor of two. The Schild slope parameter, S , was constrained to 1, and therefore, the estimated pA_2 values for each antagonist are equal to the pK_B (negative logarithm of the antagonist equilibrium dissociation constant).

NanoBRET Kinetic Binding Assay. For association binding kinetics, nonspecific binding was determined at each concentration of the fluorescent ligands at each time point by adding 1 μM SLV320, and this was subtracted from total binding to obtain specific binding measurements. The association rate (k_{on}) in $\text{M}^{-1} \text{min}^{-1}$ and dissociation rate (k_{off}) min^{-1} constants were calculated from specific binding using the following equation:

$$k_{\text{on}} = \frac{k_{\text{obs}} - k_{\text{off}}}{[L]}$$

where $[L]$ is the concentration of the fluorescent conjugate in M and k_{obs} is calculated from the global fitting of the data to the following exponential association function:

$$Y = Y_{\max}(1 - e^{-k_{\text{obs}}t})$$

where Y is the specific binding at time t , Y_{\max} represents the specific binding at infinite time (t), and k_{obs} is the rate constant for the observed rate of association.

The kinetic equilibrium dissociation constant (K_D) was determined from the data using the following equation:

$$K_D = \frac{k_{\text{off}}}{k_{\text{on}}}$$

■ ASSOCIATED CONTENT

Supporting Information

The Supporting Information is available free of charge at <https://pubs.acs.org/doi/10.1021/acs.jmedchem.0c02067>.

Additional detailed chemistry methods, analytical HPLC chromatograms, and pharmacological data of the final fluorescent ligands (PDF)

Molecular formula strings of tested compounds (CSV)

■ AUTHOR INFORMATION

Corresponding Authors

Michelle L. Halls – Drug Discovery Biology, Monash Institute of Pharmaceutical Sciences, Monash University, Parkville, Victoria 3052, Australia; Phone: +613 9903 9094; Email: michelle.halls@monash.edu

Lauren T. May – Drug Discovery Biology, Monash Institute of Pharmaceutical Sciences, Monash University, Parkville, Victoria 3052, Australia; Phone: +613 9903 9095; Email: lauren.may@monash.edu

Peter J. Scammells – Medicinal Chemistry, Monash University, Parkville, Victoria 3052, Australia; orcid.org/0000-0003-2930-895X; Phone: +613 9903 9542; Email: peter.scammells@monash.edu

Authors

Eleonora Comeo – Medicinal Chemistry, Monash University, Parkville, Victoria 3052, Australia; Division of Biomolecular Sciences and Medicinal Chemistry, School of Pharmacy, Biodiscovery Institute, University of Nottingham, Nottingham NG7 2RD, United Kingdom; Centre of Membrane Proteins and Receptors (COMPARE), University of Birmingham, B15 2TT and University of Nottingham, Birmingham NG7 2UH, United Kingdom

Phuc Trinh – Drug Discovery Biology, Monash Institute of Pharmaceutical Sciences, Monash University, Parkville, Victoria 3052, Australia

Anh T. Nguyen – Drug Discovery Biology, Monash Institute of Pharmaceutical Sciences, Monash University, Parkville, Victoria 3052, Australia

Cameron J. Nowell – Drug Discovery Biology, Monash Institute of Pharmaceutical Sciences, Monash University, Parkville, Victoria 3052, Australia

Nicholas D. Kindon – Division of Biomolecular Sciences and Medicinal Chemistry, School of Pharmacy, Biodiscovery Institute, University of Nottingham, Nottingham NG7 2RD, United Kingdom; Centre of Membrane Proteins and Receptors (COMPARE), University of Birmingham, B15 2TT and University of Nottingham, Birmingham NG7 2UH, United Kingdom

Mark Soave – Division of Physiology, Pharmacology and Neuroscience, School of Life Sciences, Queens Medical Centre, University of Nottingham, Nottingham NG7 2UH, United Kingdom; Centre of Membrane Proteins and Receptors (COMPARE), University of Birmingham, B15 2TT and University of Nottingham, Birmingham NG7 2UH, United Kingdom

Leigh A. Stoddart – Division of Physiology, Pharmacology and Neuroscience, School of Life Sciences, Queens Medical Centre, University of Nottingham, Nottingham NG7 2UH, United Kingdom; Centre of Membrane Proteins and Receptors (COMPARE), University of Birmingham, B15 2TT and University of Nottingham, Birmingham NG7 2UH, United Kingdom

Jonathan M. White – School of Chemistry and the Bio21 Molecular Science and Biotechnology Institute, The University of Melbourne, Melbourne, Victoria 3010, Australia; orcid.org/0000-0002-0707-6257

Stephen J. Hill – Division of Physiology, Pharmacology and Neuroscience, School of Life Sciences, Queens Medical Centre, University of Nottingham, Nottingham NG7 2UH, United Kingdom; Centre of Membrane Proteins and Receptors (COMPARE), University of Birmingham, B15 2TT and

University of Nottingham, Birmingham NG7 2UH, United Kingdom; orcid.org/0000-0002-4424-239X

Barrie Kellam – Division of Biomolecular Sciences and Medicinal Chemistry, School of Pharmacy, Biodiscovery Institute, University of Nottingham, Nottingham NG7 2RD, United Kingdom; Centre of Membrane Proteins and Receptors (COMPARE), University of Birmingham, B15 2TT and University of Nottingham, Birmingham NG7 2UH, United Kingdom; orcid.org/0000-0003-0030-9908

Complete contact information is available at:
<https://pubs.acs.org/10.1021/acs.jmedchem.0c02067>

Notes

The authors declare no competing financial interest.

ACKNOWLEDGMENTS

The work was funded by the Medical Research Council (Grant number MR/N020081/1 to B.K. and S.J.H.), the Australian Research Council (ARC Discovery Project Grant DP19010145 to P.J.S.), the National Health and Medical Research Council of Australia (NHMRC) (Grant number APP1145420 to L.T.M. and S.J.H.; and APP1147291 to L.T.M.), the Monash Fellowship (from the faculty of Pharmacy and Pharmaceutical Sciences and Monash University to M.L.H.), and the Centre of Membrane Proteins and Receptors (COMPARE). This work was supported by the Nottingham-Monash Joint Doctoral Training Centre program. We thank Dr. Jason Dang for assistance with the spectroscopy work. L.T.M. is an Australian Heart Foundation Future Leader Fellow.

ABBREVIATIONS

AR, adenosine receptor; BODIPY, 4,4-difluoro-4-bora-3,1,4-diaza-s-indacene; BOP, (benzotriazol-1-yloxy)tris(dimethylamino)phosphonium hexafluorophosphate; CHO, chinese hamster ovary; COMU, (1-cyano-2-ethoxy-2-oxoethylidenaminoxy)dimethylamino-morpholino-carbenium hexafluorophosphate; Cy5, cyanine5; DIPEA, diisopropylethylamine; ESI, electrospray ionization; GPCR, G-protein-coupled receptor; HEK, human embryonic kidney; HPLC, high-performance liquid chromatography; NanoBRET, nanoluciferase-bioluminescence-energy transfer; NanoLuc, nanoluciferase; NMR, nuclear magnetic resonance; RP, reverse phase; SAR, structure–activity relationship

REFERENCES

- (1) Fredholm, B. B.; IJzerman, A. P.; Jacobson, K. A.; Klotz, K. N.; Linden, J. International Union of Pharmacology. XXV. Nomenclature and Classification of Adenosine Receptors. *Pharmacol. Rev.* **2001**, *53*, 527–552.
- (2) Fredholm, B. B.; IJzerman, A. P.; Jacobson, K. A.; Linden, J. International Union of Pharmacology. XXV. Nomenclature and Classification of Adenosine Receptors—An Update. *Pharmacol. Rev.* **2011**, *63*, 527–552.
- (3) Alexander, S. P.; Christopoulos, A.; Davenport, A. P.; Kelly, E.; Marrion, N. V.; Peters, J. A.; Faccenda, E.; Harding, S. D.; Pawson, A. J.; Sharman, J. L.; Southan, C.; Davies, J. A. The Concise Guide To Pharmacology 2017 / 18: G Protein-Coupled Receptors. *Br. J. Pharmacol.* **2017**, *174*, S17–S129.
- (4) Jacobson, K. A.; Gao, Z.-G. Adenosine Receptors as Therapeutic Targets. *Nat. Rev. Drug Discov.* **2006**, *49*, 247–264.
- (5) Fredholm, B. B.; Arslan, G.; Halldner, L.; Kull, B.; Schulte, G.; Wasserman, W. Structure and Function of Adenosine Receptors and Their Genes. *Naunyn-Schmiedeberg's Arch. Pharmacol.* **2000**, *362*, 364–374.

- (6) Deb, P. K.; Deka, S.; Borah, P.; Abed, S. N.; Klotz, K.-N. Medicinal Chemistry and Therapeutic Potential of Agonists, Antagonists and Allosteric Modulators of A₁ Adenosine Receptor: Current Status and Perspectives. *Curr. Pharm. Des.* **2019**, *25*, 2697–2715.
- (7) Gao, Z.; Tosh, D. K.; Jain, S.; Yu, J.; Suresh, R. R. A₁ Adenosine Receptor Agonists, Antagonists and Allosteric Modulators. In *The Adenosine Receptors, The Receptors*; Borea, P., Varani, K., Gessi, S., Merighi, S., V. F. (eds), Ed.; Humana Press, New York, NY, 2018; 59–89.
- (8) Delacretaz, E. Supraventricular Tachycardia. *N. Engl. J. Med.* **2006**, *28*, 109–111.
- (9) Linden, J. Adenosine in Tissue Protection and Tissue Regeneration. *Mol. Pharmacol.* **2005**, *67*, 1385–1387.
- (10) Borea, P. A.; Gessi, S.; Merighi, S.; Vincenzi, F.; Varani, K. Pharmacology of Adenosine Receptors: The State of the Art. *Physiol. Rev.* **2018**, *98*, 1591–1625.
- (11) Müller, C. E.; Jacobson, K. A. Recent Developments in Adenosine Receptor Ligands and Their Potential as Novel Drugs. *Biochim. Biophys. Acta, Biomembr.* **2011**, *1808*, 1290–1308.
- (12) Gao, Z. G.; Jacobson, K. A. Purinergic Signaling in Mast Cell Degranulation and Asthma. *Front. Pharmacol.* **2017**, *8*, 1–14.
- (13) Mendiola-Precoma, J.; Padilla, K.; Rodríguez-Cruz, A.; Berumen, L. C.; Miledi, R.; García-Alcocer, G. Theobromine-Induced Changes in A₁ Purinergic Receptor Gene Expression and Distribution in a Rat Brain Alzheimer's Disease Model. *J. Alzheimer's Dis.* **2017**, *55*, 1273–1283.
- (14) Massie, B. M.; O'Connor, C. M.; Metra, M.; Ponikowski, P.; Teerlink, J. R.; Cotter, G.; Weatherley, B. D.; Cleland, J. G. F.; Givertz, M. M.; Voors, A.; DeLucca, P.; Mansoor, G. A.; Salerno, C. M.; Bloomfield, D. M.; Dittrich, H. C. Rolofylline, an Adenosine A₁-Receptor Antagonist, in Acute Heart Failure. *N. Engl. J. Med.* **2010**, *363*, 1419–1428.
- (15) Ensor, C. R.; Russell, S. D. Tonapofylline: A Selective Adenosine-1 Receptor Antagonist for the Treatment of Heart Failure. *Expert Opin. Pharmacother.* **2010**, *11*, 2405–2415.
- (16) Voors, A. A.; Bax, J. J.; Hernandez, A. F.; Wirtz, A. B.; Pap, A. F.; Ferreira, A. C.; Senni, M.; van der Laan, M.; Butler, J. Safety and Efficacy of the Partial Adenosine A₁ Receptor Agonist Neladenoson Bialanate in Patients with Chronic Heart Failure with Reduced Ejection Fraction: A Phase IIb, Randomized, Double-Blind, Placebo-Controlled Trial. *Eur. J. Heart Fail.* **2019**, *21*, 1426–1433.
- (17) Valant, C.; May, L. T.; Aurelio, L.; Chuo, C. H.; White, P. J.; Baltos, J.-A.; Sexton, P. M.; Scammells, P. J.; Christopoulos, A. Separation of On-Target Efficacy from Adverse Effects through Rational Design of a Bitopic Adenosine Receptor Agonist. *Proc. Natl. Acad. Sci. U. S. A.* **2014**, *111*, 4614–4619.
- (18) Aurelio, L.; Baltos, J. A.; Ford, L.; Nguyen, A. T. N.; Jörg, M.; Devine, S. M.; Valant, C.; White, P. J.; Christopoulos, A.; May, L. T.; Scammells, P. J. A Structure-Activity Relationship Study of Bitopic N⁶-Substituted Adenosine Derivatives as Biased Adenosine A₁ Receptor Agonists. *J. Med. Chem.* **2018**, *61*, 2087–2103.
- (19) May, L. T.; Leach, K.; Sexton, P. M.; Christopoulos, A. Allosteric Modulation of G-Protein Coupled Receptors. *Annu. Rev. Pharmacol. Toxicol.* **2007**, *47*, 1–51.
- (20) Bunnage, M. E.; Chekler, E. L. P.; Jones, L. H. Target Validation Using Chemical Probes. *Nat. Chem. Biol.* **2013**, *9*, 195–199.
- (21) Ralevic, V.; Burnstock, G. Receptors for Purines and Pyrimidines. *Pharmacol. Rev.* **1998**, *50*, 413–492.
- (22) Peakman, M.-C.; Hill, S. J. Adenosine A₁ Receptor-mediated Changes in Basal and Histamine-stimulated Levels of Intracellular Calcium in Primary Rat Astrocytes. *Br. J. Pharmacol.* **1995**, *115*, 801–810.
- (23) Ginés, S.; Ciruela, F.; Burgueño, J.; Casadó, V.; Canela, E. I.; Mallol, J.; Lluís, C.; Franco, R. Involvement of Caveolin in Ligand-Induced Recruitment and Internalization of A₁ Adenosine Receptor and Adenosine Deaminase in an Epithelial Cell Line. *Mol. Pharmacol.* **2001**, *59*, 1314–1323.

- (24) Briddon, S. J.; Middleton, R. J.; Cordeaux, Y.; Flavin, F. M.; Weinstein, J. A.; George, M. W.; Kellam, B.; Hill, S. J. Quantitative Analysis of the Formation and Diffusion of A₁-Adenosine Receptor – Antagonist Complexes in Single Living Cells. *Proc. Natl. Acad. Sci. U. S. A.* **2004**, *101*, 4673–4678.
- (25) Stoddart, L. A.; Vernall, A. J.; Briddon, S. J.; Kellam, B.; Hill, S. J. Direct Visualisation of Internalization of the Adenosine A₃ Receptor and Localization with Arrestin3 Using a Fluorescent Agonist. *Neuropharmacology* **2015**, *98*, 68–77.
- (26) Schembri, L. S.; Stoddart, L. A.; Briddon, S. J.; Kellam, B.; Canals, M.; Graham, B.; Scammells, P. J. Synthesis, Biological Evaluation, and Utility of Fluorescent Ligands Targeting the μ -Opioid Receptor. *J. Med. Chem.* **2015**, *58*, 9754–9767.
- (27) Conroy, S.; Kindon, N. D.; Glenn, J.; Stoddart, L. A.; Lewis, R. J.; Hill, S. J.; Kellam, B.; Stocks, M. J. Synthesis and Evaluation of the First Fluorescent Antagonists of the Human P2Y₂ Receptor Based on AR-C118925. *J. Med. Chem.* **2018**, *61*, 3089–3113.
- (28) Stoddart, L. A.; Vernall, A. J.; Denman, J. L.; Briddon, S. J.; Kellam, B.; Hill, S. J. Fragment Screening at Adenosine-A₃ Receptors in Living Cells Using a Fluorescence-Based Binding Assay. *Chem. Biol.* **2012**, *19*, 1105–1115.
- (29) Stoddart, L. A.; Johnstone, E. K. M.; Wheal, A. J.; Goulding, J.; Robers, M. B.; MacHleidt, T.; Wood, K. V.; Hill, S. J.; Pflieger, K. D. G. Application of BRET to Monitor Ligand Binding to GPCRs. *Nat. Methods* **2015**, *12*, 661–663.
- (30) Alcobia, D. C.; Ziegler, A. I.; Kondrashov, A.; Comeo, E.; Mistry, S.; Kellam, B.; Chang, A.; Woolard, J.; Hill, S. J.; Sloan, E. K. Visualizing Ligand-Binding to a GPCR In Vivo Using NanoBRET. *iScience* **2018**, *6*, 280–288.
- (31) Arruda, M. A.; Stoddart, L. A.; Gherbi, K.; Briddon, S. J.; Kellam, B.; Hill, S. J. A Non-Imaging High Throughput Approach to Chemical Library Screening at the Unmodified Adenosine-A₃ Receptor in Living Cells. *Front. Pharmacol.* **2017**, *8*, 1–13.
- (32) Soave, M.; Briddon, S. J.; Hill, S. J.; Stoddart, L. A. Fluorescent Ligands: Bringing Light to Emerging G Protein-coupled Receptor Paradigms. *Br. J. Pharmacol.* **2019**, 1–14.
- (33) Vernall, A. J.; Hill, S. J.; Kellam, B. The Evolving Small-Molecule Fluorescent-Conjugate Toolbox for Class A GPCRs. *Br. J. Pharmacol.* **2014**, *171*, 1073–1084.
- (34) Federico, S.; Lassiani, L.; Spalluto, G. Chemical Probes for the Adenosine Receptors. *Pharmaceuticals* **2019**, *12*, 1–21.
- (35) Kozma, E.; Suresh Jayasekara, P.; Squarciarupi, L.; Paoletta, S.; Moro, S.; Federico, S.; Spalluto, G.; Jacobson, K. A. Fluorescent Ligands for Adenosine Receptors. *Bioorg. Med. Chem. Lett.* **2013**, *23*, 26–36.
- (36) Soave, M.; Goulding, J.; Markus, R.; Hill, S. J.; Stoddart, L. A. Application of Fluorescent Purinoceptor Antagonists for Bioluminescence Resonance Energy Transfer Assays and Fluorescent Microscopy. In *Purinergic Signalling: Methods in Molecular Biology*, Vol. 2041; Walker, J.M.; Pelegrin, P., Eds.; Humana Press: New York, 2020; pp163–181.
- (37) Kecskés, M.; Kumar, T. S.; Yoo, L.; Gao, Z. G.; Jacobson, K. A. Novel Alexa Fluor-488 Labeled Antagonist of the A_{2A} Adenosine Receptor: Application to a Fluorescence Polarization-Based Receptor Binding Assay. *Biochem. Pharmacol.* **2010**, *80*, 506–511.
- (38) Duroux, R.; Ciancetta, A.; Mannes, P.; Yu, J.; Boyapati, S.; Gizewski, E.; Yous, S.; Ciruela, F.; Auchampach, J. A.; Gao, Z.-G.; Jacobson, K. A. Bitopic Fluorescent Antagonists of the A_{2A} Adenosine Receptor Based on Pyrazolo[4,3-e][1,2,4]Triazolo[1,5-c]Pyrimidin-5-Amine Functionalized Congeners. *MedChemComm.* **2017**, *8*, 1659–1667.
- (39) Comeo, E.; Kindon, N. D.; Soave, M.; Stoddart, L. A.; Kilpatrick, L. E.; Scammells, P. J.; Hill, S. J.; Kellam, B. Subtype-Selective Fluorescent Ligands as Pharmacological Research Tools for the Human Adenosine A_{2A} Receptor. *J. Med. Chem.* **2020**, *63*, 2656–2672.
- (40) Köse, M.; Gollos, S.; Karcz, T.; Fiene, A.; Heisig, F.; Behrenswarth, A.; Kiec-Kononowicz, K. J.; Namasivayam, V.; Müller, C. E. Fluorescent-Labeled Selective Adenosine A_{2B} Receptor Antagonist Enables Competition Binding Assay by Flow Cytometry. *J. Med. Chem.* **2018**, *61*, 4301–4316.
- (41) Vernall, A. J.; Stoddart, L. A.; Briddon, S. J.; Hill, S. J.; Kellam, B. Highly Potent and Selective Fluorescent Antagonists of the Human Adenosine A₃ Receptor Based on the 1,2,4-Triazolo[4,3-a]-Quinoxalin-1-One Scaffold. *J. Med. Chem.* **2012**, *55*, 1771–1782.
- (42) Vernall, A. J.; Stoddart, L. A.; Briddon, S. J.; Ng, H. W.; Laughton, C. A.; Doughty, S. W.; Hill, S. J.; Kellam, B. Conversion of a Non-Selective Adenosine Receptor Antagonist into A₃-Selective High Affinity Fluorescent Probes Using Peptide-Based Linkers. *Org. Biomol. Chem.* **2013**, *11*, 5673–5682.
- (43) Bouzo-Lorenzo; Stoddart, L. A.; Xia, L.; IJzerman, A. P.; Heitman, L. H.; Briddon, S. J.; Hill, S. J. A Live Cell NanoBRET Binding Assay Allows the Study of Ligand-Binding Kinetics to the Adenosine A₃ Receptor. *Purinergic Signal.* **2019**, *15*, 139–153.
- (44) Cooper, S. L.; Soave, M.; Jörg, M.; Scammells, P. J.; Woolard, J.; Hill, S. J. Probe Dependence of Allosteric Enhancers on the Binding Affinity of Adenosine A₁-Receptor Agonists at Rat and Human A₁-Receptors Measured Using NanoBRET. *Br. J. Pharmacol.* **2019**, *176*, 864–878.
- (45) May, L. T.; Self, T. J.; Briddon, S. J.; Hill, S. J. The Effect of Allosteric Modulators on the Kinetics of Agonist-G Protein-Coupled Receptor Interactions in Single Living Cells. *Mol. Pharmacol.* **2010**, *78*, 511–523.
- (46) Cordeaux, Y.; Briddon, S. J.; Alexander, S. P. H.; Kellam, B.; Hill, S. J. Agonist-Occupied A₃ Adenosine Receptors Exist within Heterogeneous Complexes in Membrane Microdomains of Individual Living Cells. *FASEB J.* **2007**, *22*, 850–860.
- (47) Jacobson, K. A.; Ukena, D.; Padgett, W.; Kirk, K. L.; Daly, J. W. Molecular Probes for Extracellular Adenosine Receptors. *Biochem. Pharmacol.* **1987**, *36*, 1697–1707.
- (48) Middleton, R. J.; Briddon, S. J.; Cordeaux, Y.; Yates, A. S.; Dale, C. L.; George, M. W.; Baker, J. G.; Hill, S. J.; Kellam, B. New Fluorescent Adenosine A₁-Receptor Agonists That Allow Quantification of Ligand - Receptor Interactions in Microdomains of Single Living Cells. *J. Med. Chem.* **2007**, *50*, 782–793.
- (49) Macchia, M.; Salvetti, F.; Barontini, S.; Calvani, F.; Gesi, M.; Hamdan, M.; Lucacchini, A.; Pellegrini, A.; Soldani, P.; Martini, C. Fluorescent Probes for Adenosine Receptors: Synthesis and Biology of N⁶-Dansylaminoalkyl-Substituted Neca Derivatives. *Bioorg. Med. Chem. Lett.* **1998**, *8*, 3223–3228.
- (50) Jacobson, K. A.; Ukena, D.; Padgett, W.; Daly, J. W.; Kirk, K. L. Xanthine Functionalized Congeners as Potent Ligands at A₂-Adenosine Receptors. *J. Med. Chem.* **1987**, *30*, 211–214.
- (51) Corriden, R.; Kilpatrick, L. E.; Kellam, B.; Briddon, S. J.; Hill, S. J. Kinetic Analysis of Antagonist-Occupied Adenosine-A₃ Receptors within Membrane Microdomains of Individual Cells Provides Evidence of Receptor Dimerization and Allosterism. *FASEB J.* **2014**, *28*, 4211–4222.
- (52) Briddon, S. J.; Middleton, R. J.; Yates, A. S.; George, M. W.; Kellam, B.; Hill, S. J. Application of Fluorescence Correlation Spectroscopy to the Measurement of Agonist Binding to a G-Protein Coupled Receptor at the Single Cell Level. *Faraday Discuss.* **2004**, *126*, 197–207.
- (53) Simon, G. M.; Niphakis, M. J.; Cravatt, B. F. Determining Target Engagement in Living Systems. *Nat. Chem. Biol.* **2013**, *9*, 200–205.
- (54) Singh, S.; Cooper, S. L.; Glenn, J. R.; Beresford, J.; Percival, L. R.; Tyndall, J. D. A.; Hill, S. J.; Kilpatrick, L. E.; Vernall, A. J. Synthesis of Novel (Benzimidazolyl)Isoquinolinols and Evaluation as Adenosine A₁ Receptor Tools. *RSC Adv.* **2018**, *8*, 16362–16369.
- (55) Glukhova, A.; Thal, D. M.; Nguyen, A. T.; May, L. T.; Sexton, P. M.; Christopoulos, A.; Scammells, P. J. Structure of the Adenosine A₁ Receptor Reveals the Basis for Subtype Selectivity. *Cell* **2017**, *168*, 867–877.e13.
- (56) Cheng, R. K. Y.; Segala, E.; Robertson, N.; Marshall, F. H.; Cooke, R. M.; Errey, J. C.; Marshall, F. H.; Cooke, R. M. Structures of Human A₁ and A_{2A} Adenosine Receptors with Xanthines Reveal Determinants of Selectivity. *Structure* **2017**, *25*, 1275–1285.e4.

- (57) Weyler, S.; Fülle, F.; Diekmann, M.; Schumacher, B.; Hinz, S.; Klotz, K. N.; Müller, C. E. Improving Potency, Selectivity, and Water Solubility of Adenosine A₁ Receptor Antagonists: Xanthines Modified at Position 3 and Related Pyrimido[1,2,3-Cd]Purinediones. *Chem-MedChem* **2006**, *1*, 891–902.
- (58) Baraldi, P. G.; Tabrizi, M. A.; Gessi, S.; Borea, P. A. Adenosine Receptor Antagonists: Translating Medicinal Chemistry and Pharmacology into Clinical Utility. *Chem. Rev.* **2008**, *108*, 238–263.
- (59) Kiesman, W. F.; Zhao, J.; Conlon, P. R.; Dowling, J. E.; Petter, R. C.; Lutterodt, F.; Jin, X.; Smits, G.; Fure, M.; Jayaraj, A.; Kim, J.; Sullivan, G.; Linden, J. Potent and Orally Bioavailable 8-Bicyclo[2.2.2]Octylxanthines as Adenosine A₁ Receptor Antagonists. *J. Med. Chem.* **2006**, *49*, 7119–7131.
- (60) Beaglehole, A. R.; Baker, S. P.; Scammells, P. J. Fluorosulfonyl-Substituted Xanthines as Selective Irreversible Antagonists for the A₁-Adenosine Receptor. *J. Med. Chem.* **2000**, *43*, 4973–4980.
- (61) Ballesteros, J. A.; Weinstein, H. Integrated Methods for the Construction of Three-Dimensional Models and Computational Probing of Structure-Function Relations in G Protein-Coupled. *Methods Neurosci.* **1995**, *25*, 366–428.
- (62) Dale, C. L.; Hill, S. J.; Kellam, B. New Potent, Short-Linker BODIPY-630/650 Labelled Fluorescent Adenosine Receptor Agonists. *MedChemComm* **2012**, *3*, 333–338.
- (63) Pansare, V. J.; Hejazi, S.; Faenza, W. J.; Prud'homme, R. K. Review of Long-Wavelength Optical and NIR Imaging Materials: Contrast Agents, Fluorophores, and Multifunctional Nano Carriers. *Chem. Mater.* **2012**, *24*, 812–827.
- (64) Baker, J. G.; Middleton, R.; Adams, L.; May, L. T.; Briddon, S. J.; Kellam, B.; Hill, S. J. Influence of Fluorophore and Linker Composition on the Pharmacology of Fluorescent Adenosine A₁ Receptor Ligands: Themed Section: Imaging in Pharmacology Research Paper. *Br. J. Pharmacol.* **2010**, *159*, 772–786.
- (65) Karolin, J.; Johansson, L. B. A.; Strandberg, L.; Ny, T. Fluorescence and Absorption Spectroscopic Properties of Dipyrrometheneboron Difluoride (BODIPY) Derivatives in Liquids, Lipid Membranes, and Proteins. *J. Am. Chem. Soc.* **1994**, *116*, 7801–7806.
- (66) Ulrich, G.; Zissel, R.; Harriman, A. The Chemistry of Fluorescent Bodipy Dyes: Versatility Unsurpassed. *Angew. Chem., Int. Ed.* **2008**, *47*, 1184–1201.
- (67) Hill, S. J.; May, L. T.; Kellam, B.; Woolard, J. Allosteric Interactions at Adenosine A₁ and A₃ Receptors: New Insights into the Role of Small Molecules and Receptor Dimerization. *Br. J. Pharmacol.* **2014**, *171*, 1102–1113.
- (68) Rose, R. H.; Briddon, S. J.; Hill, S. J. A Novel Fluorescent Histamine H(1) Receptor Antagonist Demonstrates the Advantage of Using Fluorescence Correlation Spectroscopy to Study the Binding of Lipophilic Ligands. *Br. J. Pharmacol.* **2012**, *165*, 1789–1800.
- (69) Ma, Z.; Lin, Y.; Cheng, Y.; Wu, W.; Cai, R.; Chen, S.; Shi, B.; Han, B.; Shi, X.; Zhou, Y.; Lupei, D.; Li, M. Discovery of the First Environment-Sensitive Near-Infrared (NIR) Fluorogenic Ligand for α_1 -Adrenergic Receptors Imaging in Vivo. *J. Med. Chem.* **2016**, *59*, 2151–2162.
- (70) Müller, C. E. Synthesis of 3-Substituted 6-Aminouracils. *Tetrahedron Lett.* **1991**, *32*, 6539–6540.
- (71) Müller, C. E.; Sandoval-Ramirez, J. A New Versatile Synthesis of Xanthines with Variable Substituents in the 1-, 3-, 7- and 8-Positions. *Synthesis* **1995**, *10*, 1295–1299.
- (72) Baraldi, P. G.; Borea, P. A.; Preti, D.; Tabrizi, M. A. Novel Adenosine A₃ Receptor Modulators. WO 2006/083916 A2, Aug 10, 2006.
- (73) Marx, D.; Wingen, L. M.; Schnakenburg, G.; Müller, C. E.; Scholz, M. S. Fast, Efficient, and Versatile Synthesis of 6-Amino-5-Carboxamidouracils as Precursors for 8-Substituted Xanthines. *Front. Chem.* **2019**, *7*, 1–15.
- (74) Olsson, R. A.; Holschbach, M. H.; Schrader, J. Adenosine Receptor Antagonists With Improved Bioactivity. WO 99/31101, Jun 24, 1999.
- (75) Draper-joyce, C. J.; Khoshouei, M.; Thal, D. M.; Liang, Y.-L.; Nguyen, A. T. N.; Furness, S. G. B.; Venugopal, H.; Baltos, J.; Plitzko, J. M.; Danev, R.; Baumeister, W.; May, L. T.; Wootten, D.; Sexton, P. M.; Glukhova, A.; Christopoulos, A. Structure of the Adenosine-Bound Human Adenosine A₁ Receptor–Gi Complex. *Nature* **2018**, *558*, 559–563.
- (76) Mattedi, G.; Deflorian, F.; Mason, J. S.; de Graaf, C.; Gervasio, F. L. Understanding Ligand Binding Selectivity in a Prototypical GPCR Family. *J. Chem. Inf. Model.* **2019**, *59*, 2830–2836.
- (77) Bolcato, G.; Bissaro, M.; Deganutti, G.; Sturlese, M.; Moro, S. New Insights into Key Determinants for Adenosine 1 Receptor Antagonists Selectivity Using Supervised Molecular Dynamics Simulations. *Biomolecules* **2020**, *10*, 1–11.
- (78) Mason, J. S.; Bortolato, A.; Weiss, D. R.; Deflorian, F.; Tehan, B.; Marshall, F. H. High End GPCR Design: Crafted Ligand Design and Druggability Analysis Using Protein Structure, Lipophilic Hotspots and Explicit Water Networks. *Silico Pharmacol.* **2013**, *1*, 1–12.
- (79) Mason, J. S.; Bortolato, A.; Congreve, M.; Marshall, F. H. New Insights from Structural Biology into the Druggability of G Protein-Coupled Receptors. *Trends Pharmacol. Sci.* **2012**, *33*, 249–260.
- (80) Stoddart, L. A.; Kilpatrick, L. E.; Hill, S. J. NanoBRET Approaches to Study Ligand Binding to GPCRs and RTKs. *Trends Pharmacol. Sci.* **2018**, *39*, 136–147.
- (81) Dale, N. C.; Johnstone, E. K. M.; White, C. W.; Pflieger, K. D. G. NanoBRET: The Bright Future of Proximity-Based Assays. *Front. Bioeng. Biotechnol.* **2019**, *7*, 1–13.
- (82) Hall, M. P.; Unch, J.; Binkowski, B. F.; Valley, M. P.; Butler, B. L.; Wood, M. G.; Otto, P.; Zimmerman, K.; Vidugiris, G.; MacHleidt, T.; Robers, M. B.; Benink, H. A.; Eggers, C. T.; Slater, M. R.; Meisenheimer, P. L.; Klaubert, D. H.; Fan, F.; Encell, L. P.; Wood, K. V. Engineered Luciferase Reporter from a Deep Sea Shrimp Utilizing a Novel Imidazopyrazinone Substrate. *ACS Chem. Biol.* **2012**, *7*, 1848–1857.
- (83) Mercier, J. F.; Salahpour, A.; Angers, S.; Breit, A.; Bouvier, M. Quantitative Assessment of B1- and B2-Adrenergic Receptor Homo- and Heterodimerization by Bioluminescence Resonance Energy Transfer. *J. Biol. Chem.* **2002**, *277*, 44925–44931.
- (84) Marullo, S.; Bouvier, M. Resonance Energy Transfer Approaches in Molecular Pharmacology and Beyond. *Trends Pharmacol. Sci.* **2007**, *28*, 362–365.
- (85) Pflieger, K. D. G.; Eidne, K. A. Illuminating Insights into Protein-Protein Interactions Using Bioluminescence Resonance Energy Transfer (BRET). *Nat. Methods* **2006**, *3*, 165–174.
- (86) Uhlén, M.; Fagerberg, L.; Hallström, B. M.; Lindskog, C.; Oksvold, P.; Mardinoglu, A.; Sivertsson, Å.; Kampf, C.; Sjöstedt, E.; Asplund, A.; Olsson, I.; Edlund, K.; Lundberg, E.; Navani, S.; Al-Khalili Szigartyo, C.; Odeberg, J.; Djureinovic, D.; Ottosson Takanan, J.; Hober, S.; Alm, T.; Edqvist, P. H.; Berling, H.; Tegel, H.; Mulder, J.; Rockberg, J.; Nilsson, P.; Schwenk, J. M.; Hamsten, M.; von Feilitzen, K.; Forsberg, M.; Persson, L.; Johansson, F.; Zvalnen, M.; von Heijne, G.; Nielsen, J.; Pontén, F. Tissue-Based Map of the Human Proteome. *Science* **2015**, *347*, 394.
- (87) *The Human Protein Atlas* <https://www.proteinatlas.org/ENSG00000163485-ADORA1/cell> (accessed Nov 1st, 2020).
- (88) Schwehm, C.; Kellam, B.; Garces, A. E.; Hill, P. S. J.; Kindon, N. D.; Tracey, D.; Li, J.; Macdonald, S. J. F.; Rowedder, J. E.; Stoddart, L. A.; Stocks, M. J. Design and Elaboration of a Tractable Tricyclic Scaffold to Synthesize Drug-like Inhibitors of Dipeptidyl Peptidase-4 (DPP-4), Antagonists of the C-C Chemokine Receptor Type 5 (CCRS5), and Highly Potent and Selective Phosphoinositol-3 Kinase δ (PI3K δ) Inhibitors. *J. Med. Chem.* **2017**, *60*, 1534–1554.
- (89) May, L. T.; Bridge, L. J.; Stoddart, L. A.; Briddon, S. J.; Hill, S. J. Allosteric Interactions across Native Adenosine-A₃ Receptor Homodimers: Quantification Using Single-Cell Ligand-Binding Kinetics. *FASEB J.* **2011**, *25*, 3465–3476.
- (90) Hoffmann, C.; Castro, M.; Rinken, A.; Leurs, R.; Hill, S. J.; Vischer, H. F. Ligand Residence Time at G-Protein-Coupled

Receptors - Why We Should Take Our Time to Study It. *Mol. Pharmacol.* **2015**, *88*, 552–560.

(91) Guo, D.; Heitman, L. H.; Ijzerman, A. P. Kinetic Aspects of the Interaction between Ligand and G-Protein-Coupled Receptor: The Case of the Adenosine Receptors. *Chem. Rev.* **2017**, *117*, 38–66.

(92) Sykes, D. A.; Stoddart, L. A.; Kilpatrick, L. E.; Hill, S. J. Binding Kinetics of Ligands Acting at GPCRs. *Mol. Cell. Endocrinol.* **2019**, *485*, 9–19.

(93) Stoddart, L. A.; Vernall, A. J.; Bouzo-Lorenzo, M.; Bosma, R.; Kooistra, A. J.; De Graaf, C.; Vischer, H. F.; Leurs, R.; Briddon, S. J.; Kellam, B.; Hill, S. J. Development of Novel Fluorescent Histamine H₁-Receptor Antagonists to Study Ligand-Binding Kinetics in Living Cells. *Sci. Rep.* **2018**, *8*, 1–19.

(94) Sykes, D. A.; Parry, C.; Reilly, J.; Wright, P.; Fairhurst, R. A.; Charlton, S. J. Observed Drug-Receptor Association Rates Are Governed by Membrane Affinity: The Importance of Establishing 'Micro-Pharmacokinetic/Pharmacodynamic Relationships' at the β_2 -Adrenoceptor. *Mol. Pharmacol.* **2014**, *85*, 608–617.

(95) Gherbi, K.; Briddon, S. J.; Charlton, S. J. Micro-Pharmacokinetics: Quantifying Local Drug Concentration at Live Cell Membranes. *Sci. Rep.* **2018**, *8*, 1–8.

(96) Kalk, P.; Eggert, B.; Relle, K.; Godes, M.; Heiden, S.; Sharkovska, Y.; Fischer, Y.; Ziegler, D.; Bielenberg, G. W.; Hocher, B. The Adenosine A₁ Receptor Antagonist SLV320 Reduces Myocardial Fibrosis in Rats with 5/6 Nephrectomy without Affecting Blood Pressure. *Br. J. Pharmacol.* **2007**, *151*, 1025–1032.

(97) De Lig, R. A. F.; Rivkees, S. A.; Lorenzen, A.; Leurs, R.; Ijzerman, A. P. A 'Locked-on,' Constitutively Active Mutant of the Adenosine A₁ Receptor. *Eur. J. Pharmacol.* **2005**, *510*, 1–8.

(98) Iredale, P. A.; Alexander, S. P. H.; Hill, S. J. Coupling of a Transfected Human Brain A₁ Adenosine Receptor in CHO-K1 Cells to Calcium Mobilisation via a Pertussis Toxin-sensitive Mechanism. *Br. J. Pharmacol.* **1994**, *111*, 1252–1256.

(99) Baker, J. G.; Hill, S. J. A Comparison of the Antagonist Affinities for the Gi- and Gs- Coupled States of the Human Adenosine A₁-Receptor. *J. Pharmacol. Exp. Ther.* **2007**, *320*, 218–228.

(100) Townsend-Nicholson, A.; Schofield, P. R. A Threonine Residue in the Seventh Transmembrane Domain of the Human A₁ Adenosine Receptor Mediates Specific Agonist Binding. *J. Biol. Chem.* **1994**, *269*, 2373–2376.

(101) Rivkees, S. A.; Barbaiya, H.; Ijzerman, A. P. Identification of the Adenine Binding Site of the Human A₁ Adenosine Receptor. *J. Biol. Chem.* **1999**, *274*, 3617–3621.

(102) Gao, Z. G.; Mamedova, L. K.; Chen, P.; Jacobson, K. A. 2-Substituted Adenosine Derivatives: Affinity and Efficacy at Four Subtypes of Human Adenosine Receptors. *Biochem. Pharmacol.* **2004**, *68*, 1985–1993.

(103) Steyer, J. A.; Almers, W. A Real-Time View of Life within 100 NM of the Plasma Membrane. *Nat. Rev. Mol. Cell Biol.* **2001**, *2*, 268–275.

(104) Calebiro, D.; Rieken, F.; Wagner, J.; Sungkaworn, T.; Zabel, U.; Borzi, A.; Cocucci, E.; Zürn, A.; Lohse, M. J. Single-Molecule Analysis of Fluorescently Labeled G-Protein-Coupled Receptors Reveals Complexes with Distinct Dynamics and Organization. *Proc. Natl. Acad. Sci. U. S. A.* **2013**, *110*, 743–748.

(105) Halls, M. L.; Yeatman, H. R.; Nowell, C. J.; Thompson, G. L.; Gondin, A. B.; Civciristov, S.; Bunnett, N. W.; Lambert, N. A.; Poole, D. P.; Canals, M. Plasma Membrane Localization of the μ -Opioid Receptor Controls Spatiotemporal Signaling. *Sci. Signaling* **2016**, *9*, 1–14.

(106) Lin, K.-C.; Vu, C. Condensed Purine Derivative as A₁ Adenosine Receptor Antagonists. WO 02/44182 A1, Jun 6, 2002.

(107) Stewart, G. D.; Valant, C.; Dowell, S. J.; Mijaljica, D.; Devenish, R. J.; Scammells, P. J.; Sexton, P. M.; Christopoulos, A. Determination of Adenosine A₁ Receptor Agonist and Antagonist Pharmacology Using *Saccharomyces Cerevisiae*: Implications for Ligand Screening and Functional Selectivity. *J. Pharmacol. Exp. Ther.* **2009**, *331*, 277–286.

(108) Nguyen, A. T. N.; Baltos, J. A.; Thomas, T.; Nguyen, T. D.; Muñoz, L. L.; Gregory, K. J.; White, P. J.; Sexton, P. M.; Christopoulos, A.; May, L. T. Extracellular Loop 2 of the Adenosine A₁ Receptor Has a Key Role in Orthosteric Ligand Affinity and Agonist Efficacy. *Mol. Pharmacol.* **2016**, *90*, 703–714.

(109) Schindelin, J.; Arganda-Carreras, I.; Frise, E.; Kaynig, V.; Longair, M.; Pietzsch, T.; Preibisch, S.; Rueden, C.; Saalfeld, S.; Schmid, B.; Tinevez, J.-Y.; White, D. J.; Hartenstein, V.; Eliceiri, K.; Tomancak, P.; Cardona, A. Fiji: An Open-Source Platform for Biological-Image Analysis. *Nat. Methods* **2012**, *9*, 676–682.